universität wien

DIPLOMARBEIT

Titel der Diplomarbeit

„Applikation von Cumarin 6 als sensibler Marker zur Krebszell-Detektion“

Verfasser

Christoph MIKSCH

angestrebter akademischer Grad

Magister der Naturwissenschaften (Mag.rer.nat.)

Wien, 2011

Studienkennzahl lt. Studienblatt:	A 490
Studienrichtung lt. Studienblatt:	Diplomstudium Molekulare Biologie
Betreuerin / Betreuer:	ao. Univ.-Prof. Dr. Gottfried Köhler

Dedicated to my family

Acknowledgements

Without claiming completeness, I want to give thanks to the following people:

I am very grateful to ao. Univ.-Prof. Dr. Gottfried KÖHLER, who was supervising my work and leading it in the right directions, and being patient with the delay I was producing because I was confronted with many different things that took time to gel. He was mentoring me together and with the help of Dr. Michael EDETS-BERGER, who tried to help me as much as possible and did a really good job, taking into consideration that he was obviously sieged by many other people, who demanded most of his time.

Further, I want to thank Dr. Martin KNAPP, who accepted me as the person I am and gave me lots of advice, as he was very willing to share his profound knowledge in chemistry and thus, providing me with all the necessary information to write a big part of this thesis, as he did most of the work that led to the theoretical knowledge about the Onkovidon® dye.

Special thanks goes to Julia SCHINDELAR, as she was providing me with the little funny guys, called cancer cells, as she really has a sense for their behavior and needs, and can be seen as an institution concerning tissue culture. I also want to thank Karin MÜLLER, Erwin GAUBITZER and Arthur SEDIVY for being really nice colleagues, the latter known for his intelligence and outstanding funny behavior, found only in a handful of extraordinary primates.

I also want to thank all the people who formed and/or worked for OnkoTec, as they offered me the opportunity to be part of a big project that will hopefully earn profit in the future.

Moreover, I really want to thank some members of Prof. Gerhard WICHE's group, namely Dr. Gernot WALKO, one of the most erudite and cool persons I know, Dr.

Peter FUCHS, for his support and friendship, and Mag. Karl Leopold WÖGENSTEIN, who really knows who I am, and stands out as one of my oldest real friends at the university. This feature can only be ascribed to one other university mate, Mag. Matthias PARRINI, who exactly knows what I have to thank him for. I also want to thank Annika SCHMID, as she could not resist asking if she was going to find her name in this acknowledgement, and for being a real good friend.

Further, I want to thank Christina DRIMMEL and Marvin T. MILES for their nice support in the final days of completing this work.

Additionally, I want to give credit to all of my friends that I know from my time consuming sport, as they are a spring of happiness and joy, and thus, make my life better and easier.

I cannot even describe how deeply grateful I am to have found inspiration, happiness and relaxation through the intelligent and understanding woman, Silvia HEISS, who turned out to be my girlfriend and brought me back on track to finish my studies. I am curious where the future will take us. Thank you!

Last, but always first, I say thank you to my family. Without you, I would be nothing. You made me the person I am. You supported me in every way to reach this point in my life and I can only hope that you know how important you are to me and will always be.

Index of contents

1 Introduction

The plasma membrane

Membranes are crucial in regulating cellular function. The plasma membrane isolates the cytosol from the extracellular space and other membranes surround all the intracellular organelles and are, therefore, responsible for the maintenance of the typical differences between the contents of each organelle and the cytosol. The plasma membrane is even more crucial, because it shields the whole interior of the cell, thus the cytosol and all underlying membranous structures, from the extracellular environment. Specialized membrane proteins, no matter if found in the plasma membrane or any other intracellular compartment, help to fulfill a big range of different membrane functions. For example, there is the establishment of ion gradients [1]. These serve as the driving force for transportation of selected solutes across the membrane, for production of electrical signals, as in nerve and muscle cells, or for synthesis of ATP (for review see [2]), as in the mitochondria. Another function of membrane proteins is to serve as receptors [3], thus to gather, alter and transfer information by detection of extracellular signals, produced by other cells or the harboring organism as a whole, and then react with changes in cell behavior.

All biological membranes, so also the plasma membrane, show the same general structure. They are composed of a 5nm thin continuous double layer of lipid molecules, the most abundant being so-called phospholipids, held together mainly through noncovalent interactions, which build a fluidic structure that also harbors a big range of protein molecules (see Figure 1-10 A). The lipid double layer's main function is to serve as a barrier, as it is impermeable to most water soluble molecules [4].

Nearly all other tasks, like catalyzing membrane associated functions, as again ATP synthesis or membrane bound signaling or providing attachment points for the cytoskeleton [5], are fulfilled by proteins, whereupon one of the most important tasks is the transport across the membrane. In this case, membrane-spanning proteins are used to carry nutrients, metabolic waste products or small ions across the membrane. Ions are used to establish gradients, which are then again used as a driving force for motor-proteins or for co-transport of other substances mostly against their concentration gradients.

The plasma membrane further shelters glycoproteins and proteoglycans, both consisting of a protein part, as well as of one or more covalently O- or N-linked sugar chains [6], which get attached during so-called posttranslational modification. These molecules are responsible for diverse cellular functions, but their key role, together with glycolipids, is to form the so-called and cell type specific glycocalyx. Glycolipids exhibit a special class of lipids with sugars attached to their head groups. Glycocalices are exclusively located on the extracellular side of the plasma membrane and are not only found in all cells of epithelial origin, as in uroepithelial cells, but also in red blood cells, and often protect these cells from injury by toxic compounds and from invasion through microorganism [7], but some contributing molecules may also provide attachment sides for those [8].

1.1.1 Lipids

As noted before, phospholipid molecules, or simply phospholipids, are the major constituents of mammalian membranes besides cholesterol. Both, phospholipid- and cholesterol-synthesis are executed at the cytosolic leaflet of the endoplasmic reticulum (ER) by membrane bound enzymes, because all necessary metabolites are found in the cytosol [4]. Thus, all newly synthesized phospholipids would stay in the outer leaflet of the ER, if there was not scramblase, a lipid translocator, equilibrating phospholipids between the ER-leaflets (for review see [9]). From the ER, phospholipids bud off in double-layered vesicles and are transported to their target

membrane, where they fuse by SNARE-associated vesicle-membrane fusion [10]. This vesicle transport is mainly bound to the cytoskeleton. Along the microtubule network, vesicles connected to motor proteins [11], such as dyneins and kinesins, move to their target membrane. Every target membrane shows a distinct distribution of certain lipids between its inner and outer leaflet. As noted before, glycolipids, for example, are only located in the outer leaflet of the plasma membrane. Because lipids can only diffuse laterally in their according leaflet, they have either to be sorted before incorporation into their target membrane or need another lipid translocator. For the plasma membrane, this would be an enzyme called, flipase [4]. It was shown, that in artificial membranes, mostly lacking this enzyme, no flip-flop of phospholipids can be observed.

The main phospholipids are the phosphoglycerides. These show a general structure (see Figure 1-1), that consists of a three-carbon glycerol backbone, with two long-chain fatty acids, one normally harboring one or more cis-double bonds, connected through ester bonds to two adjacent carbon atoms of the glycerol. The third glycerol carbon is linked to a phosphate group, which is again bound to one of several different head groups [4]. Cis-double bonds produce unsaturated fatty acids, and further introduce kinks in these otherwise straight hydrocarbon molecules, which directly contribute to the membrane fluidity. Lipids that harbor unsaturated fatty acids cannot stay as close together as saturated lipids, and because the fatty acid tails are further more spread apart, membranes containing them are thinner (see Figure 1-2) [12].

By modulating the arrangement of head groups and fatty acids, mammalian cells can produce many different phosphoglycerides, but phosphatidylethanolamine, phosphatidylserine and phosphatidylcholine are the three main ones, in mammalian membranes. A fourth important phospholipid is sphingomyelin, which originates from sphingosine rather than glycerol. Sphingosine consists of a long acyl chain, with one amino group in between two hydroxyl groups, at one end of the molecule. This structure gets altered in sphingomyelin by attachment of a fatty acid to the

amino group and a phosphocholine group to the terminal hydroxyl group (for review see [13]). This leaves a free hydroxyl group to form hydrogen bonds to either the head group of an adjacent protein, a neighboring lipid or surrounding water molecules or a small drug or dye molecule. Sphingomyelin and the three glycerol derived phospholipids contribute up to nearly 50% of the total mass of mammalian membranes.

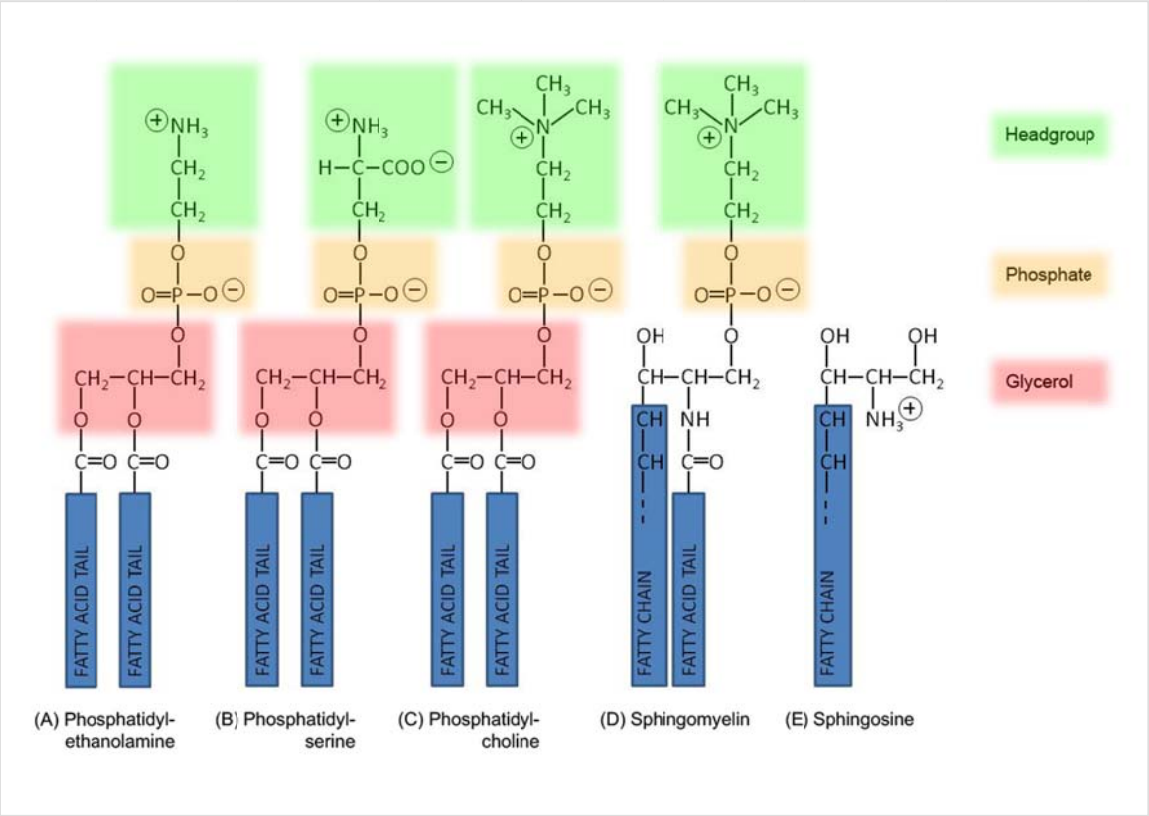

Figure 1-1: The four major phospholipids in mammalian cell membranes.
The lipids shown in (A-C) are phosphoglycerides, derived from glycerol, whereas the lipid shown in (D) is a sphingolipid, derived from sphingosine (E). Note the free OH-group on the backbone of sphingomyelin (D), which is capable of forming H-bonds to other molecules. Highlighted in green are the different head groups of the phospholipids, which actually determine the differences between (A-C), and in case of (B) give a net negative charge. Highlighted in yellow is the phosphate group, typical for all phospholipids, and shown in red is the glycerol backbone, if present in the lipid. (Modified from [14])

1.1.2 Cholesterol

Cholesterol is a sterol, consisting of a rigid ring structure connected to a short hydrocarbon chain and a single polar hydroxyl group on the other end of the molecule. Thus, cholesterol molecules automatically position themselves in a lipid bilayer, in a structure dependent manner. The hydroxyl group is always located close to the polar head groups of adjacent phospholipids. Hence, cholesterol modulates membrane properties by interacting and thus, immobilizing the hydrocarbon region closest to the polar head groups of the phospholipids (see Figure 1-10) [14]. This is achieved through noncovalent interaction of its rigid, plate-like steroid rings, with the nearby hydrocarbon groups, which prevents rotation around C-C bonds. So, it makes the bilayer more rigid, by packing unsaturated lipids closer together, and enhances its barrier function to small water soluble molecules. In contrast, and very interestingly, it does not alter the fluidity of the bilayer itself, it seems to be the main regulator of membrane fluidity in mammalian cells, where it is found in high concentrations and even prevents fatty acids from crystallizing.

The mammalian plasma membrane shows many cholesterol-, sphingolipid- and sphingomyelin-enriched membrane domains [15], so-called lipid rafts, which are thicker than other parts of the plasma membrane, due to the longer hydrocarbon chains of the saturated fatty acids (see Figure 1-2). Lipid rafts show a reduced water permeability, but higher proton permeability, compared to other membrane regions [16]. The activity of several membrane proteins is dependent on association with lipid rafts, as it is the case for clathrin-independent endocytosis [6].

Because cholesterol is the main constituent of lipid rafts their function can be altered, and thus studied, with pharmacological substances that deplete membrane cholesterol, as for example β-cyclodextrin and its derivates [6], [17], [18]. Overall cholesterol is found in huge amounts, in the plasma membrane of eukaryotic cells. There possibly exists one cholesterol molecule beside each phospholipid.

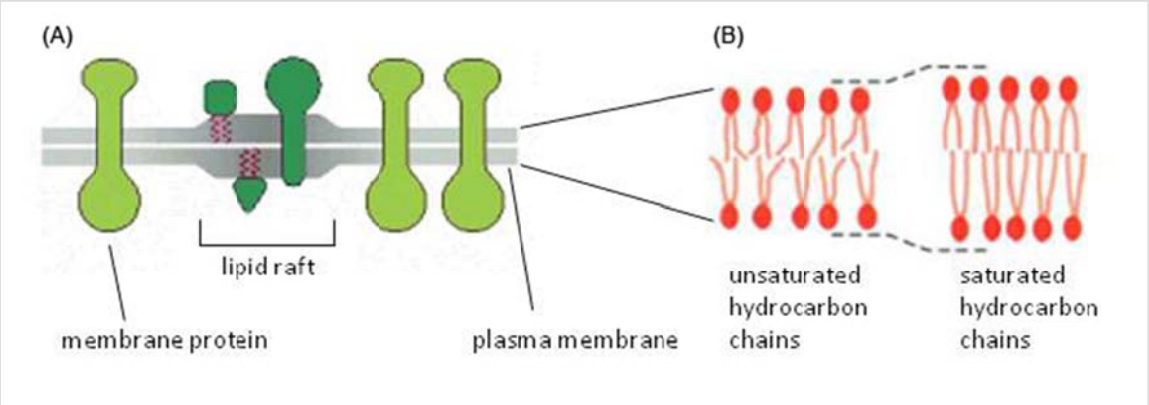

Figure 1-2: Lipid rafts and membrane composition.
(A) Schematic drawing of a lipid raft. Because of their increased thickness and their different lipid composition, rafts are thought to concentrate a variety of special membrane proteins (dark green) as they are the location of clathrin-dependent endocytosis.
(B) The influence of cis-double bonds in hydrocarbon chains. The double bonds produce kinks, which makes it more difficult to pack the two hydrocarbon chains together, and thus making the lipid bilayer more difficult to freeze. Further, because the hydrocarbon chains of unsaturated lipids are more spread apart, lipid bilayers containing them are thinner than bilayers formed only from saturated lipids (like lipid rafts). (A and B modified from [19])

De novo cholesterol synthesis involves many steps and occurs in the cytoplasm as well as at the ER, mainly in the liver, in the intestines, and is turned off when blood cholesterol levels are high [20]. Because it is only slightly water soluble, cholesterol gets stored and further transported in either lipid droplets or lipoprotein particles, such as chylomicrons, very-low-density lipoprotein (VLDL), intermediate-density lipoprotein (IDL), low-density lipoprotein (LDL) and high-density lipoprotein (HDL). The higher the cholesterol fraction and thus, the lower the protein fraction is, the less dense the particle is. The group of lipoprotein particles is necessary for clearance and transportation of free blood cholesterol taken in from food and they carry cholesterol molecules either in their alcoholic state or as fatty acyl esters, also known as cholesterol esters. Whereas HDL particles are responsible for reverse cholesterol transport, from tissue to the liver, the other lipoprotein particles transport cholesterol towards certain tissues. This is achieved through different apolipoprotein cell-targeting signals on the surface of each particle type. Lipoprotein particles are the subject of extensive research, as the understanding of choles-

terol metabolism is crucial for the development of therapies to some cholesterol-bound diseases in man [21].

1.1.3 Membrane transport

Membrane transport is necessary for cells to maintain differences in solute concentrations between the cytosol and the extracellular fluid, as well as between organelles and the cytosol. This is due to the hydrophobic interior of membranes, which makes them impermeable for most polar molecules. The smaller and the more hydrophobic a molecule is [16], the more easily it will pass through membranes. However, to carry inorganic ions, small water-soluble molecules and even large particles, such as sugars, amino acids or nucleotides across their membranes, cells express a high number of transport proteins on their cell surface. Up to 30 percent of all membrane proteins might function in transport processes and some cells allow nearly two-thirds of their energy to be utilized for this purpose.

Mainly, there are two classes of transport proteins. First of all, transporters, which constitute a class of proteins which undergo conformational changes to transport distinct molecules across membranes. And second channels, which form hydrophilic pores that facilitate passive transmembrane transport, always in direction of the electrochemical gradient of the transported molecule [22].

Transporters can be divided into two subsets, those using the electrochemical gradient of the transported molecule or thereby co-transporting a second molecule and those which are in need of an energy source, such as ATP, to fulfill their transportation task [22], [1]. Thus, it can be said, that channels and many transporters allow transport “downhill” only, a process referred to as passive transport, and only some transporters are capable of transporting molecules against their electrochemical gradient in need of energy, which is then so-called active transport. However, each transport protein is specialized in transporting only a particular class of mole-

cules across a membrane, which is why cells need so many of these proteins to supply all their needs.

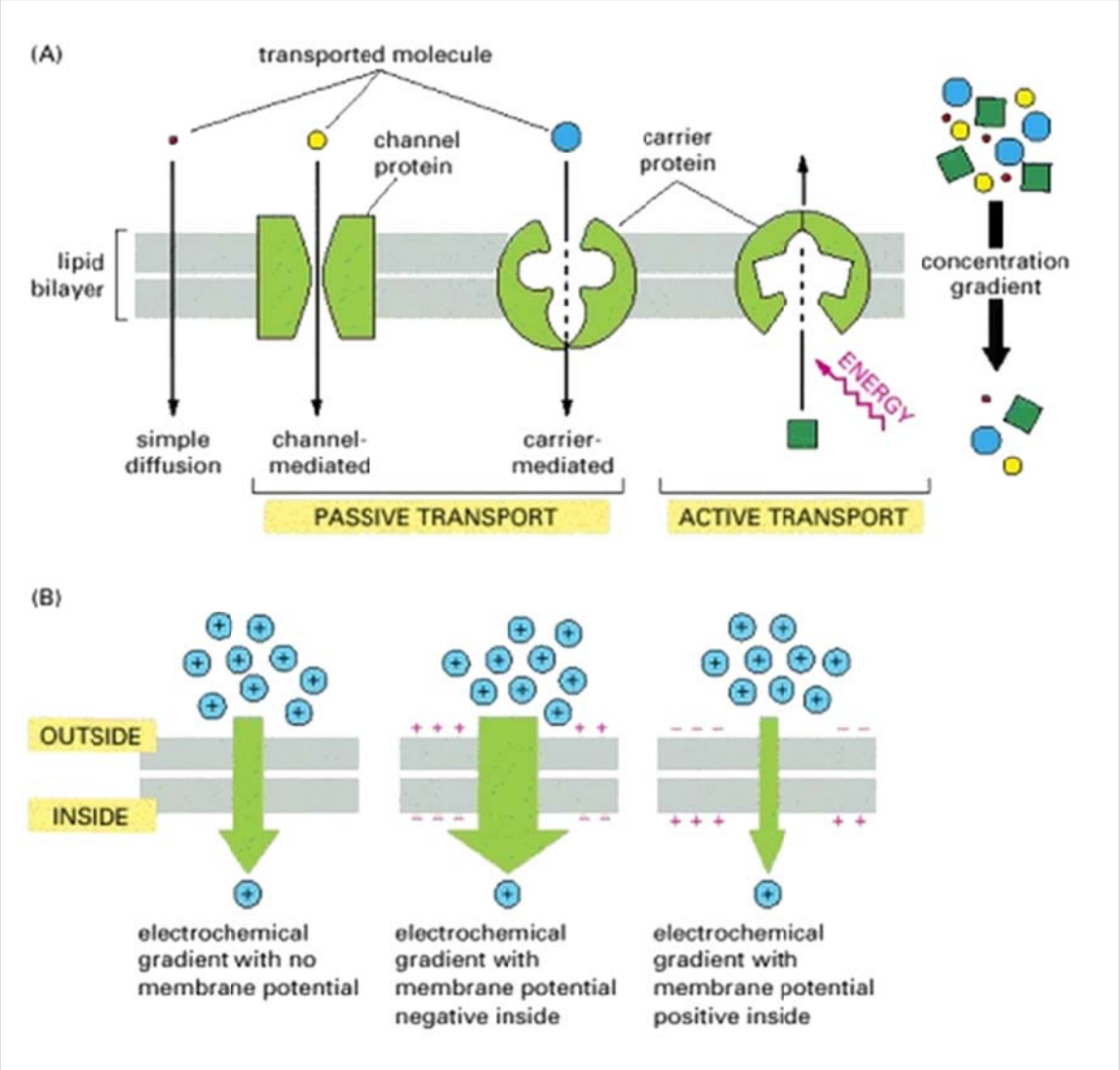

Figure 1-3: Passive and active transport.
(A) Passive transport down an electrochemical gradient is a spontaneous process, which happens simply by diffusion through the bilayer or by facilitated diffusion trough channels or by passive carrier proteins. These proteins undergo conformational changes and are the class of proteins that are also used for active transport of molecules. In contrast, active transport uses metabolic energy to pump the molecule against its electrochemical gradient.
(B) Electrochemical gradients combine membrane potentials and concentration gradients, in either a summative (middle) or subtractive way (right).

For the study of uptake mechanisms inhibition of active transport is of high importance. This can either be achieved on a molecular level for a specific transport protein or for the entity of active transporters.

Organelles

A fundamental feature of eukaryotic cells is that they are not only filled with cytoplasm, but also harbor a nucleus and different membrane-bound organelles, which fulfill a variety of different functions. The most important of these are the ER, the Golgi apparatus, mitochondria, lysosomes, endosomes as well as peroxisomes and numerous so called lipoprotein particles. Eukaryotic cells orchestrate organelle functions, as they arrange their number to satisfy their needs and to execute the functions they have to fulfill in their specialized tissue. Further, organelles support, as it is the case for lipid and cholesterol trafficking [23], and influence each other [24]. Thus, it is highly possible that a plasma membrane staining compound may be delivered to nearly every other intracellular organelle.

1.1.4 Mitochondria

Mitochondria are the most important intracellular organelles, as their main function is the oxidative degradation of nutrients for the production of energy. They are seen as very specialized organelles because they consist of a double membrane system, with an outer membrane and a highly folded inner membrane. This is probably due to incorporation by membranous engulfment of an aerobic prokaryote by a primitive anaerobic eukaryotic cell, to ensure survival in an oxygen-rich environment. Mitochondria indeed show many similarities to free-living prokaryotes, as they are of the same size, have a small genome, can synthesize proteins and divide into two for reproduction. The specialized double membrane system creates an intermembrane space, between the inner and the outer membrane, and the matrix space, within the inner membrane. The mitochondrial genome encodes only a

few proteins, mainly found in the inner membrane, whereas the majority of mitochondrial membrane proteins is synthesized from transcripts of nuclear genes and needs later translocation, driven through ATP hydrolysis, into the mitochondrial membranes. As mitochondria can occupy up to 25% of the volume of a single cell, they are leading recipients of membrane proteins and lipids in a typical eukaryotic cell [25].

The double membrane system, together with the specialized setup of proteins, the electron transport chain, allows the establishment of an electrochemical proton gradient in the intermembrane space. This gradient then drives the production of ATP by the ATP-synthase. The whole process, of establishment and use of the electrochemical proton gradient is also known as oxidative phosphorylation (for review see [26]) and marks the importance of mitochondria to eukaryotic cells, together with the citric acid cycle that takes place in the matrix space of these unique organelles. Mitochondria further play a role in apoptosis, as disruption of their membranes leads to loss of cytochrom C from the electron transport chain, which than activates caspases. These enzymes are key players in apoptosis [27].

Concerning lipid biosynthesis, it has to be mentioned that beside some steps in phosphatidylethanolamine synthesis no lipid synthesis is carried out at the mitochondrial membrane system, they are, therefore, non-autonomous organelles. Mitochondrial lipids are mainly synthesized at the mitochondria associated membranes (MAMs) of the ER, which harbor lipid-synthesizing enzymes of high specific activity and when in close vicinity to mitochondria, directly transfer lipids to the organelles, avoiding vesicle mediated transfer. Lipid droplets are also thought to deliver lipids to Mitochondria [23].

Phosphatidylcholine is the most abundant phospholipid found in mitochondrial membranes, comprising around 40% of total phospholipids, followed by high amounts of phosphatidylethanolamine. Phosphatidylserine concentration is low, but this lipid is necessary for the production of phosphatidylethanolamine, as the

synthesizing enzyme, phosphatidylserine decarboxylase, is bound to the inner mitochondrial membrane. Mitochondria are devoid of sphingolipids, such as sphingomyelin, and glycolipids.

Cholesterol, on the other hand, is needed in mitochondria as the first step of steroid hormone synthesis, the conversion of cholesterol to pregnenolone, occurs at the outer mitochondrial membrane in steroidogenic mammalian cells. Unknown protein based mechanisms are involved in the import into mitochondria, as well as for the transfer between the inner and outer mitochondrial membrane. Although the inner membrane of mammalian cells is nearly devoid of cholesterol, this exchange might occur, especially at contact sites, between the two membranes [25].

1.1.5 Lysosomes

Lysosomes are membrane bound organelles, with an acidic lumen, filled with degradative acid hydrolase enzymes, such as phosphatases, nucleases, glycosidases, proteases, peptidases, sulfatases, and lipases that work at pH 4.5 [28]. They can be seen as a garbage disposal unit, as they are responsible for macromolecule breakdown and breakdown of all endocytic compounds taken up by cells from their extracellular environment.

Among proteases, cathepsins are the most understood hydrolases. These do not only digest proteins intralysosomal and, upon release from lysosomes, degrade the extracellular matrix, they are also thought to fulfill some functions in bone remodeling, antigen presentation and epidermal homeostasis as they are of importance to angiogenesis, cell death and cancer cell invasion [27].

Cathepsins are released to the cytosol following a process called lysosomal membrane permeabilization (LMP), which can be triggered by various factors, but also through high concentrations of sphingosine, an acid ceramidase generated metabolite of ceramide. Ceramide itself, which belongs to the group of sphingolipids, as

sphingomyelin, becomes degraded in lysosomes through incorporation and breakdown of intraendosomal membranes [27].

All major membrane lipids are degraded in the same way as sphingolipids, by lipases that only digest intralysosomal membranes, which were formed by the sorting of lipids in late endosomes as intraendosomal membranes, without harming the lysosomal limiting membrane. The lipases can also perform the corresponding back-reaction, thus offering a switch to regulate the intralysosomal concentration of lipid metabolites and thereby, triggering or avoiding LMP. As lysosomes take up cargo from endosomes, which are also thought to stay in contact with lipid droplets [23], they comprise a second source for lipids, for the lysosomal limiting membrane, beside membrane fusion between endosomes and lysosomes. Cholesterol gets removed from incorporated membranes in the stage of endosomes, thus intralysosomal membranes are nearly devoid of sterols [28].

Upon LMP, cathepsins are released to the cytosol, which then, among other factors such as reactive oxygen species, trigger the breakdown of mitochondrial membranes. This leads to the release of cytochrome C from the mitochondrial membranes, resulting in the activation of caspases, which are thought to be the main enzymatic activators in apoptosis. Cathepsins can also trigger apoptosis by themselves, in a mitochondria independent manner. This observation makes lysosomes highly interesting in the treatment of cancer, because cancer cells, which normally prevent all major apoptotic mechanisms, are still sensitive to apoptosis through lysosomal breakdown [27].

1.1.6 Lipid droplets and lipoprotein particles

Lipid droplets, also known as lipid bodies, are increasingly recognized as dynamic and multifunctional organelles in different cell systems and organisms. Originally found in adipocytes, they were long considered to be a storage-organelle for lipids, but nothing else. They consist of a hydrophobic core, made of neutral lipids, tri-

acylglycerides and cholesterol esters. This core is surrounded by a monolayer of polar lipids and core-anchored proteins [29]. Recent studies propose a formation model of lipid droplets, which indicates that they bud off the endoplasmic reticulum after neutral lipids, produced in the ER itself, get deposited into the ER membrane, where they form a three-dimensional droplet [30].

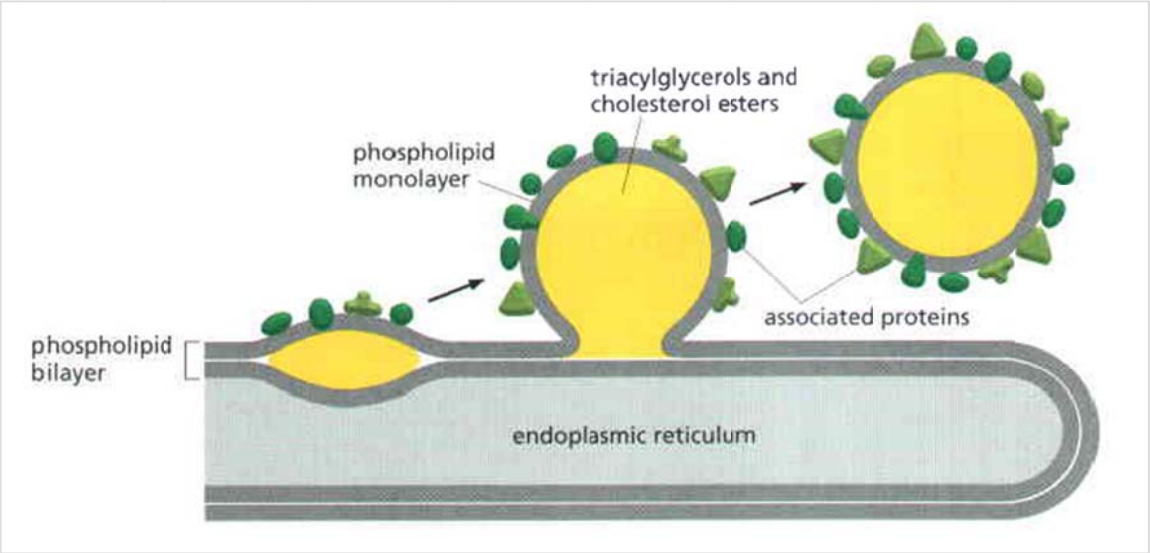

Figure 1-4: A model for the formation of lipid droplets.
Neutral lipids are deposited between the two monolayers of the ER membrane. There, they aggregate into a 3-dimensional droplet, which buds and pinches off the ER membrane as a unique organelle, surrounded by a single monolayer of phospholipids and associated proteins. (Taken from [19])

Meanwhile, they are considered as discrete organelles, with some really important functions in lipid-metabolism, as well as in steroid hormone synthesis [31], and they have a strong similarity to lipoprotein particles, such as VLDL, IDL, LDL and HDL. Further, they are more and more recognised as key-players in inflammation and cancer [32].

While the occurrence and functions of lipid droplets in cancer cells are largely unknown, a large number of cancer cells show lipid bodies as a common feature. Thus, lipid bodies may function as collecting- and storage-organelles for lipids and cholesterol esters, thereby being an energy reservoir and a supplier for synthesis of charged lipids, and for the synthesis of steroid hormones and prostaglandins. All

these proposed functions seem to, obviously, support cancer cells, taking into consideration that one of their striking problems is the acquisition of nutrients and causing influence on the adjacent tissue. The surface of lipid bodies, in cancer cells, was shown to be enriched with the protein ADRP (Adipophilin) [33], which is in agreement with previous demonstrations that ADRP is the main surface protein of lipid bodies in different mammalian cells, including epithelial cells.

Lipid droplets are prescribed to localize close to the nucleus and the ER, these being the starting points for lipid- and hormone synthesis. Imaging of droplets, in living cells, often shows them as relatively immobile organelles that move rapidly within small areas, although directed movement along the microtubules is observed, too. Dyneins are thought to be the motor proteins responsible for this motion. Beside these common motor proteins, droplets are thought to comprise another, frequently used, cellular machinery. For the fusion process they take advantage of the SNARE molecules, which are normally found on transport vesicles [10]. The difference between droplets and normal vesicles is, obviously, the membrane composition, droplets bearing only a monolayer, whereas lipid bilayers are found on vesicles. Thus, the melting of the outer leaflets on vesicle fusion is comparable to the whole droplet-fusion-process. Fusion events are observed and confirmed. Lipid droplets do not only fuse with themselves, but also with other organelles, such as peroxisomes, lysosomes, and mitochondria [23], [34].

Uroepithelium and bladder cancer

1.1.7 Normal Uroepithelium

Uroepithelium is a multilayered epithelial tissue, classified as a transitional epithelium, consisting of 3-6 layers of 3 distinct cell types. One layer of big luminal, superficial, squamoid cells, or so-called umbrella cells [35], is followed by underlying multiple layers of medium sized intermediate cells, again followed by one layer of

small basal cells, sitting on the lamina propria [36]. All layers are commonly connected through interdigitations of cytoplasmic processes and by desmosomes, between adjacent cells of the same and neighboring cell layers. Concerning the uroepithelium itself, an increase in the complexity of morphology and differentiation can be observed from base to surface [37].

The luminal surface of the typical umbrella cell shows a very specialized plasma membrane, with many invaginations, and below the membrane one can see many vesicles. The outer and the inner leaflet of the plasma membrane are different. Depending on the degree of distension these vesicles start to disappear, because they fuse with the plasma membrane to extend the surface of the umbrella cell. Superficial cells are densely coated with a layer of glycosaminoglycan (GAG), consisting of glycoproteins and proteoglycans [35], and concerning morphology, the cell differs between a cuboidal and a stretched form [38], also depending on the degree of distension, with the long axis parallel to the lamina propria. Numerous, fine cytoplasmatic filaments are found in these cells, which are either lined up parallel or in a criss-cross pattern and are thought to be of the intermediate type. Further, tight junctions were observed on the lateral edges of these cells [37], as the apical plasma membrane shows interdigitations, which might function as a zipper for sealing the luminal surface of the uroepithelium [38]. These features cannot be observed in the layers of intermediate or basal cells. Additionally, desmosomes connect these cells to the underlying intermediate cells. Two (in 19% of cells) or more (in 3% of cells) nuclei are sometimes found in these cells [37], [36]. Thus, multinucleation should not be seen as criteria for malignancy, which makes it very hard to distinguish between normal and aberrant uroepithelium. Nuclei are circular and chromatin was found to be fine-structured, compared to the other two cell types, an indication for higher transcriptional activity, and thus, a high rate of intracellular repair [36]. Bi- or trinucleate cells show a very small internuclear space, densely packed with organelles, such as Golgi membranes and associated vesicles, other coated vesicles, mitochondria and thin filaments. Mitochondria are

found in high numbers, in the apical region of superficial cells, as well as a very high number of lysosomes, of different sizes ranging from normal to very big. This makes sense, taking into account that these cells are constantly in production of new proteins and other cellular products, which is energy consuming, as well as in need of replacement of parts of the luminal membrane and thereby, digestion of cellular material. These two organelles may, thus, contribute to a large part, together with the high rate of intracellular repair, to the longevity of urothelial cells [38].

Intermediate cells appear, apparently, smaller than the umbrella cells and contribute the biggest amount of cells to the uroepithelium. They are connected to each other through desmosomes and the cytoplasm of these cells shows a unique feature, not found very often in eukaryotic cells, namely vacuolization. This might help the cells to compensate pressure alterations caused by the filling of the urinary bladder. Intermediate cells constitute 1 to 4 layers of cells to the uroepithelium and a small number is attached to the lamina propria [37]. Many indentations can be found on the cell nuclei, and nucleoli, as well as nuclear bodies are similar, but not the same, to those of basal cells, thus indicating a lower rate of transcriptional activity compared to the umbrella cells. Close to the surface layer intermediate cells resemble superficial cells, by showing less indented nuclei and a higher number of lysosomes. The number of lysosomes seems to decrease from surface to base in uroepithelium. Mitochondria are found in clusters, in cells subjacent to surface cells and are mainly located in the apical region. Also, lipid inclusions can be seen in these cells [37].

The underlying basal cells are tightly bound to the lamina propria and make up the smallest portion of the uroepithelium concerning the total cell volume. In cross-sections they look nearly cubic. A big part of the cytoplasm of these cells is occupied by the nucleus, showing a typical indented morphology, with densely packed chromatin, showing only few nucleoli and nuclear bodies, and thereby, nearly no transcriptional activity. Golgi membranes and rough endoplasmic reticulum are ra-

re. Mitochondria are clustered and found in small numbers compared to intermediate and superficial cells [37]. No unusual amounts of lysosomes can be observed.

1.1.8 Bladder cancer

Bladder cancer, or urothelial carcinoma, is the fifth most common malignancy in Europe. In most cases, conventional urothelial carcinoma accounts for carcinoma of the urothelial tract lining, but because the urinary bladder is in close proximity to the urethra, which is lined by stratified epithelium, as it is to the prostate gland in males, there is big potential for enormous plasticity and divergent differentiation in neoplastic urothelium [39]. Further, the urothelium is constantly in contact with sometimes harmful substances, as it is in physical stress due to filling and voiding of the bladder. And because the urothelium has many similarities to normal epithelium, it shows epithelial-like behavior concerning the formation of neoplastic lesions. Thus, it is not astonishing that one can see many differences in the morphology of urothelial cells, even in a healthy urothelium, because it is reacting to environmental changes [40]. Thus, some of the urothelial carcinoma, such as nested, microcystic and inverted variants can be mistaken as benign tumors or reactive urothelial processes. In contrast, other variants, such as the micropapillary, discohesive and plasmacytoid variant, mimic metastatic tumors from other sites. Furthermore, divergent differentiation is found with squamous carcinoma, which is definitely derived from stratified endothelium, as with glandular, sarcomatoid or lymphoepithelioma-like carcinoma. In many cases bladder cancer is not only limited to one variant, but patients show mix-types of different variants.

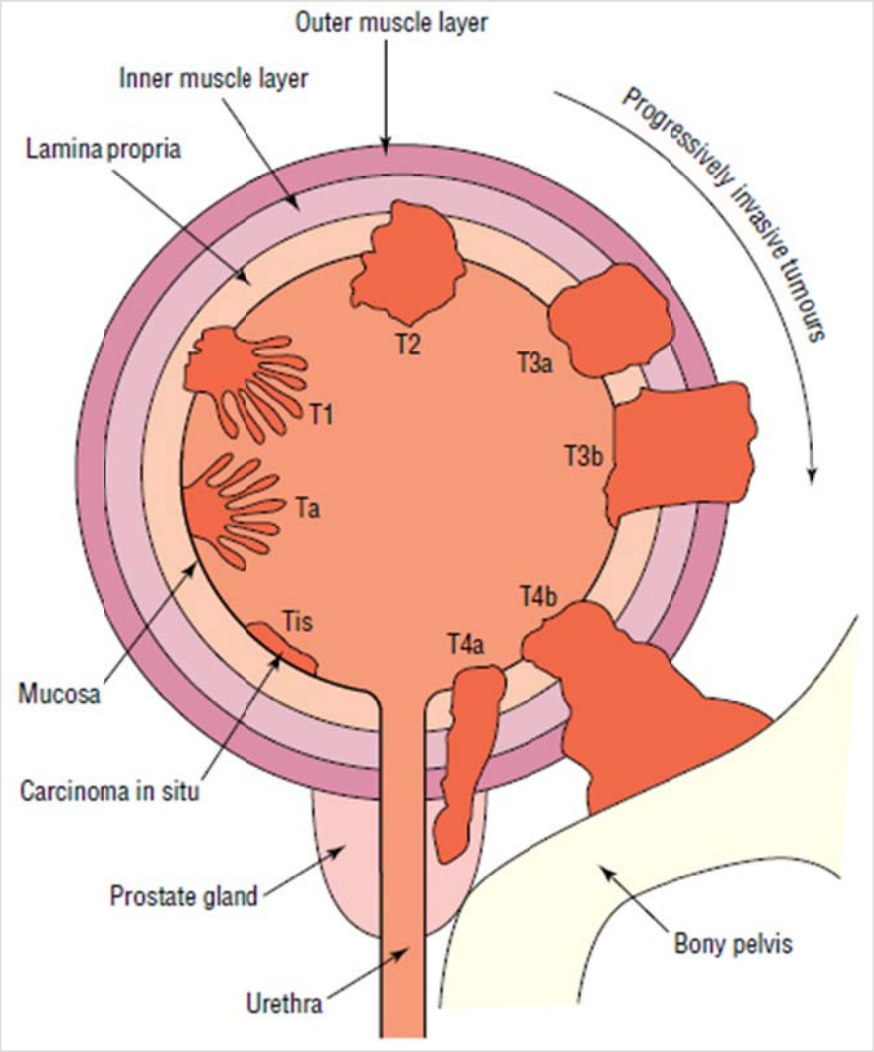

Figure 1-5 Tumor staging in bladder cancer according to the TNM system of 1997.
A tumor that is only found on the mucosa and lies flat is Tis (a carcinoma in situ) and a papillary lesion that is also limited to the mucosa is Ta. As soon as it penetrates the lamina propria, but not the muscle layer, a tumor is T1. When the tumor invades muscle it is staged from T2 to T4, according to the depth of infiltration of muscle tissue and other surrounding tissue. Tumors that invade the bladder muscle are highly malignant and often harbor a high potential for metastasis. (Taken from [41])

As voided urine is normally taken for diagnostic purposes, it is of high interest to find methods to distinguish between all cell types found in this body fluid and to sort out circulating tumor cells (CTCs) [42]. As, for example, high malign bladder cancer cells look similar to stratified epithelial cells from the urethra, concerning size and shape of the cell-body, but not the nucleus, microscopic detection without any markers is a time consuming task, which further needs experienced investiga-

tors and cannot be done automatically. Further, lots of red and white blood cells, as well as macrophages, can be found in the urine, especially in samples derived from cancer positive patients. These also need to be distinguished from potential bladder cancer cells or removed from urine prior to diagnosis. Overall, this implicates the potential of many false positive diagnosed samples.

Origin	Variant	Markers
Urothelial carcinoma (infiltrating)	Usual type (conventional) invasive urothelial carcinoma	CK7 with or without CK20, p63, 34βE12, CK5/6, thrombomodulin and uroplakin3
	Inverted urothelial papilloma	Ki67, p53 and CK20
	Tubular variant of urothelial carcinoma	CK7, CK20 and 34βE12 are positive. Prostate-specific antigen is negative.
	With squamous differentiation	
	With trophoblastic differentiation	
	Clear cell	
	Nested	
	Microcystic	
	Micropapillary	CK20 negative and oestrogen receptor positive, (TTF)-1 negative
	Lymphoepithelioma-like	Focal CK20 positive
	Lymphoma-like	
	Plasmacytoid	CD138 positive. Sometimes CK20. E-cadherin negative. Small intracytoplasmic mucin vacuoles are demonstrable in at least a proportion of tumour cells in both the plasmacytoid and discohesive variants.
	Sarcomatoid	
	Stromal giant cell	CD68, leucocyte common antigen, CD51 and CD54, CK negative
	Giant Cell	

Origin	Variant	Markers
	Lipid-cell variant	CK7 and CK20
	Undifferentiated	
Squamous neoplasms	Squamous cell carcinoma	
	Verrucous carcinoma	
Glandular neoplasms	Adenocarcinoma	
	Not otherwise specified	
	Enteric	
	Mucinous	
	Signet ring cell	
	Clear cell	
	Hepatoid	
	Mixed	
Neuroendocrine tumors	Small cell carcinoma	
	Carcinoid	
Miscellaneous	Metastatic tumors	

Table 1-1: Listing of different bladder cancer variants and their origin, together with molecular marker proteins, if described.

Still, there is a staging system for histological samples derived through cytoscopy or after tumor excision for conventional urothelial carcinoma (see Figure 1-5), as there is the ongoing trial of classifying all the variants (as shown in Table 1-1), which is not possible by means of histology or cytology of voided urine alone (for review see [41]). This might be possible, combined with the detection of molecular markers, or maybe by this method alone. Expression of cytokeratin 20 is common among many of the bladder cancer variants. Many differences concerning marker proteins have been found to date, in the different bladder cancer variants, which makes it possible, even though expensive, to distinguish some of the variants by the use of antibodies. But because not all of the markers are expressed on the cancer cells' surfaces, fixation is needed in many cases, which is time consuming. There is the need for more markers, maybe not only protein markers, but also morphological ones, which can be detected on living cells in the urine, without any

fixation procedures. Still then, the development of a diagnostic tool, which is fast, sensitive and specific is a very complex task.

1.1.9 Established human bladder cancer cell lines and murine fibroblasts

In this study, the 3 used human bladder cancer cell lines were named HTB2, HTB9 and HTB5. HTB9 cells were adherent tumorigenic epithelial cells derived from a benign transitional cell papilloma. HTB9 cells were adherent tumorigenic epithelial malign grade II carcinoma cells, and HTB5 cells were adherent malign grade IV carcinoma cells. Tumor malignancy staging was done with the old nomenclature, before change to the TNM system in the year 1997, since these cell lines have existed for over 30 years. Little is known about these cell lines, but HTB5 cells are described to show the presence of microvilli and lipid droplets, and to no longer be capable of forming desmosomes. L929 fibroblasts are derived from murine subcutaneous connective tissue and serve as a control cell line.

Cyclodextrins

Cylodextrins, also known as cycloamyloses or simply as CDs, are produced from starch by enzymatic conversion through cyclomaltodextrin glucanotransferase, CGTase, that was first discovered in bacillus macerans [43]. They were first discovered by Villiers in 1891, but were not extensively studied before the early 1950ies, long after Schardinger identified both, α- and β-cyclodextrin, between 1903 and 1911 [44]. Today they are used in many fields ranging from pharmacology to agricultural-, to the food industry. The most often used cyclodextrins in biochemical and pharmaceutical applications are cyclic oligosaccharides, consisting of six to eight dextrose units (α-, β- and γ-cyclodextrins, respectively) connected by 1 -> 4 gycosidic linkages. These are the natural or so-called “parent cyclodextrins” (see Figure 1-6 A and B) [45].

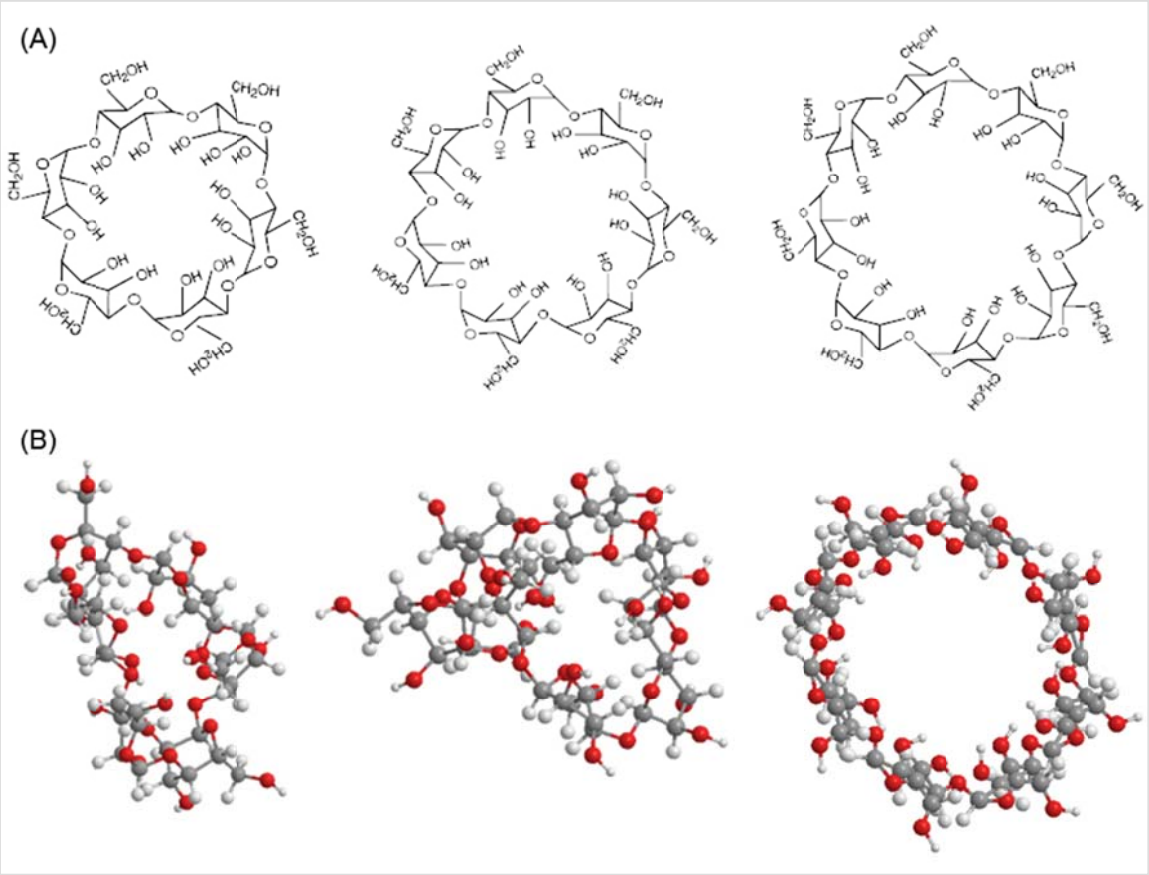

Figure 1-6: Parent or natural CDs.
(A) Parent CDs, namely α-, β- and γ-cyclodextrin (from left to right), represented by formulas.
(B) Parent CDs, namely α-, β- and γ-cyclodextrin (from left to right), represented by ball stick models. (A, modified from [46]; B, courtesy of Ao. Univ. Prof. Dr. Karl Peter Wolschann).

Cyclodextrins show a blunted torus structure [47], a hydrophilic outer surface and a hydrophobic inner cavity [48] and are able to form inclusion complexes, with apolar organic guest molecules, by including those molecules or parts of them in their inner hydrophobic cavity. They are, thus, widely used as drug-carriers for often poorly water-soluble substances, with the side effect of often enhancing their bioavailability and stability [49].

The parent cyclodextrins do not only vary in the number of glucose-molecules, they also show morphologically different torus structures. Ball stick models (see Figure 1-6 A) show the differences in cavity-size and shape [46]. γ-cyclodextrin offers the

best accessible cavity [50], whereas β-cyclodextrin is more stable, because secondary hydroxyl groups on the wider rim of the torus (whereas primary hydroxyl groups are located on the narrow rim of the torus) form H-bonds [47]. This results in a reduced hydrophilic exterior surface, thus reducing its water-solubility [47], but thereby increasing the affinity of complexed guest molecules for biological membranes [49].

Regarding encased molecules, it has to be mentioned that they have to fit exactly, concerning size and shape, into the central hydrophobic cavity of the chosen cyclodextrin molecule [48]. Furthermore, the enclosed molecule is insulated from the surrounding, as it is protected from UV-light, heat and oxygen [51].

Cyclodextrins can, therefore, be used as alternative solvents to overcome some of the formulation and delivery problems of otherwise problematic drugs. For example, solvents, for hydrophobic drugs, such as dimethylsufoxide (DMSO), polyethylene glycol, propylene glycol, ethanol, etc. might increase solubility when mixed with water, but most often they do this in a nonlinear fashion. Thus, a drug may be well soluble in one of these pure solvents, but once the drug-solvent mixture is diluted in water, the once poorly water-soluble drug normally precipitates in big amounts. This does not happen when cyclodextrins are used for drug complexation [45].

Concerning preservation of formed complexes, cyclodextrins offer numerous methods, of which a very useful one is the lyophilization method, which results in the production of a long lasting water-soluble powder [52].

The most important feature of cyclodextrins is their capability of facilitating the uptake of the encased molecule into the plasma membrane of living cells, simply by obviating the hydration of the complexed drug, when switching from the cyclodextrin into the membrane, while dilution seems to be the main driving force for drug release [45] and the proximity of the inclusion complex to the membrane alleviates

the drugs' uptake. A model for the mode of penetration enhancement of biological membranes by cyclodextrins, is given in Figure 1-7.

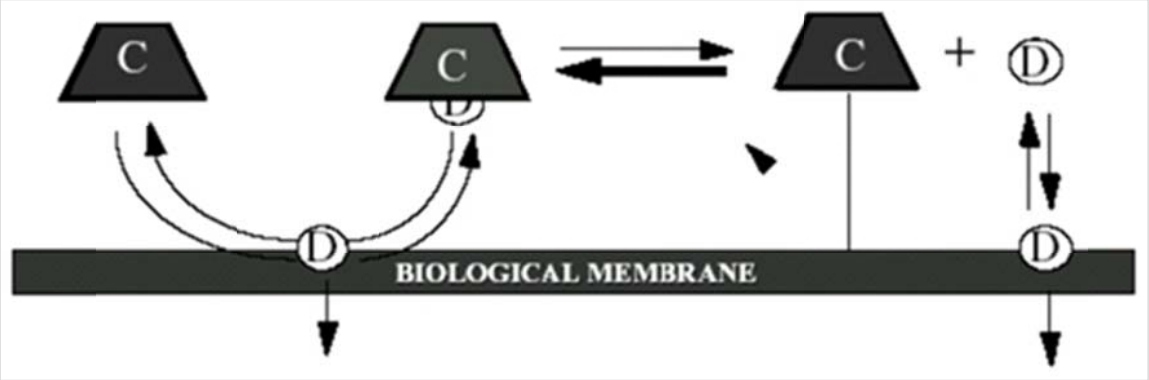

Figure 1-7: Model for the mode of penetration enhancement by cyclodextrins.
Abbreviations: C, cyclodextrin-molecule and D, drug. (Taken from [48])

However, cyclodextrins should not be seen as the "weapon of choice" when hydrophobic compounds need to be delivered to biological membranes, which always exist in hydrophilic environments. Besides, delivering drugs safely and with only a few side effects, they have a major weakness. Only molecules with the right size, shape and solubility can be complexed, which are the main limitations in the use of cyclodextrins. Further, α- and β-cyclodextrin [53], and especially the derivate methyl-β-cyclodextrin [54] are known to disrupt membranes, as β-cyclodextrin and its methylated derivate are capable of depleting membranous cholesterol. In addition, they seem to be renally toxic at high doses, when applied on mammalians. Still, they are a very strong and useful instrument and have been used extensively over the last 60 years, in the pharmaceutical field [45], and can normally be used at non toxic concentrations.

Coumarin 6

Natural coumarin, 1-benzopyran-2-one, is a chemical compound found in many plants, especially the tonka-bean [55], which brought about the name of the com-

pound, the french word for tonka-bean being coumarou. It is produced in plants by hydroxylation, glycolysis and cyclization of cinnamic acid [56].

It is the basic structure for many other naturally appearing compounds, which show a wide range of interesting and diverse physiological activities. There are more than a thousand derivates, ranging from simple coumarins containing hydroxyl- or alkyl side chains to complex coumarins with furanoyl, benzoyl, pyranoyl or alkylphosphorothionyl substituents [57].

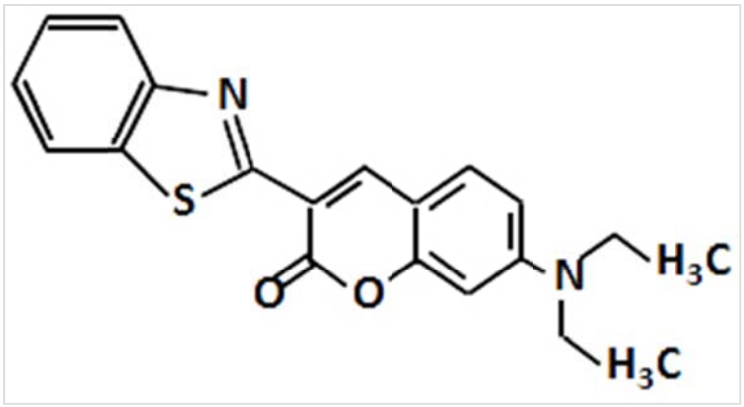

Figure 1-8: Chemical structure of Coumarin 6, or 3-(2-benzothiazolyl)-7-(diethylamino)-coumarin

Coumarin 6, or 3-(2-benzothiazolyl)-7-(diethylamino)-coumarin, or simply C6, is a member of the 7-aminocoumarins, with a molecular weight of 350 Da. It consists of a probably conjugated double-bond 4-ring structure, with delocalized electrons and an amino group in the 7th position, thus making it a very efficient fluorescent compound, and is also used as a laser dye [58]. Existence of a rotational axis in between the first and the second two ring-structures is possible, even probable. The structure of coumarin 6 can be seen in Figure 1-8. Excitation of coumarin 6, at 488nm, leads to fluorescence emission between 500nm and 520nm, dependent on the solvent.

When dissolved in different organic solvents, such as dimyristoylphosphatidylcholine (DMPC), ethanol, tetrahydrofuran (THF) or isooctane, one can see (Figure 1-9 A), that the fluorescence intensity of coumarin 6 is not altered, but that there is

a slight left shift to shorter wavelengths of the fluorescence emission compared to the wavelength, when dissolved in water. Dissolution in isooctane, as an example for a non-polar hydrocarbon solvent, induced two vibrational bands, with peaks at 457.5 nm and 489 nm [59]. It has to be mentioned, that coumarin 6 is poorly water-soluble, thus favoring organic solvents [60], [58], which generally lead to shorter wavelengths regarding fluorescence emission, than more polar compounds.

It is responsible for the sweet scent of newly mown hay, as it is known to be a bitter-tasting appetite suppressant, which is probably produced by plants, as a chemical defense against plant eating animals. Having no anticoagulant activity by itself, it can be transformed into the anticoagulant dicumarol [61]. Dicumarol, first discovered in 1939, was the starting point for the development of many other anticoagulant drugs as, for example, warfarin and its metabolites [62].

In addition, coumarin 6 meets the assumptions for complexation with cyclodextrins, being a mainly hydrophobic [63], which, still, weakly dissolves in water, and stretched rod-like molecule [59], [64], [58], compared to other coumarins. Thus, it can either be complexed by β- or γ-cyclodextrin; β-cyclodextrin being the better complex forming cyclodextrin (data not published). For these reasons and after measuring several other coumarins, dissolved in ethanol or in attempting to complex with β-cyclodextrin, via fluorometry (data not shown), it stood out as fluorescent, at the longest wavelength, compared to the other candidates, and the only one that could be complexed with cyclodextrins. Long wavelength fluorescence was important to excite the molecule on the lab-owned confocal, microscope and to measure the dynamics of complex formation between coumarin 6 and β-cyclodextrin by fluorescence correlation spectroscopy (FCS) [64].

When complexed with β-cyclodextrin, again a shift of the fluorescence of coumarin 6 can be observed (see Figure 1-9 B). Fluorescence emission values change for aqueous coumarin 6, from wavelengths at 520 nm to 500nm, when complexed with β-cyclodextrin in 10000-fold excess (data not published).

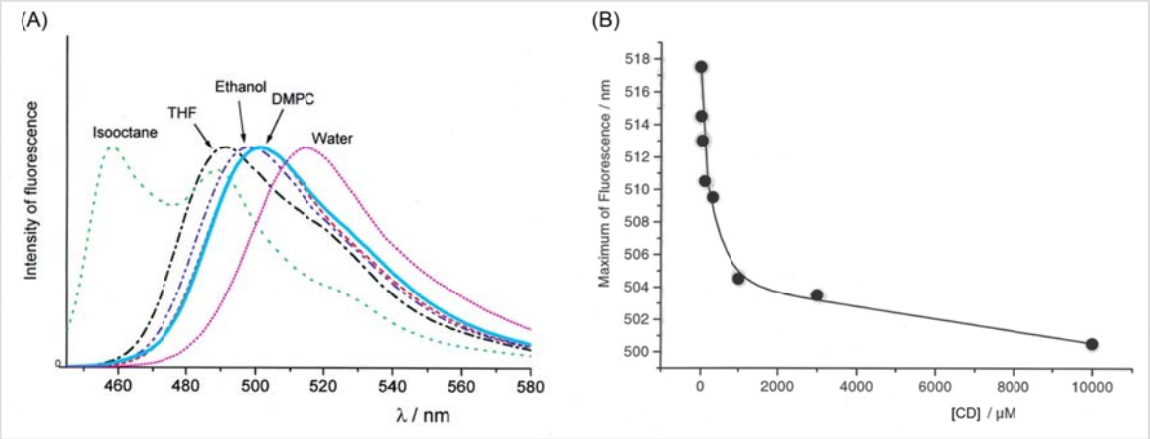

Figure 1-9: Shifts in fluorescence of C6, depending on solvents and on complexation with β-CD.
(A) Solvent shift of the C6 fluorescence measured via fluorometry. Fluorescence emissions of C6 shift to shorter wavelengths, when dissolved in dimyristoylphosphatidylcholine (DMPC), ethanol, tetrahydrofuran (THF) or isooctane, instead of water.
(B) Shift of the fluorescence of 10^{-8}M C6 with rise of the concentration of β-CD, measured via fluorometry. (A and B, courtesies of Dr. Martin Knapp)

Being aware of the fact that coumarin 6 molecules are mostly hydrophobic, the idea came up, that if they somehow come close to a plasma membrane, they will be incorporated into the hydrophobic region generated by the carbohydrate tails of the phospholipid molecules, but the polar parts of the molecules will also stick out of the hydrophobic region. Furthermore, the oxygen molecule sticking out of one of the four rings of coumarin 6 is capable of forming hydrogen bonds, with the free hydroxyl group, in the polar head region of sphingomyelin. Thus, coumarin 6 molecules may automatically position themselves at distinct regions in the plasma membrane and might compete for space with cholesterol molecules (see Figure 1-10 C).

Onkovidon®

Onkovidon®, is a new and patent registered green fluorescent dye [65], that consists of the two above described molecules (see Figure 1-10). Precisely, β-cyclodextrin forms an inclusion complex with coumarin 6.

As existence of other than 1:1 complexes was shown before [66], [67], it was not astonishing that ab initio calculations on the interaction proposed a model of one, two or three β-cyclodextrin molecules forming an inclusion complexes, with only one coumarin 6 molecule [64], depending on the absolute concentration of applied β-cyclodextrin and not the concentration of coumarin 6, that was kept constant at 30nM. Thus, complexes weigh between 1450 and 3650 Da, calculating 1100 Da for each β-cyclodextrin molecule and 350 Da for C6, as said before.

Distinct absolute concentrations of applied β-cyclodextrin demonstrated to be the key factor for forming percental higher amounts of one of the 3 possible complexes compared to the other two and free ethanolic coumarin 6, when measured by FCS. It can be seen (Figure 1-11 A), that at a concentration of 100µM β-cyclodextrin, 40% of the formed complexes are of a 1:1 stoichiometry, whereas only 20% are 1:2 and that there are still 40% of free ethanolic coumarin 6. At concentrations of 1mM β-cyclodextrin, 1:2 and 1:3 stoichiometries contribute to 43% each, compared to only 13% of 1:1 complexes being formed. The percentage of free coumarin 6 is already negligible at this β-cyclodextrin concentration. At 5mM β-cyclodextrin, mainly 1:3 complexes were found (80%), whereas only 18% of the formed complexes showed a 1:2 stoichiometry, and nearly no complexes of a 1:1 stoichiometry or free coumarin 6 could be observed [59].

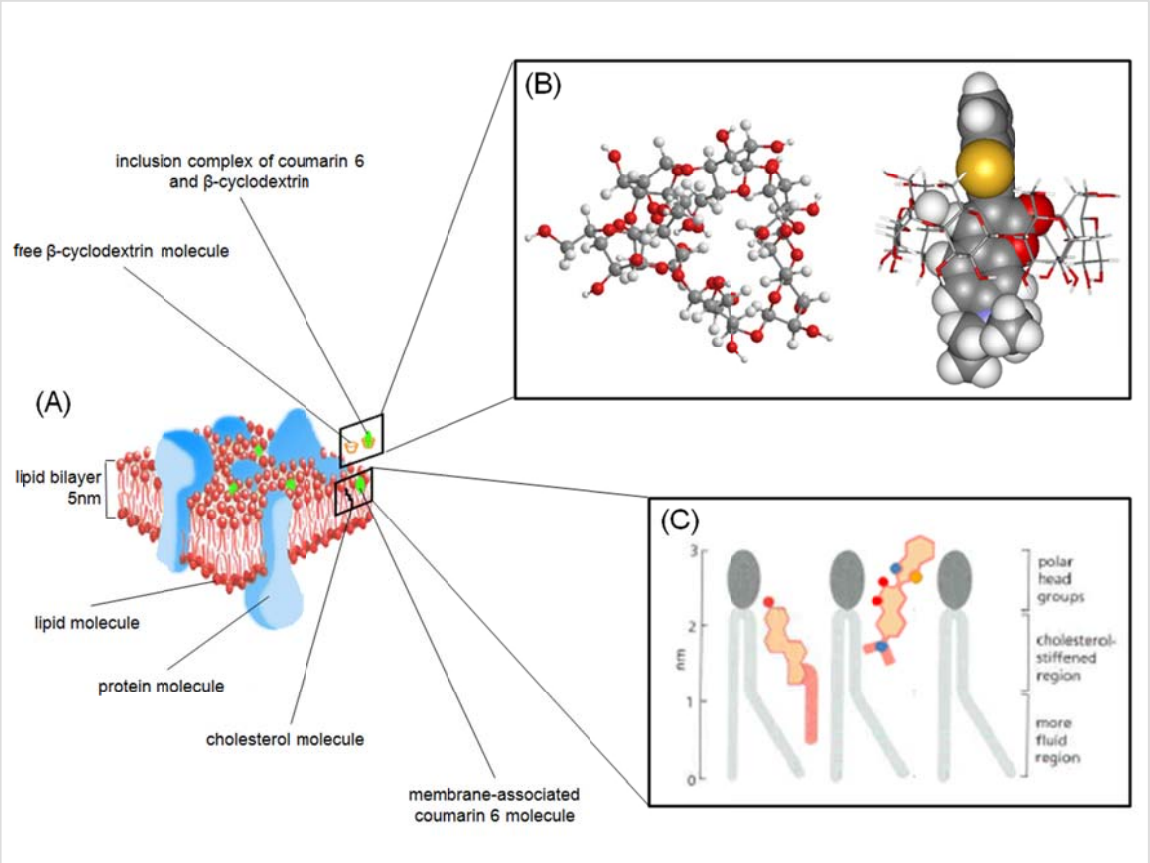

Figure 1-10: A schematic overview of the Onkovidon® dye, it's localization in the plasma membrane of living cells and possible competition with cholesterol.
Onkovidon® is a lipohilic dye, obtained through forming an inclusion complex between the basket-shaped sugar molecule β-cyclodextrin and a green fluorescent laser-dye molecule, named coumarin 6.

(A) A three-dimensional view of a lipid bilayer. Shown in the upper rectangle are, a free β-CD molecule, after delivery of the C6 molecule to the plasma membrane, as well as the inclusion complex between a β-CD molecule and a C6 molecule. The lower rectangle shows a cholesterol molecule and a C6 molecule located in the plasma membrane.

(B) β-CD, represented by a ball stick model (left). The inclusion complex between β-CD and C6, represented by a combined model of a stick model for the sugar molecule and a space filling model for the C6 molecule (right). Shown in this figure is the 1:1 complex due to reasons of simplification, although 1:2 and 1:3 complexes of C6 and β-CD do exist.

(C) Schematic drawing of a cholesterol molecule (left colored molecule) and a C6 molecule (right colored molecule) interacting with three mono-unsaturated phospholipid molecules in one monolayer of a lipid bilayer. It can be seen, that only one of both molecules can interact with the same two phospholipid molecules, because otherwise, they would compete for the hydrophobic region of the plasma membrane. Further, C6 may form a hydrogen bond to sphingomyelin. (A, modified from [19]; B, courtesies of Ao. Univ. Prof. Dr. Karl Peter Wolschann ; C, modified from [19]).

Ab initio calculations on the structures of the different complexes also reveal a possible rotation in the coumarin 6 molecule, around the C-C axis between the two double-ring structures (see Figure 1-11 B to E).

In this study, all experiments were performed using staining solutions of 30nM coumarin 6 and 100µM β-cyclodextrin, giving a ratio of 1:3333, between coumarin 6 and β-cyclodextrin and thus, leading to equally distributed 1:1 complexes of coumarin 6:β-CD and free coumarin6. When the majority of present complexes was 1:1, as found at this β-cyclodextrin concentration, we observed the best staining properties on live cells, whereas lower or higher concentrations of the sugar, which led to the before described ratios of complexes, resulted in rather bad staining properties [64].

But, as described before, coumarin 6 was first dissolved in absolute ethanol, which gave a clear and green fluorescent solution [64]. Before complexation attempts, the fluorescence intensity of ethanolic coumarin 6 was examined. Compared to the cyclodextrin-complexed form of coumarin 6, the observed fluorescence quantum yield was nearly identical [59].

However, when applied onto established cancer cell lines, we sighted that ethanolic coumarin 6 did not stain cells very well. This was most likely due to the inhibition of normal cellular function caused by membrane breakdown, that comes along with high concentrations of ethanol [64], and because the affinity of ethanolic coumarin 6, to the membrane, is low compared to the β-cyclodextrin-complexed form. When complexed with β-cyclodextrin, which was used at rather non-toxic concentrations [18] compared to the concentration of ethanol, the dye molecule stains plasma membranes, as proposed before for coumarin 6 molecules (see Figure 1-10). And when present in a majority of 1:1 complexes membrane staining seemed to follow the proposed model of penetration enhancement by cyclodextrins (see Figure 1-7).

Preservation of the formed complexes was achieved through lyophilization, as described above. The resulting powder was dissolved in water or 1 x PBS prior to every experiment, to gain staining solutions.

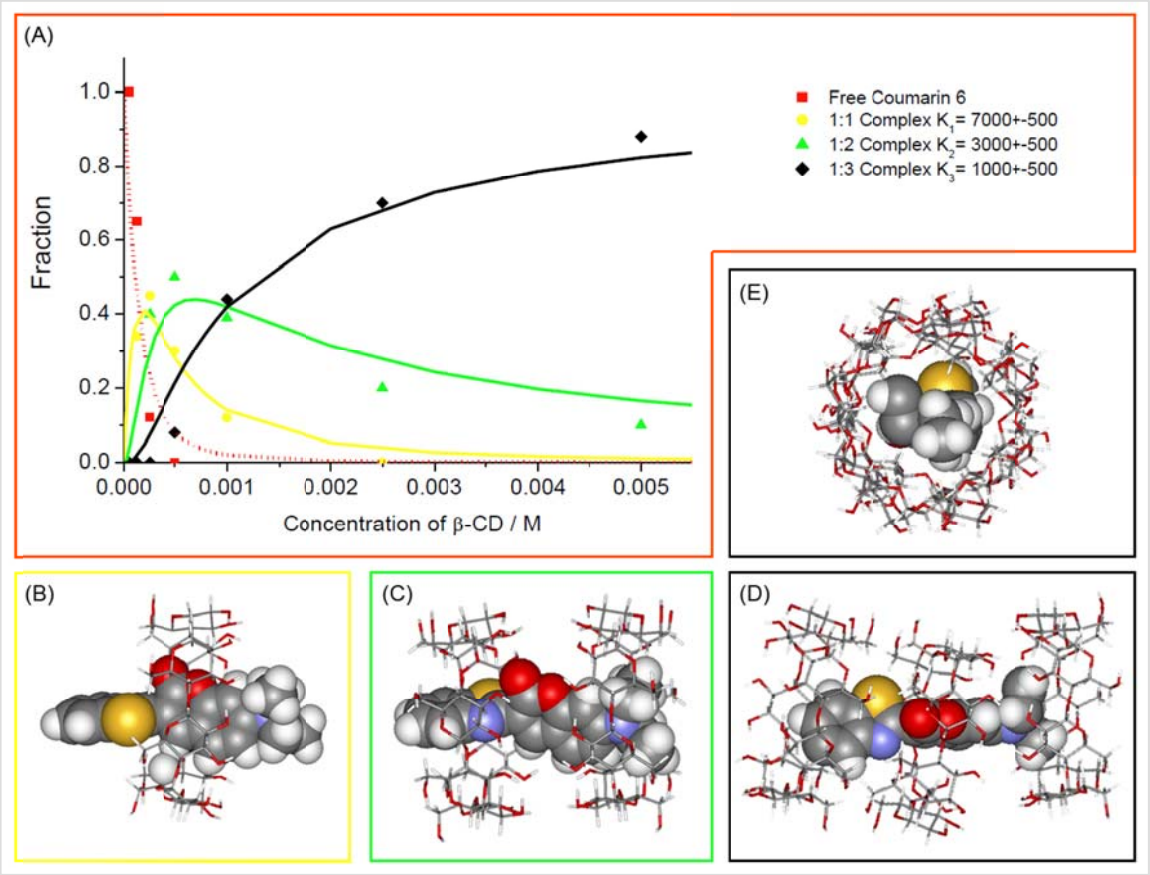

Figure 1-11: Fractions of the three different C6-β-CD-complexes and free C6, as well as the three possible models of C6-β-CD-complexes, originating from ab initio calculations

(A) Illustration of fractions of the 3 possible complexes of C6:β-CD, namely 1:1, 1:2 and 1:3, and free coumarin 6, pointing out the importance of absolute β-CD-concentrations on the ratio of formed complexes. At concentrations around 100µM β-CD there is a ratio of 40% 1:1 complex to 40% free C6 and 20% 1:2 complex, and no 1:3. At this β-CD-concentration, the best staining properties were observed.

(B) Complex of a 1:1 stoichiometry of C6:β-CD, represented by a combined model of a stick model for the β-CD molecule and a space filling model for the C6 molecule.

(C) Complex showing a 1:2 stoichiometry of C6:β-CD. In contrast to B the space filling model for C6 is rotated around the C-C bond between the two double-ring structures to properly fit into the 2 sugar baskets, without causing rejection between the sugar molecules.

(D) 1:3 stoichiometric C6:β-CD complex. This time the space filling model for the C6 molecule is not rotated around the C-C bond, when compared to (C), but the whole angle of view is different for better illustration.

(E) 1:3 stoichiometric C6:β-CD complex as shown in (D) rotated by 90° to the left. (A, modified from [59]; B to E, courtesies of Ao. Univ. Prof. Dr. Karl Peter Wolschann)

Besides a staining of the plasma membrane it seemed likely that all other intracellular membrane systems, meaning organelles like mitochondria, endosomes, lysosomes, endoplasmatic reticulum and the nuclear lamina could be stained too, with the coumarin 6 dye, although the further intracellular distribution, without a cyclodextrin as a delivery compound, remains unknown.

2 Aims

The aim of this study was to gain basic information about a newly developed fluorescent dye formulation, Onkovidon®. The intention was to prove that it can be used in vitro as a lipophilic, not cytotoxic staining compound for cultured cell lines. Another objective was to examine staining patterns for different cell lines and to quantify the uptake properties by comparing the mean fluorescence intensities for each cell line. Gaining information about mean cell size and perimeter was of high interest, too.

Determining, whether the staining process is related to active uptake mechanisms or to passive diffusion processes was of the highest interest. This can be achieved by decreasing of active transport mechanisms, by chilling cultured cells to 4°C and through observation of giant unilamellar vesicles obtained by electroformation. These are artificial test-systems and do not contain any membrane associated protein machineries necessary for active transportation.

Counterstaining of cell organelles, like mitochondria, lysosomes and lipid droplets, with other fluorescent dyes, and observation through a laser scanning microscope, will give insights in the intracellular distribution of the dye formulation. Additionally, exploration of the role of membrane cholesterol, which theoretically opposes one part of the dye, on cell staining, had to be done. This was completed by measurement of the total membrane cholesterol content of the cultured cell lines and correlation to the results from staining experiments.

The expected results provide information on the uptake mechanism of the dye, its intracellular processing and its effect on the viability of the cells. It shows potential for life cell staining and for improvements, like increase the of specifity or red-shifted fluorescence.

3 Results and Discussion

Evaluation of the influence of active transport and cell viability on the staining behavior of cultured cells

Microscopic imaging pointed out, that Onkovidon® does not only stain the plasma membrane, but also intracellular structures, in different patterns and intensity. In a first approach, determination of the relevance of active transport mechanisms on the staining behavior of cultured human bladder cancer cells and murine fibroblasts, was the subject of investigation. Theoretically, the dye-molecule would incorporate in lipid bilayers and, thus, it seemed likely that this process would be supported by transport proteins. It is known that, when cells are chilled to 4°C most active transport mechanisms are reduced to minimal functioning [68]. Further, killing cells by ribosomal translation blockade, through incubation with the antibiotic neomycin [69], should, finally, allow for the staining of membranes, only by passive diffusion of Onkovidon®.

Thus, cells were either treated as described in the Viable staining of adherent cells for epifluorescence and laser scanning microscopy or Inactivation of active transport processes or Neomycin-induced cell death. The resulting images, showing cells that were either stained at 4°C, at 37°C or when dead, were subsequently analyzed as described in Image analysis. Mean fluorescence intensities were calculated, as well as up to now unknown data for mean cell size and perimeter. Results of these analyses are shown in Figure 3-1 and representative images can be seen in Figure 3-2.

Expectations were that cells would stain best at 37°C, followed by weaker staining at 4°C and that killed cells would either not stain at all, or very weakly. Interestingly, this is only true for HTB5 and HTB9 cells, the more aberrant bladder cancer lines

(see Figure 3-1 A and B). The benign HTB2 cells stain better at 4°C than at 37°C and when killed, whereas L929 cells follow the exact reverse pattern. A reason for better staining of L929 cells on incubation, with neomycin, might be that these cells did not die at the chosen dose of the antibiotic. This idea comes from observation of these fibroblasts, during this study, where they were found to grow faster and to survive longer, when left untreated, than the three human cell lines (data not shown). Thus, it is possible that the majority of L929 cells were still alive or almost dying when stained with Onkovidon®. Moreover, the fibroblasts showed a different behavior on the occasion of cell death, compared to the human cell lines, as they were not breaking apart in pieces, but getting round and budding off the cell culture dish's surface. This behavior led to images of unusual amounts of round shaped, brightly stained cells (see Figure 3-2 L), hardly distinguishable from the also, often round shaped and less stained adherent fibroblasts, and thereby producing signals that are not avoidable and bias the results gathered from these images.

It has to be mentioned further, that the neomycin induced killing of cells was a difficult task, because incubation time and neomycin concentration had to be chosen and monitored very carefully. Otherwise, sudden detachment of the majority of cells was not unusual. Thus, prior to that, a screen was performed (data not shown) before to acquire the necessary data, that can be seen in Neomycin-induced cell death.

Because of the expected misleading results produced by neomycin killing, a possibly weaker staining of killed cells had to be verified by the not quantitatively evaluable method, in case of adherent cells, of Trypan Blue staining [70]. This was performed posterior to normal staining with Onkovidon®, as described in Neomycin-induced cell death. Indeed, a weaker Onkovidon® staining on killed cells was observed, consistent over all 4 lines (see Figure 3-3). Trypan Blue is not thought to interfere with Onkovidon®. Thus, it seems likely that the weaker signal is derived from weaker staining on dead cells. It seems that Onkovidon® staining is, thus,

supported through active transport, and works fine on “healthy” cells, but the staining is mainly due to passive diffusion.

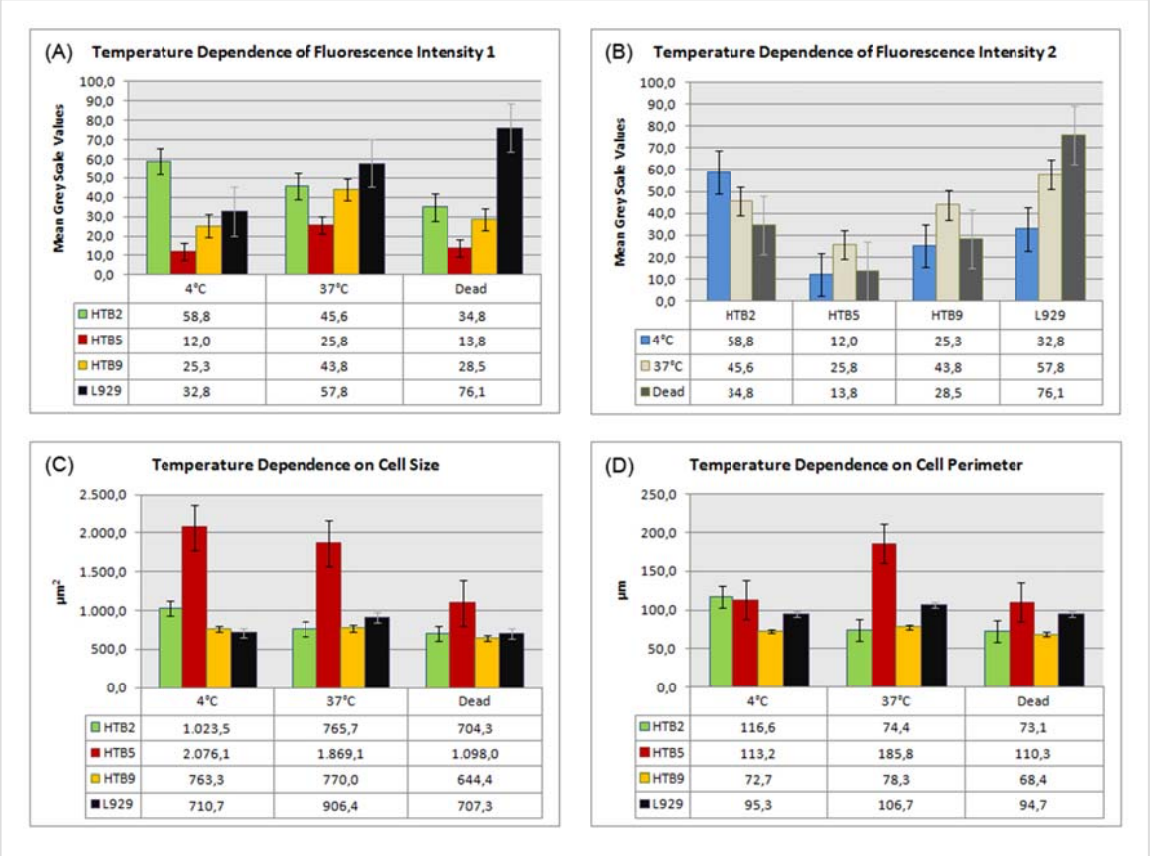

Figure 3-1: Graphs calculated from evaluated images derived from three experiments to eliminate active transportation for being responsible for the staining of membranes.

(A) Bar chart with mean standard error showing mean grey scale values (=fluorescence intensities) for three bladder cancer cell lines (HTB2, HTB5, HTB9) and a control cell line (L929), at the two chosen temperatures (4°C and 37°C) and after killing of cells, through incubation with neomycin (Dead). Grade IV malign cells, of the HTB5 strain (red), show weaker staining than the less aberrant HTB9 (yellow) and the benign HTB2 (green) strains. The control strain L929 (black) ranges in between the values of the bladder cancer cells.

(B) Bar chart with mean standard error showing mean grey scale values (=fluorescence intensities) for all 4 cell lines, at the two chosen temperatures or after killing. Values for staining at 4°C (blue) were expected to be stronger than for staining after killing (dark grey), but less intense than for staining at 37°C.

(C) Bar chart with mean standard error showing mean cell sizes in μm^2. Color code is the same as in (A).

(D) Table showing mean cell perimeters of cells as described in (A). Bar chart with mean standard error showing mean cell perimeters in µm. Color code is the same as in (A).

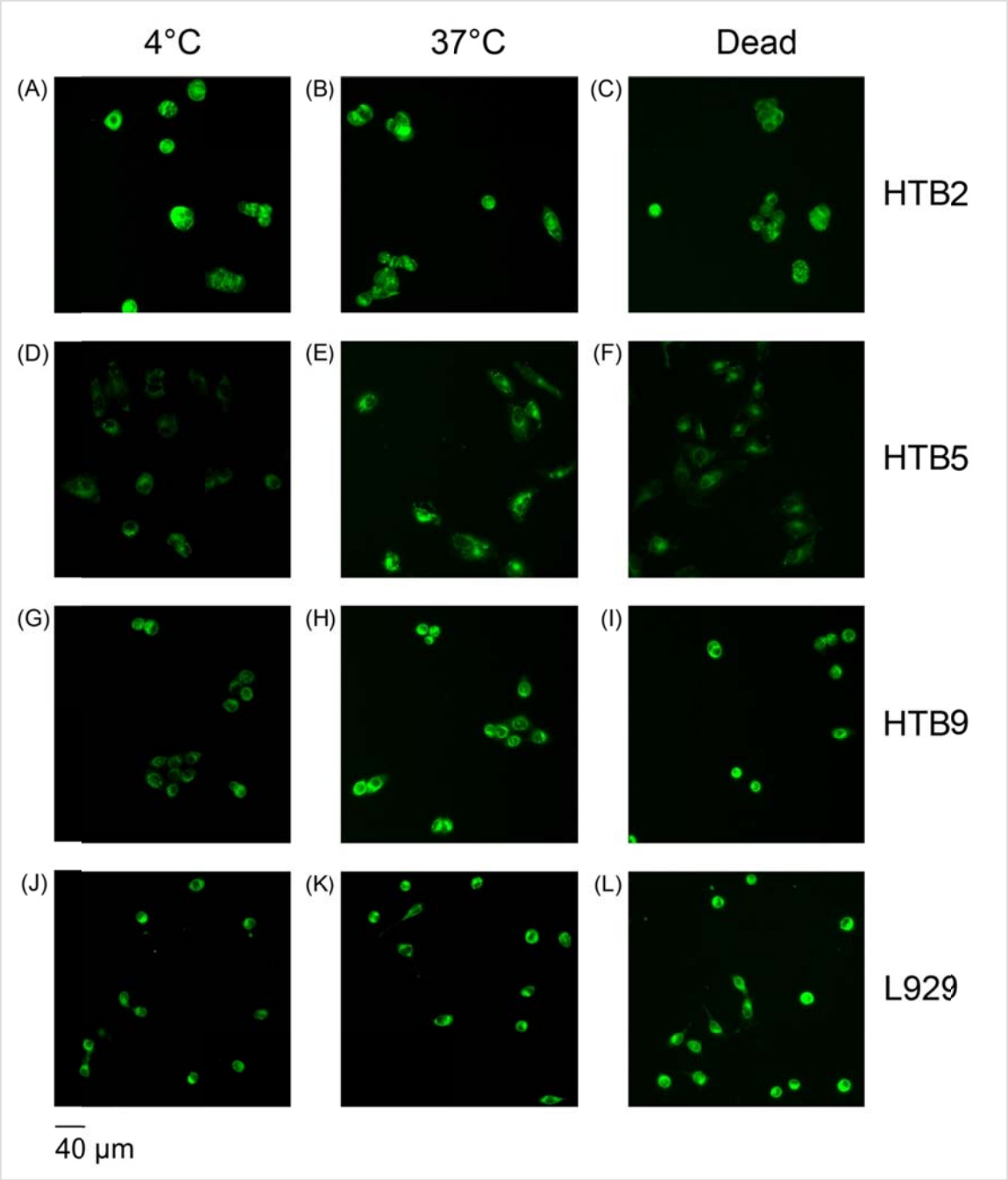

Figure 3-2: Representative images of mean fluorescence intensities from different staining procedures reflecting data arranged in Figure 3-1
Staining of human bladder cancer cell lines (HTB2, HTB5 and HTB9) and a control cell line (L929), at 4°C and 37°C, as well as after neomycin induced cell death.

The, obviously, better staining of HTB2 cells at 4°C (see Figure 3-1 B) might also result from the automated image analysis, as the pictures of HTB2 cells overall showed cell type typical aggregation of these cells. Thus, those cells were mistakenly identified as a single cell, instead of skipping the aggregate, and thereby resulted in a stronger gray scale value at 4°C.

Calculation of the mean cell size (see Figure 3-1 C) resulted in the finding that, bladder cancer cells seem to shrink a little, when getting more aberrant, as a difference between the benign HTB2 strain and the grade II malign HTB9 strain, in size, is not deniable (Figure 3-1 C and Figure 3-2 A to C and G to I). However, on progression of disease, when having a glance at the grade IV malign HTB5 strain, phenotype and cell size change dramatically, as the cell size is being doubled (see Figure 3-1 B).

Concerning the mean cell perimeter (see Figure 3-1 D), HTB5 cells stick out, when stained at 37°C, from all other values, thus making it possible to distinguish those cells from the other cell types. This finding seems very interesting, taking into consideration that HTB5 cells harbor metastatic potential, which might be supported by extending the cell surface.

Overall, and quite interesting, cells seem to stain well at 4°C, although active transport should be reduced at this temperature, as they do, when incubated with neomycin. These findings, moreover, indicate that the staining process functions by passive diffusion processes, but might be supported through active transport. The effect of reduced diffusion on colder temperatures seems to be deniable for the staining procedure.

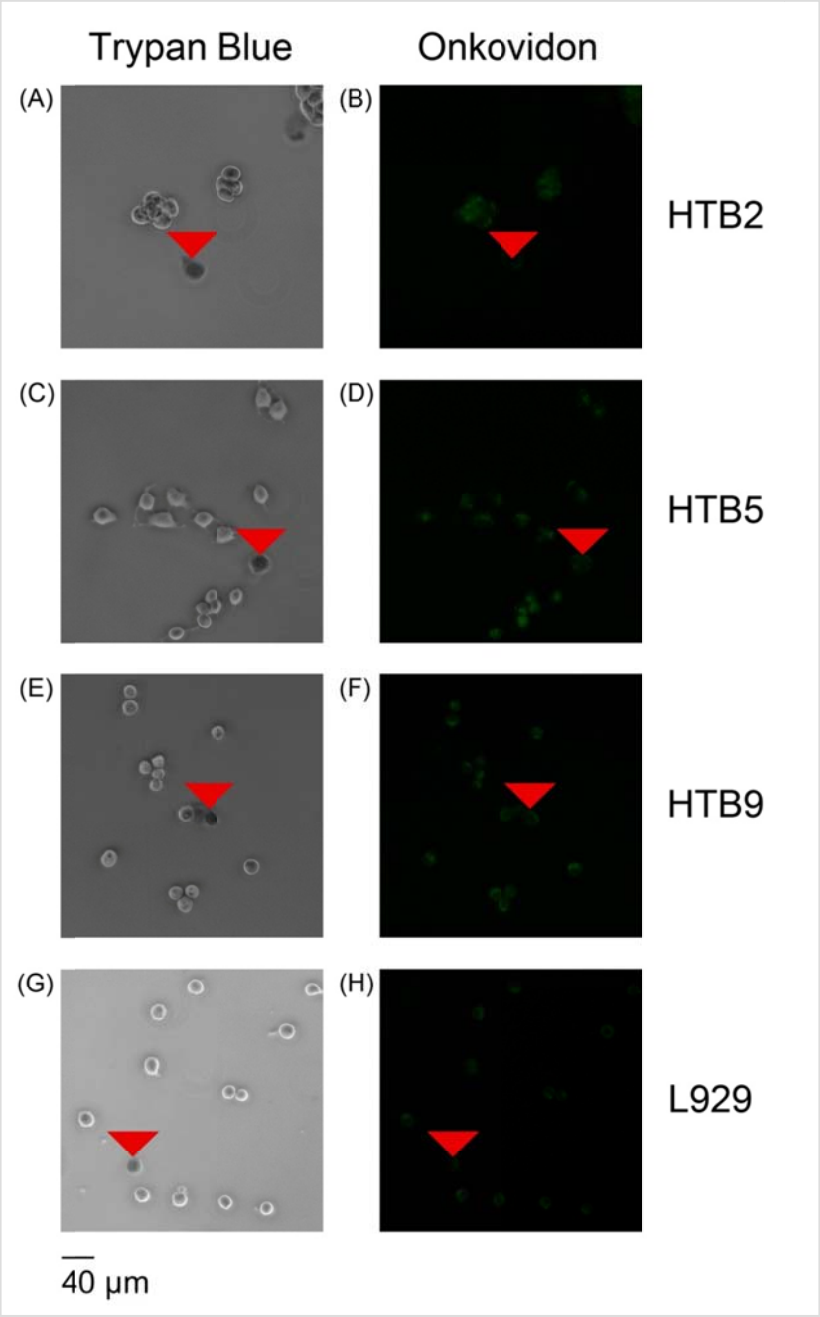

Figure 3-3: Trypan Blue and Onkovidon® stained cells.
Pictures A, C, E and G show dead, but still adherent cells (indicated through red triangles) in transmitted light. Pictures B, D, F and H show the same cells stained with Onkovidon®, in the fluorescence mode of the microscope. Dead cells appear to be stained weaker.

Longtime Incubation with Onkovidon®

Many fluorescent dyes obviously harm living cells, when they are applied on them. This is most often caused by their solvents, such as DMSO or acetonitrile, which appear to be cytotoxic in many cases [71], [72].

β-cyclodextrin, as well as methyl-β-cyclodextrin, have cholesterol depleting properties [73], [74], [54]. Thus, it might be possible that, β-cyclodextrin, constituting the delivery vector portion of the Onkovidon® dye, when exchanging coumarin 6 between the complex and the plasma membrane, takes-off the cholesterol, as a side effect. Although the used cyclodextrin concentration is far below the needed concentration for effective cholesterol depletion, β-cyclodextrin might still have an influence on the membrane properties, maybe leading to membrane breakdown, as it is the case for methyl-β-cyclodextrin.

Also, coumarin 6 is known to be toxic, when applied in high concentrations on tissue cultured cells or multicellular organisms, leading to bile duct carcinoma in rats [75]. Because both components of the dye harbor cytotoxic potential we wanted to examine the dye's effect, when not only used in a staining procedure for 10min, where cells are allowed to recover afterwards, but when kept in the surrounding media solution of tissue cultured cell lines for a longer time period. Thus, human bladder cancer cell lines (HTB2, HTB5 and HTB9) and murine fibroblasts (L929) were treated, as described in Long term incubation with Onkovidon®. A representative choice of pictures, taken at distinct time points, is shown in Figure 3-4

While the dye-clogged media were not removed after incubation, but kept on the cells for the next 48 hours, cells did not show any abnormal behaviour concerning growth or cell death. After 24 hours, as well as after 48 hours, higher cell numbers were observed and counted (data not shown). Thus, it seems that the dye is of no harm to cells and is, therefore, easy to handle for investigators.

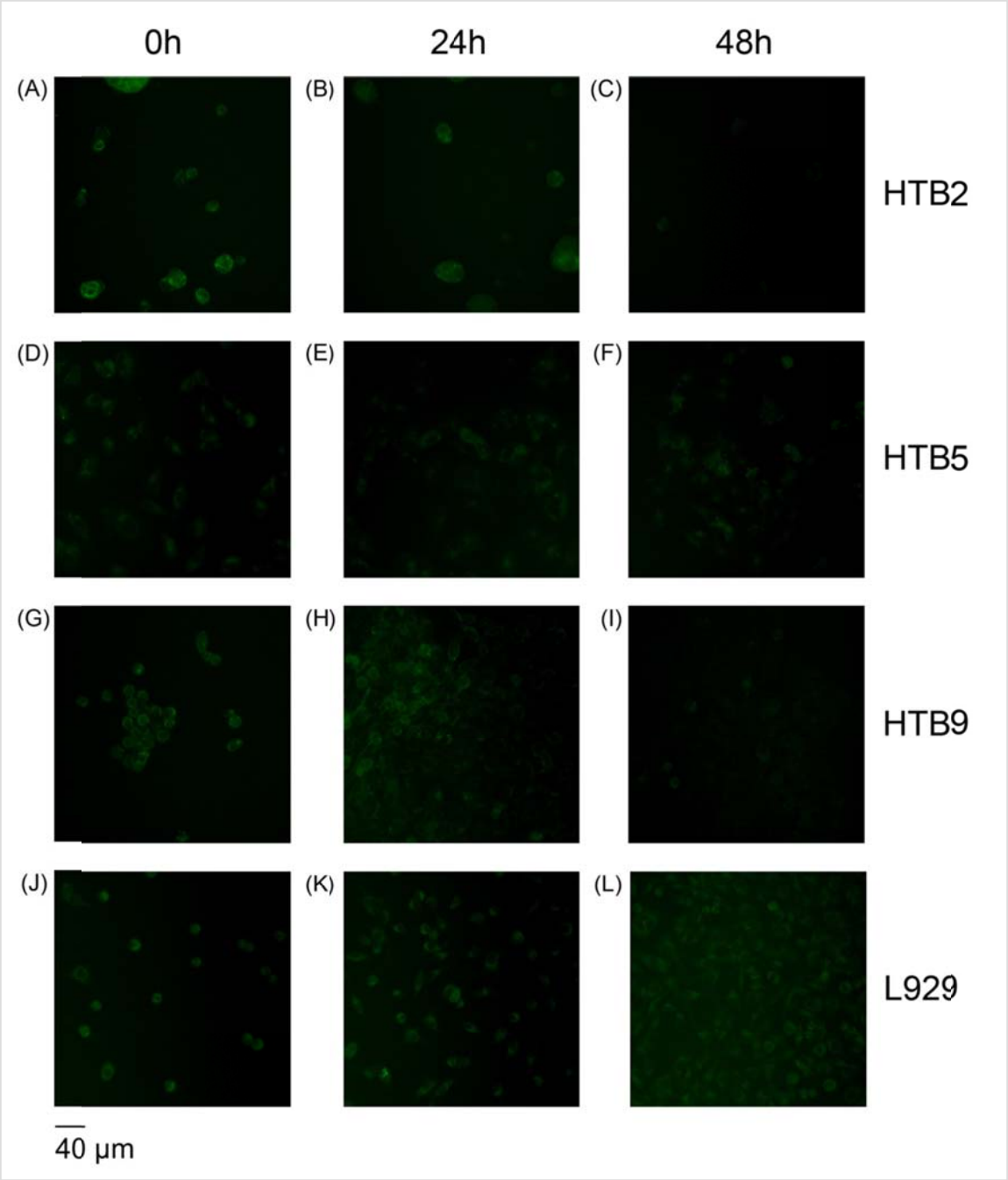

Figure 3-4: Choice of pictures taken at distinct time points from all 4 cell lines, when grown for 48 hours, in Onkovidon®-clogged medium.
(A, D, G, J) Photos taken 10min after start of incubation. (B, E, H, K) Photos after 24 hours. (C, F, I, L) Photos after 48 hours. Cells of all strains, obviously, not only survive treatment with Onkovidon®, they show normal growth behavior.

Strong background fluorescence was observed with all 4 strains after 24 hours, which got worse after 48 hours. This was most probably due to stained cellular waste products and cellular fragments from dead cells.

Giant Unilamellar Vesicles

In the next step, we searched for an artificial system to examine both, the dependence on active transport and the cholesterol dependence on the staining procedure. The latter was of quite big interest, taking into account that β-cyclodextrin is capable of the complexation of cholesterol and that the delivered coumarin 6 is possibly competing for space, with cholesterol molecules, in the plasma membrane.

We came up with the idea of producing giant unilamellar vesicles (GUVs) using the electroformation method, described in Giant unilamellar vesicle formation and staining. Thus, it was possible to grow and observe vesicles of different lipid- and cholesterol assemblies and concentrations. After the formation process, the vesicles were attempted to be stained in the same way as the cell lines. The following listing gives an overview of the tested lipid- and cholesterol-compositions for the electroformation:

- 100% EggPC
- 100% POPC
- 90% POPC and 10% SM
- 90% POPC and 10% PE
- 90% POPC and 10% PI
- 90% POPC and 10% PS
- 70% POPC and 30% Cholesterol

4 chambers of each type, were always prepared; because the procedure does not work safely all the time. Thus, and because of the known problems concerning the

formation of GUVs, as it seems that only some possible compositions allow effective GUV production, only a few of the chosen compositions worked properly. Shown in Figure 3-5 are the 4 different compositions, that led to formation of GUVs. These were 100% EggPC, 100% POPC, 90% POPC and 10% PE, and 90% POPC and 10% PE. Interestingly, 70% POPC with 30% Cholesterol did not work either, as it is known that GUVs, with approximately 25 mol %, should actually form [76].

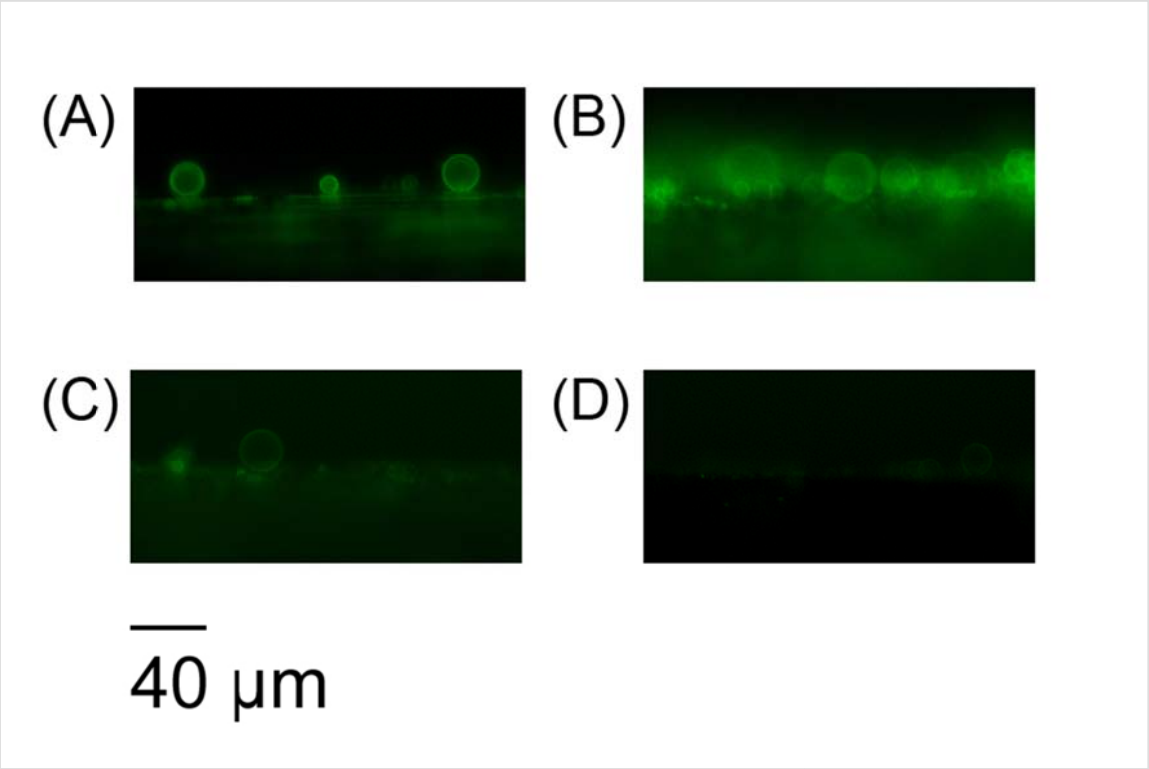

Figure 3-5: Giant unilamellar vesicles stained with Onkovidon®.
GUVs were formed from (A) EggPC. (B) 100% POPC, (C) 90% POPC and 10% PE and (D) 90% POPC and 10% PS.

The gathered images show that GUVs, and thereby, artificial membranes, also stain with Onkovidon®, but because neither all chosen compositions worked out nor did the cholesterol composition, we were not able to determine the effect of cholesterol, on the staining procedure, in the artificial system.

Cholesterol Measurement

In addition, evaluation of the role of membrane associated cholesterol, of living cells on the staining procedure, was another point of interest. Thus, cultured cells were digested and to extract all membrane fractions as described in Cholesterol Measurement, which were then loaded onto SDS-gels (see Polyacrylamid gels and Coomassie-staining and -destaining), which in turn were subjected to Photodensiometric analysis of PAA-gels with Quantiscan (see Figure 3-6 A to C). After this, the obtained membrane fractions were analyzed spectroscopically, as described in the Spectroscopic measurement of membrane cholesterol. The measured values were then compared to the mean fluorescence values gathered from Evaluation of the influence of active transport and cell viability on the staining behavior of cultured cells (see Figure 3-7).

(A)

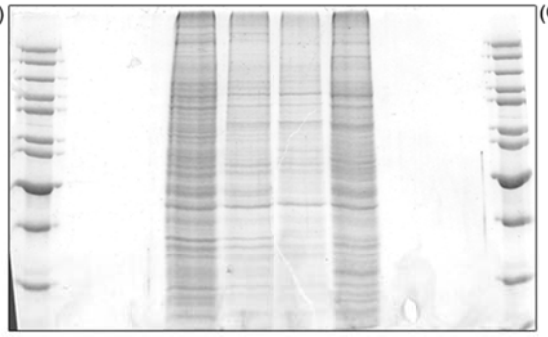

(C)

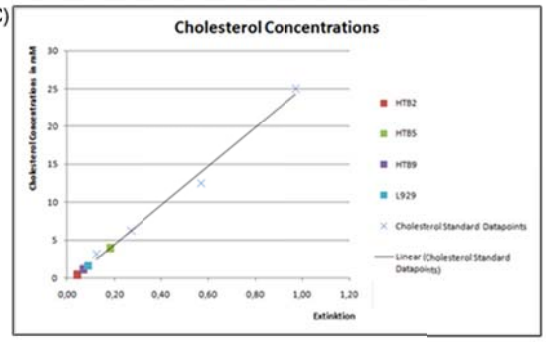

(B)

Cellline	Measured Grayscale Values	Calculated Ratio
HTB9	6.871,49	0,30
HTB5	15.336,98	0,68
L929	22.629,75	1,00
HTB2	26.133,45	1,15

Figure 3-6: Cholesterol Measurement.
(A) Grayscale photo of PAA-gel for better contrast, for use with Quantiscan. Each lane shows one cell line. From left to right bladder cancer cells (HTB2, HTB5 and HTB9), and control fibroblasts (L929).
(B) Measured grayscale values for bladder cancer cells (HTB2, HTB5 and HTB9) and control fibroblasts (L929), and calculated ratios that show which sample had the biggest lipid fraction.
(C) Straight calibration line produced after measurement of extinction values of cholesterol standards, with plotted extinction values for bladder cancer cells (HTB2, HTB5 and HTB9) and control fibroblasts (L929).

The obtained results are surprising, as they point out that the more cholesterol is present in the membrane systems of the different cell lines the weaker the staining of the Onkovidon® dye seems to be. HTB5 cells, showing the highest cholesterol concentrations, stain worst. This implements a possible competition of coumarin 6, with cholesterol, for space in the membranous systems of stained cells.

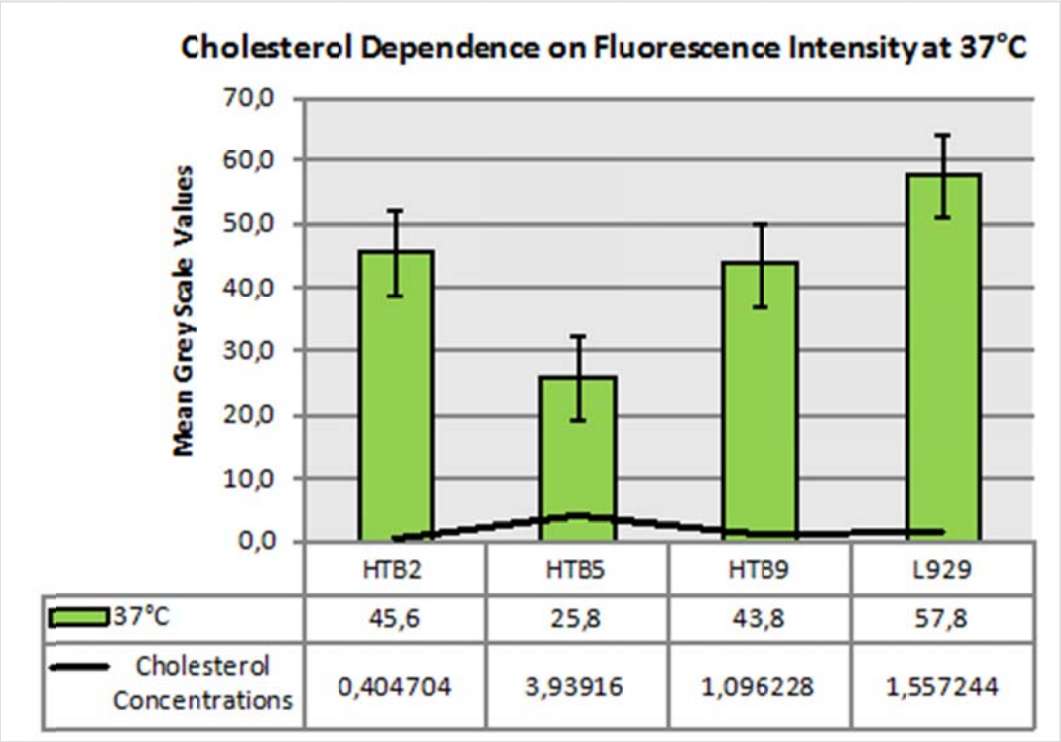

Figure 3-7: Cholesterol dependence on fluorescence intensity for staining at 37°C.
Green bars show data gathered from Evaluation of the influence of active transport and cell viability on the staining behavior of cultured cells. Black line shows cholesterol concentrations for each bladder cancer cell line (HTB2, HTB5 and HTB9) and control fibroblasts (L929) in mM.

Laser scanning microscopic imaging

Images taken with the fluorescence microscope showed staining of intracellular structures on all 4 cell lines. Thus, it seemed obvious that not only the plasma membrane is stained, but somehow coumarin 6 molecules also reach intracellular membranes. Because coumarin 6 is, also, slightly soluble in water, it might be possible that once it crosses the barrier of the plasma membrane, either by diffusion or

by flip-flop of certain lipids of the outer leaflet, such as sphingomyelin, it might dissolve in the cytosol and thereby reach intracellular membrane systems, such as mitochondria and lysosomes. Besides the theory that cytosolic coumarin 6 is responsible for intracellular staining, it might be possible that vesicular transport, along the cytoskeleton, starting with budding vesicles from the plasma membrane, is triggering the staining of intracellular membranes. This theory cannot be taken for granted as some preliminary experiments (data not shown) pointed out that the staining process takes place within milliseconds.

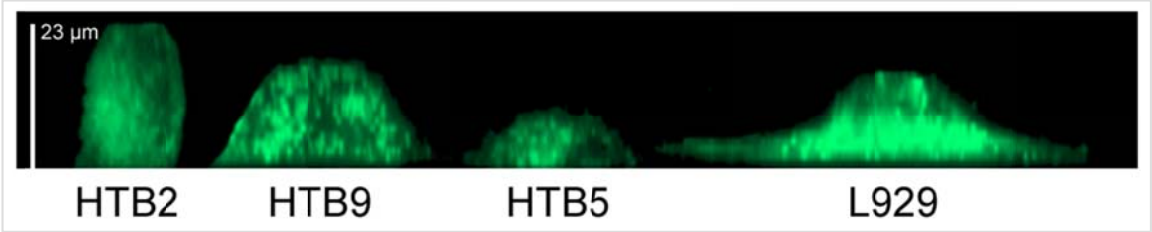

Figure 3-8 Change in cell morphology.
3D-reconstruction of viable stained single cells in the LSM Image Browser and capturing of the side view shows the difference in cell morphology. Benign HTB2 cells harbor an intact cytoskeleton and show a cone-like morphology. The more aberrant the cell line, the more flattened the morphology seems to be. Grade II malign HTB9 cells appear more ball-like and this morphology is nearly lost on grade IV malign HTB5 cells.

Besides the known intracellular membrane systems, we observed well stained dots in the cytosol of each of the used cell lines, that might be lipid droplets. These might also be responsible for intracellular staining of cells with Onkovidon®, as they seem to play a role in inter-membrane lipid traffic [23]. Existence of lipid droplets was approved for HTB5 cells, as there was evidence for the existence of microvilli and the lack of desmosomes, published by the purchasing company, but not yet for the other two bladder cancer cell lines and the fibroblasts. Lipid droplets are described to be localized close to the nucleus and the ER, and to show rapid non targeted movement between small areas [29]. This could be seen using fluorescence microscopy, when observing our bladder cancer cells, but not when having a glance at the fibroblasts. Here the droplet-like structures do not move at all.

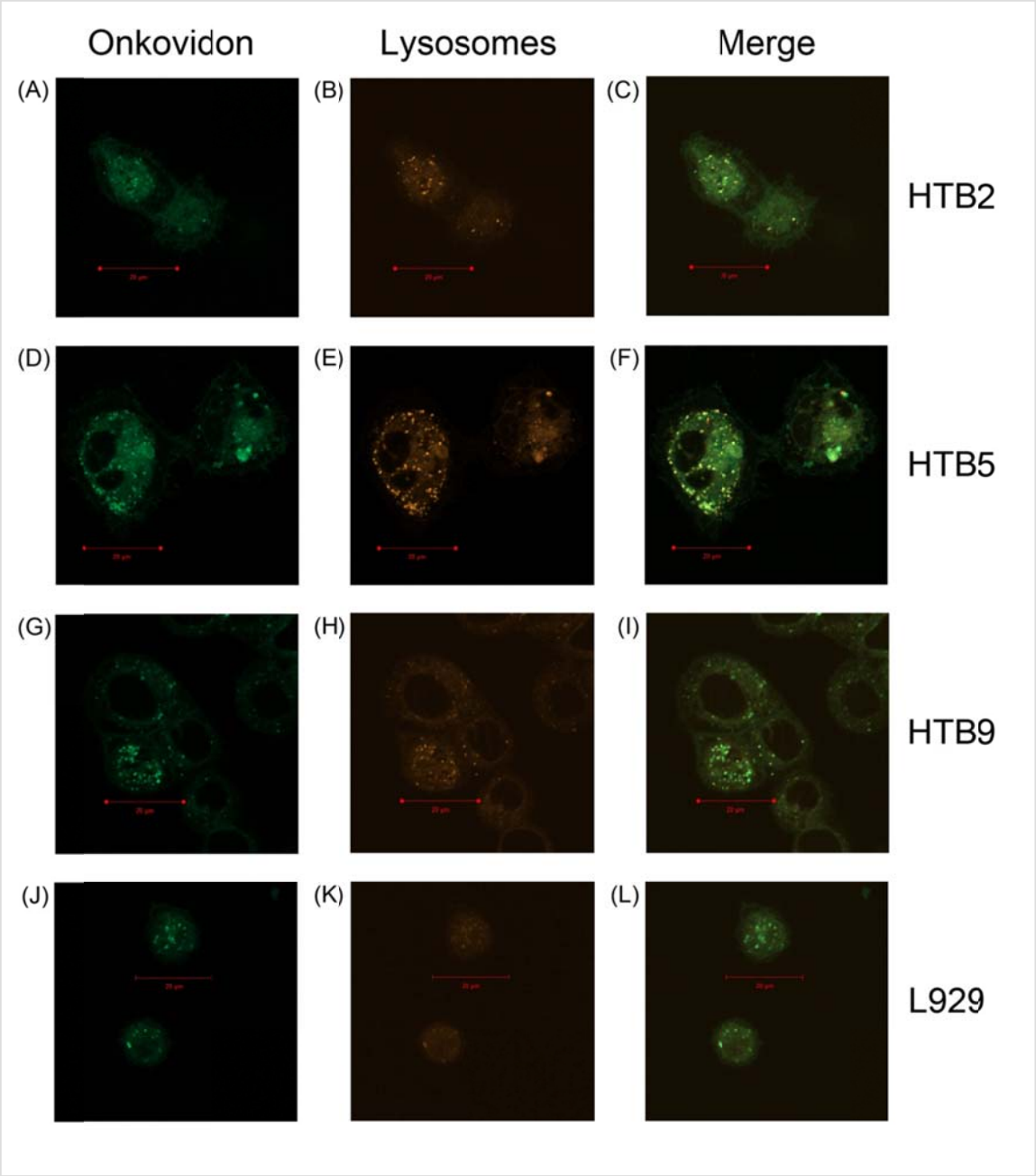

Figure 3-9: Stained lysosomes.
Pictures in a row are taken from the same cell and the same plane.
(A) shows two HTB2 cells 3µm from the ground plate of the observation chamber, stained with Onkovidon®.
(B) covers the same cell, at the same plane, stained with Lyso-Tracker® Red DND-99 (577/590).
(C) Merged image of (A) and (B). Yellow dots indicate that this structure is stained by both dyes.
Pictures (D) to (F), (G) to (I) and (J) to (L) follow the same setup, but for HTB5 cells (two cells 3µm from the ground plate of the observation chamber), HTB9 cells (three cells forming tissue 6µm from the ground plate of the observation chamber) and L929 cells (two cells 3µm from the ground plate of the observation chamber), respectively.

Further, the localization to exactly these two organelles is not consistent over the different bladder cancer populations, but still, all of them show lipid droplet like structures.

Thus, we decided to take advantage of a laser scanning microscope to determine which of the intracellular structures were stained and to verify if the bright green dots were lipid droplets, by colocalisation. Besides this, laser scanning microscopy allows for the capturing of so-called Z-stack images, which describes images taken from different planes within a cell, and subsequent three-dimensional reconstruction. We intended to stain lysosomes, mitochondria and lipid droplets, first on living cells as described in the Viable staining of adherent cells for epifluorescence and laser scanning microscopy, and later on fixed samples, as described in the Staining and fixing of adherent cells for epifluorescence and laser scanning microscopy.

There was serious difficulty in our attempt to stain and fix bladder cancer cells and fibroblasts, as the fixation, with 3.7% PFA, disrupted the plasma membrane. Instead of improved resolution, pictures appeared waxier, compared to viable stainings (data not shown). Also, staining with Mito-Tracker® Orange CMTMRos (554/576), as described in Staining with Mito-Tracker® Orange CMTMRos (554/576), was only partly successful, as the tracker substance for unknown reasons seemed to coincidently stain the nucleus, besides the mitochondria (data not shown).

After three-dimensional reconstructions of images taken from viable stained single cells of each cell line (see Figure 3-8), one can see the difference in cell morphology. Cells of higher malignancy seem to lose the integrity of their cytoskeleton and thus, appear much more flattened. They also no longer build up tissue like structures (data not shown), and no longer express the epithelial cell adhesion molecule (EpCAM), which is typically expressed in epithelia forming cells types (data not shown). EpCAM expression is observed with HTB2 and HTB9, but not with HTB5 cells, nor with the L929 fibroblasts.

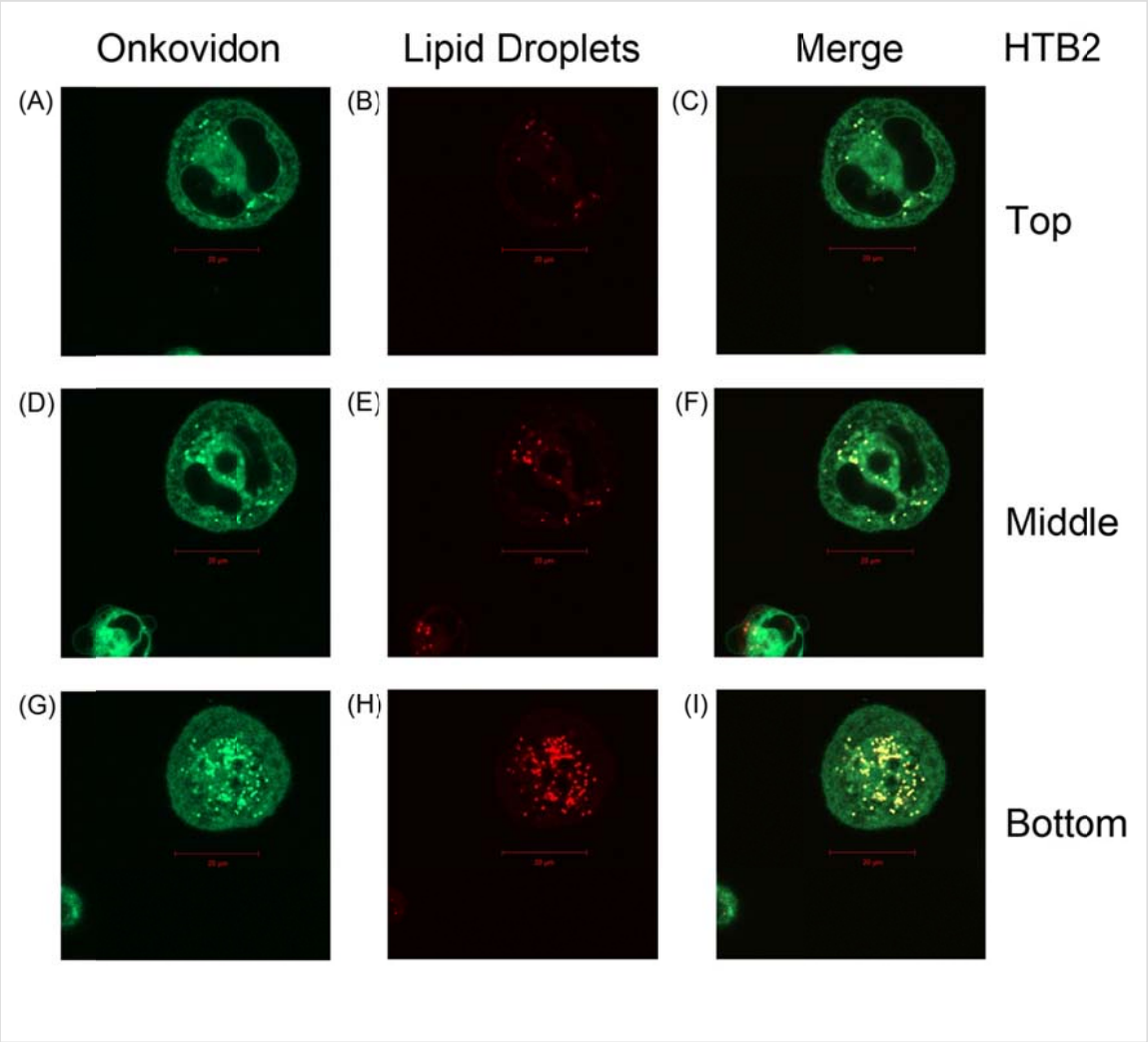

Figure 3-10: Lipid droplets in HTB2 cells.
Pictures (A) to (I) are from the same cell and pictures in a row are of the same plane.
(A) shows an HTB2 cell 13µm from the ground plate of the observation chamber stained with Onkovidon®.
(B) covers the same cell, at the same plane, stained with BODIPY® 558/568 C_{12}
(C) Merged image of (A) and (B). Yellow dots indicate that this structure is stained by both dyes.
Pictures (D) to (F) and (G) to (I) follow the same setup, but are taken 9µm and 5µm from the ground plate of the observation chamber. Note that lipid droplets are located more or less basal, and that bladder cancer cells sometimes show fragmented nuclei and vacuolated cytoplasm.

Another fascinating finding was the different staining pattern observed with the three bladder cancer cell lines. The benign HTB2 cells were stained homogenously all over the surface, as well intracellular membranous structures were stained. The grade II malign HTB9 cells show a more baso-lateral staining pattern, whereas the completely devolutioned HTB5 cells stain in a fragmented pattern. This strange

staining pattern led to confusion before the discovery of lipid droplets, and that these might be responsible for “sucking” away the hydrophobic dye from the cell surface (data not shown). Further, LSM imaging showed cytoskeletal components to be stained, which can be due to stained vesicles that are transported along the cytoskeleton.

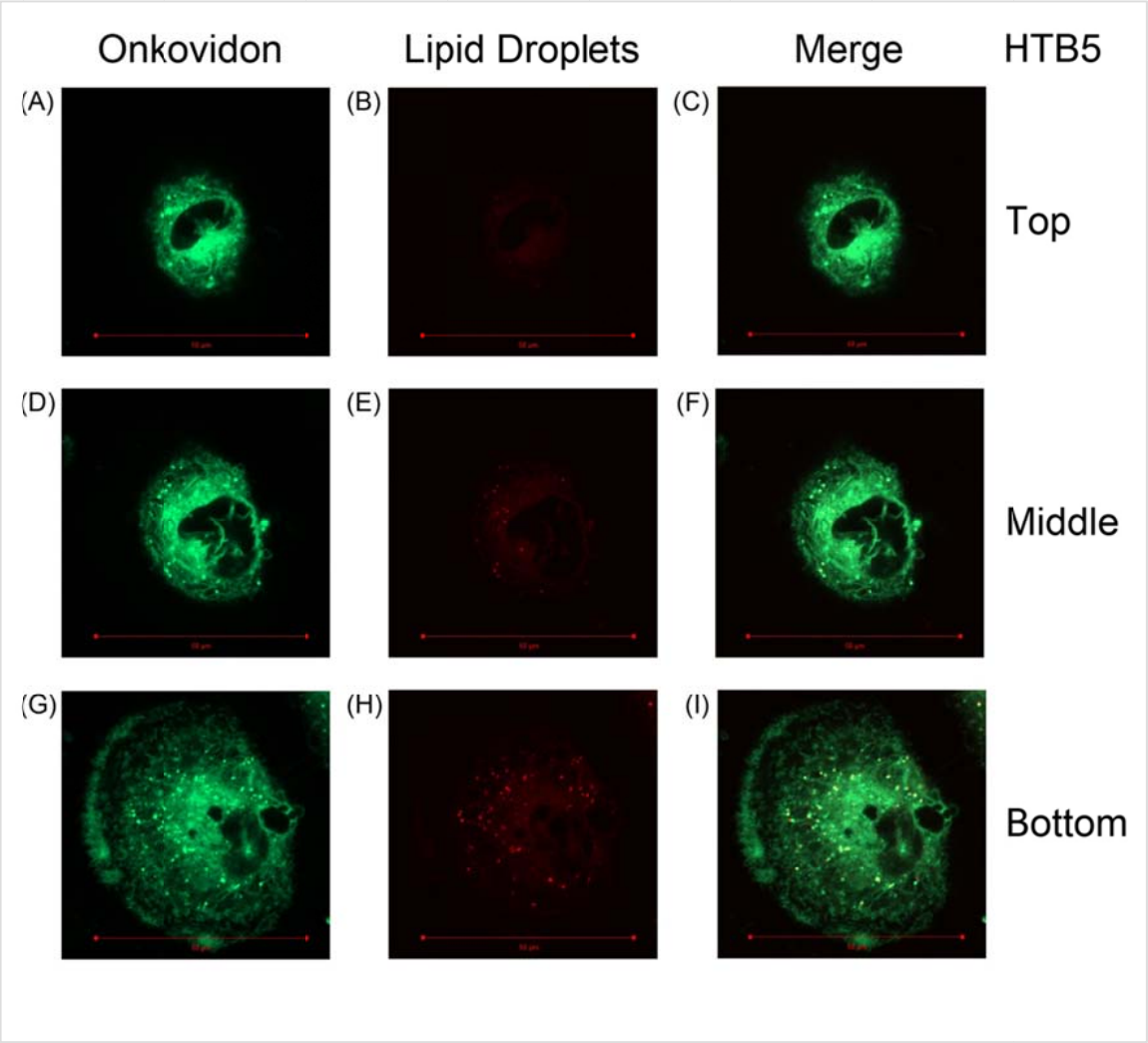

Figure 3-11: Lipid droplets in HTB5 cells.
Pictures (A) to (I) are from the same cell and pictures in a row are of the same plane.
(A) shows an HTB5 cell 17µm from the ground plate of the observation chamber stained with Onkovidon®.
(B) covers the same cell, at the same plane, stained with BODIPY® 558/568 C_{12}
(C) Merged image of (A) and (B). Yellow dots indicate that this structure is stained by both dyes.
Pictures (D) to (F) and (G) to (I) follow the same setup, but are taken 11µm and 5µm from the ground plate of the observation chamber. Note that lipid droplets are located more or less basal and appear smaller than in HTB2 cells, and that bladder cancer cells sometimes show fragmented nuclei and vacuolated cytoplasm.

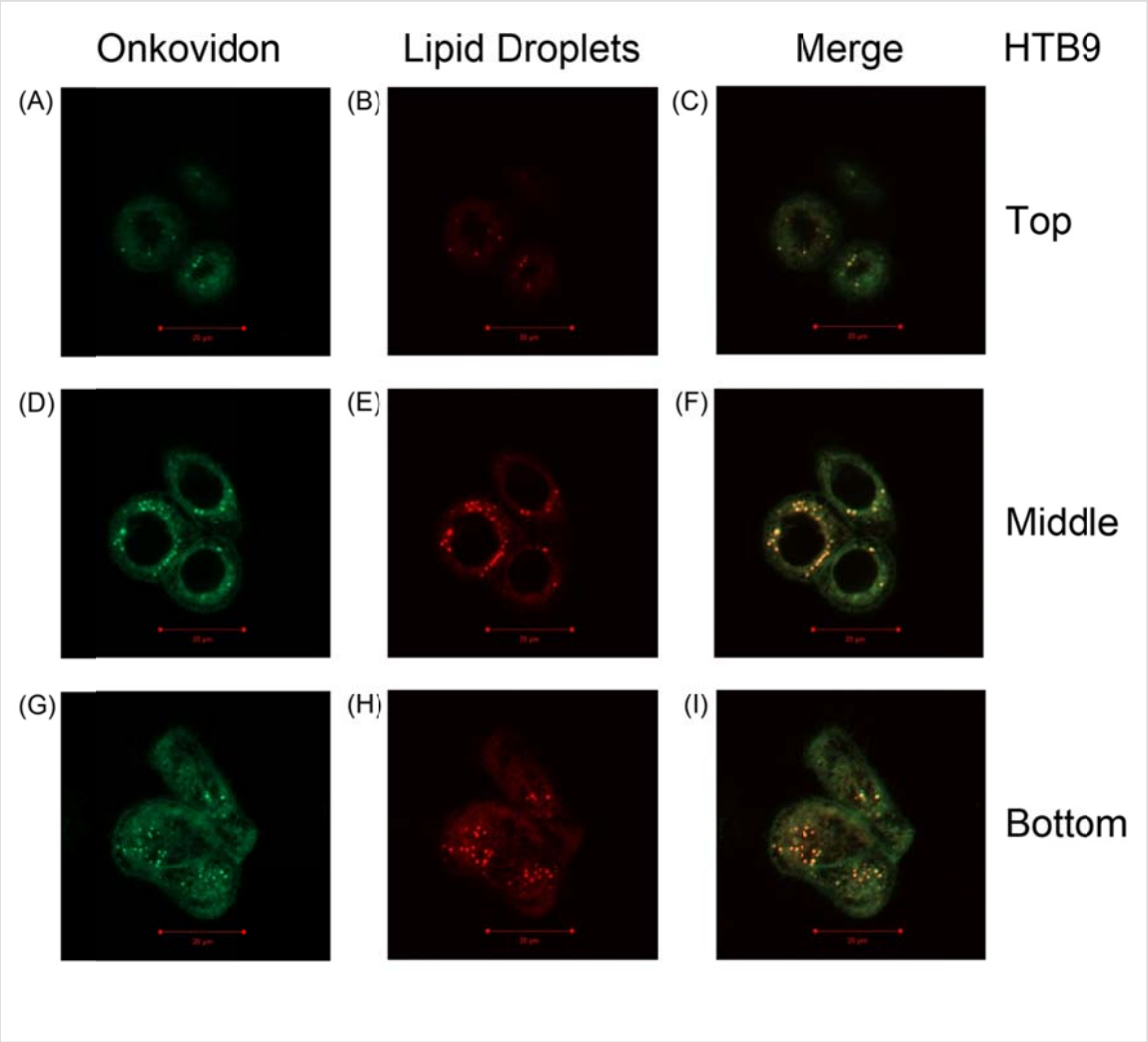

Figure 3-12: Lipid droplets in HTB9 cells.
Pictures (A) to (I) are from the same cell and pictures in a row are of the same plane.
(A) shows three HTB9 cells 15µm from the ground plate of the observation chamber stained with Onkovidon®.
(B) covers the same cell, at the same plane, stained with BODIPY® 558/568 C_{12}
(C) Merged image of (A) and (B). Yellow dots indicate that this structure is stained by both dyes.
Pictures (D) to (F) and (G) to (I) follow the same setup, but are taken 9µm and 3µm from the ground plate of the observation chamber. Note that lipid droplets are located more or less basal and appear bigger than in HTB2 cells, and that these bladder cancer cells do not show fragmented nuclei and vacuolated cytoplasm.

Viable staining with the Lyso-Tracker® Red DND-99 (577/590), as described in Staining with Lyso-Tracker® Red DND-99 (577/590) worked out fine. It was known before that this tracker substance produces a strong background signal and thus, stained lysosomes are hard to distinguish from the overall staining. Pictures for all 4 cell lines are summarized in Figure 3-9.

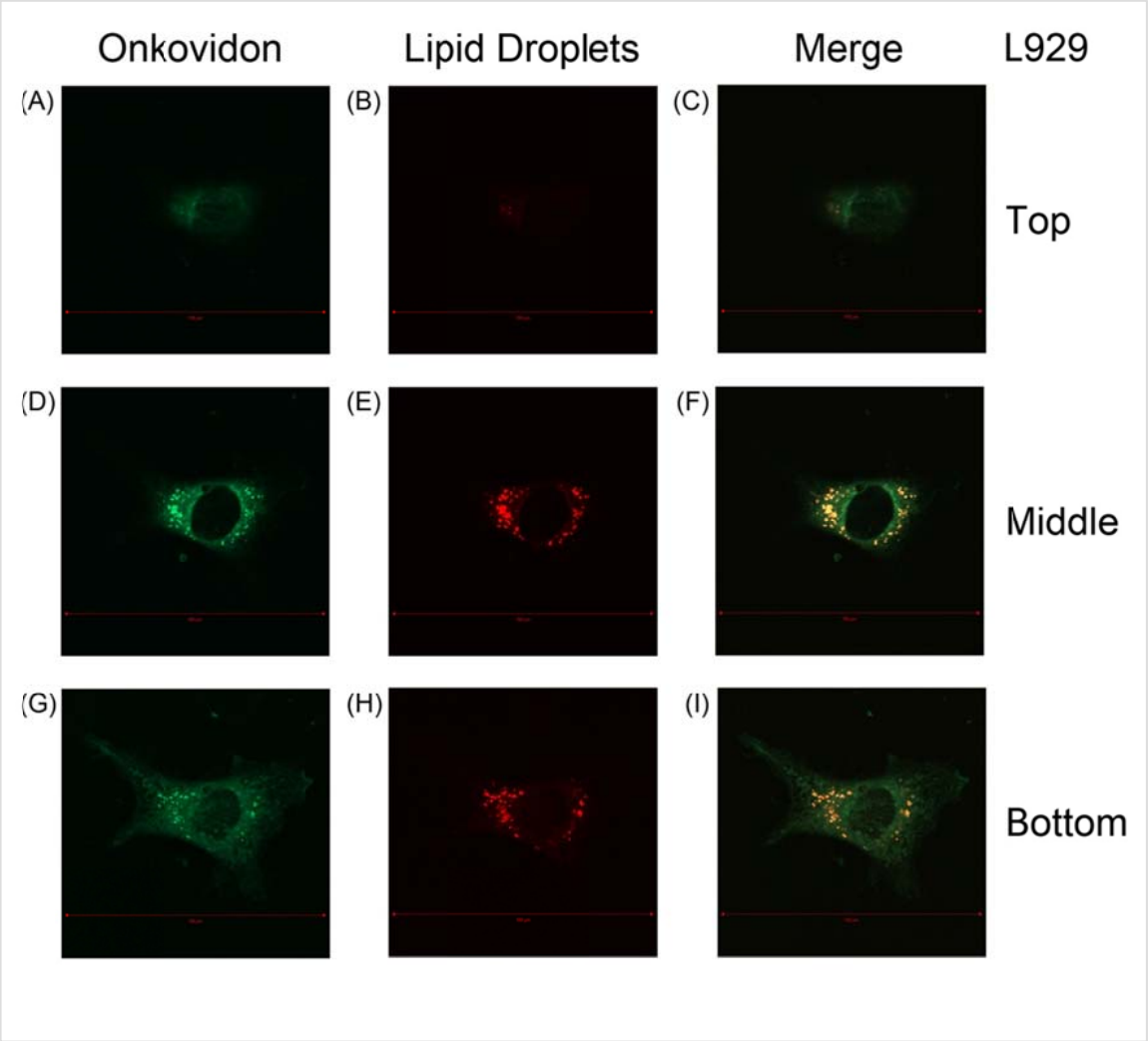

Figure 3-13: Lipid droplets in L929 cells.
Pictures (A) to (I) are from the same cell and pictures in a row are of the same plane.
(A) shows a L929 fibroblast 6µm from the ground plate of the observation chamber stained with Onkovidon®.
(B) Covers the same cell, at the same plane, stained with BODIPY® 558/568 C_{12}
(C) Merged image of (A) and (B). Yellow dots indicate that this structure is stained by both dyes.
Pictures (D) to (F) and (G) to (I) follow the same setup, but are taken 4µm and 2µm from the ground plate of the observation chamber. Note that lipid droplets are located more or less basal and appear as big as in HTB9 cells, and that fibroblast show a completely different morphology.

Viable staining with BODIPY® 558/568 C_{12}, as described in Staining with BODIPY® 558/568 C_{12} was successful, too. It has to be mentioned that the stained structures might basically be lipid droplets, but because this dye comprises a twelve-hydrocarbon-tail it is not impossible that some of the stained structures are other lipoprotein particles.

Consistent over all 4 lines, even with the control fibroblasts, is the finding that droplets do not only localize close to ER and nucleus, but are more or less distributed basal, as can be seen in Figure 3-10, Figure 3-11, Figure 3-12 and Figure 3-13. Further, there are differences in droplet number and size. Cells with wider cytoplasm seem to harbor more, but smaller droplets, compared to cells where the nucleus takes most of the intracellular space.

4 Conclusion

Experimental data, from experiments with chilled (4°C), normally treated (37°C) and killed cells, and artificial membranes, affirm that Onkovidon® is a membrane staining dye formulation. It consists of coumarin 6 and β-cyclodextrin, in a 1:1 inclusion complex in an aqueous solution, which incorporates into bilayers, basically through, passive diffusion processes. Staining takes place within milliseconds, when applied on living cells or on artificial membranes, which do not harbor transport proteins.

The staining procedure is supported by active transport mechanisms, when cells are held under perfect environmental conditions. Cell staining is not only bound to the plasma membrane, but also to cytosolic membrane systems such as lysosomes and lipid droplets, and is independent of cell viability. Further, no cytotoxicity was observed on incubation, with the dye formulation, for 48 hours.

Lipid droplets are interestingly not only found in HTB5 bladder cancer cells, as known before. During this study they were also discovered in the three other investigated cell lines and localize in all four cell populations basally.

Membrane bound cholesterol seems to play a role in the staining mechanism. Cells with a high membrane cholesterol concentration stain weaker at optimal growing conditions, which is consistent with the idea that coumarin 6 molecules are competing with cholesterol molecules for space in lipid bilayers.

Although automated analysis of microscopic images declares that the fibroblast control cell line stains better when cells are killed, data from counterstaining, with Trypan Blue, revealed that this finding is not true. All four tested cell lines stain much weaker when cells are killed. HTB2 cells in contrast, appear to stain better at 4°C, which is a bias produced by automated cell counting. Comparing the data of

all 4 cell lines does not build up a consistent picture, but this is due to an obvious inhomogeneity in between the three bladder cancer populations. Highly malign HTB5 cells, for example, cover more area, show a flattened phenotype, due to cytoskeletal breakdown, and no longer express EpCAM. Thus, these cells should be investigated more precisely and detailed evaluation for every single cell line seems necessary.

5 Materials and Methods

Chemicals and Solutions

Compound	Catalogue- or Cas-Number	Purchaser
1-palmitoyl-2-0leoyl-sn-glycero-3-phosphoethanolamine	850757 P	Avanti Polar Lipids (USA)
2-oleoyl-1-palmitoyl-sn-glycero-3-phosphocholine	42773	Sigma-Aldrich (Austria)
3-(2-benzothiazolyl)-7-(diethylamino)-coumarin ($C_{20}H_{18}N_2O_2S$) (C540)	120	Radiant Dyes (Germany)
30 % Acrylamide mix (29:1)	1108	Gerbu (Germany)
4,4-difluoro-5-(2-thienyl)-4-bora-3a,4a-diaza-*s*-indacene-3-dodecanoic acid (BOD-IPY® 558/568 C_{12})	D-3835	Invitrogen (Austria)
Acetic acid	100063	Merck (Austria)
Acetonitrile	00688	Sigma-Aldrich (Austria)
Ammonium persulfate	13375	Serva (Germany)
Bromphenolblue Solution	B7021	Sigma-Aldrich (Austria)
Cholesterol	700000 P	Avanti Polar Lipids (USA)
Coomassie blue R250	1097	Gerbu (Germany)
Diethylether	31670	Sigma-Aldrich (Austria)
Dimethyl sulfoxide	D8418	Sigma-Aldrich (Austria)
Disodium hydrogen phosphate Na_2HPO_4	71645	Sigma-Aldrich (Austria)
Dithiothreitol (DTT)	1008	Gerbu (Germany)
Dulbecco's Modified Eagle's Medium (DMEM)	D5648-10X1L	Sigma-Aldrich (Germany)
Eagle's Minimum essential medium	M0268-10X1L	Sigma-Aldrich (Germany)
Egg PC L-α-phosphatidylcholine (Egg, Chicken)	840051 P	Avanti Polar Lipids (USA)
Ethanol	32221	Sigma-Aldrich (Austria)
Ethyl acetate	320307	Sigma-Aldrich (Austria)

Compound	Catalogue- or Cas-Number	Purchaser
Ethylenediaminetetraacetic acid (EDTA)	1034	Gerbu (Germany)
Fetal bovine serum	A15-104	PAA Laboratories (Austria)
Formaldehyde Solution	47608	Sigma-Aldrich (Austria)
Glycerol	2006	Gerbu (Germany)
Glycine	G7126-1G	Sigma-Aldrich (Austria)
Hydrochloric acid (HCl)	100317	Merck (Austria)
Iron (III) chloride hexahydrate	236489	Sigma-Aldrich (Austria)
Isopropanol	109634	Merck (Austria)
LysoTracker® Red DND-99 *1mM solution in DMSO* *special packaging*	L-7528	Invitrogen (Austria)
Mc Coy's 5A medium	M4892-10XL	Sigma-Aldrich (Germany)
Methanol	34860-1L-R	Sigma-Aldrich (Austria)
$MgCl_2$	63072	Sigma-Aldrich (Austria)
MitoTracker® Orange CMTMRos *special packaging*	M-7510	Invitrogen (Austria)
Neomycin trisulfate salt hydrate	N6386	Sigma-Aldrich (Austria)
Non essential amino acids	M11-003	PAA Laboratories (Austria)
Penicilin/Streptomycin	P11-010	PAA Laboratories (Austria)
Phenylmethanesulfonylfluoride (PMSF)	P-7626	Sigma-Aldrich (Austria)
Phosphatase Inhibitor Cocktail 2	P0044	Sigma-Aldrich (Austria)
Phosphatase Inhibitor cocktail 3	P5726	Sigma-Aldrich (Austria)
Phosphate buffered saline 100x (PBS)	P5368	Sigma-Aldrich (Austria)
Protease Inhibitor Cocktail Complete Mini	11836153001	Roche (Austria)
Roti®Mount Fluo Care	Art: HP 19.1	Carl ROTH (Germany)
Roti®Mount Fluo Care DAPI	Art: HP 20.1	Carl ROTH (Germany)
RPMI-1640 with L-glutamine	R6504-10X1L	
Sodium bicarbonate	S-5761	Sigma-Aldrich (Germany)
Sodium dihydrogen phosphate NaH_2PO_4	71506	Sigma-Aldrich (Austria)
Sodium Dodecyl Sulfate (SDS)	L-4509	Sigma-Aldrich (Austria)
Sodium hydroxide solution (NaOH)	2020	Gerbu (Germany)
Sodium pyrovate	P2256-5G	Sigma-Aldrich (Germany)

Compound	Catalogue- or Cas-Number	Purchaser
Sucrose	1366	Gerbu (Germany)
Sulfuric Acid	CAS-Number 7664-93-9	Riedel-deHaën (Germany)
TEMED	35925	Serva (Germany)
Tris(hydroxymethyl)-aminomethan/hydrochloric acid (Tris/HCl)	1018	Gerbu (Germany)
Triton X-100	9002-93-1	Gerbu (Germany)
Trypan Blue solution	T8154	Sigma-Aldrich (Austria)
Trypsin	L11-658	PAA Laboratories (Austria)
Trypsin-EDTA	L11-660	PAA Laboratories (Austria)
Urea	1044	Gerbu (Germany)
β-cyclodextrin $(C_6H_{10}O_5)_7$	17688	Serva (Germany)

Table 5-1 Description of all chemicals and solutions, with Catalogue- or CAS-number and respective purchasing company, used in experiments.

Methods

5.1.1 Cell Culture

Cell culture reagents were obtained from Sigma Aldrich (Austria), Euroclone (Austria) and PAA-Laboratories (Austria). Cell lines were purchased from American Type Culture Collection (ATCC, Manassas, USA).

5.1.1.1 L929 murine subcutaneous connective tissue fibroblasts

L929 cells were routinely grown in DMEM (high glucose - 4500mg glucose), containing 4.5mM L-glutamine, 18mM sodium-bicarbonate, 100U/ml penicillin, 100µg/ml streptomycin and 10% fetal bovine serum, in a 6% CO_2 humidified atmosphere, at 37°C. Cells were fed 3 times a week and passaged once a week. For passaging, the cells were treated with 1x trypsin and a new medium is inoculated with a 1:20 dilution of cells.

5.1.1.2 HTB2 benign human urinary bladder transitional papilloma cells

HTB2 cells were routinely grown in Mc Coy's 5A medium, containing 26 mM sodium-bicarbonate, 100U/ml penicillin, 100µg/ml streptomycin and 10% fetal bovine serum, in a 6% CO_2 humidified atmosphere, at 37°C. Cells were fed 3 times a week and passaged once a week. For passaging, the cells were treated with 1x trypsin EDTA, containing 0,5mg/ml trypsin and 0,22mg/ml EDTA (Titriplex III), and a new medium is inoculated with a 1:6 dilution of cells.

5.1.1.3 HTB9 grade II malign human urinary bladder carcinoma cells

HTB9 cells were routinely grown in RPMI-1640 with L-glutamine, containing 18mM sodium-bicarbonate, 100U/ml penicillin, 100µg/ml streptomycin and 10% fetal bovine serum, in a 6% CO_2 humidified atmosphere, at 37°C. Cells were fed 3 times a week and passaged once a week. For passaging, the cells were treated with 1x trypsin EDTA, containing 0,5mg/ml trypsin and 0,22mg/ml EDTA (Titriplex III), and a new medium is inoculated with a 1:6 dilution of cells.

5.1.1.4 HTB5 grade IV malign human urinary bladder transitional carcinoma cells

HTB5 cells were routinely grown in Eagle's Minimum essential medium, containing 26mM sodium-bicarbonate, 110mg/l sodium-pyruvate, 1% non essential amino acids, 100U/ml penicillin, 100µg/ml streptomycin and 10% fetal bovine serum, in a 6% CO_2 humidified atmosphere, at 37°C. Cells were fed 3 times a week and passaged once a week. For passaging, the cells were treated with 1x trypsin EDTA, containing 0,5mg/ml trypsin and 0,22mg/ml EDTA (Titriplex III), and a new medium is inoculated with a 1:5 dilution of cells.

5.1.2 Cell Counting

Cell counting was performed using a Bürker-Türk counting chamber, for calculating the cell numbers of L929, HTB2, HTB9 and HTB5 cells before seeding and when splitting. Scrapped or trypsinized cells were diluted to a countable cell density and after counting the cells in all 16 squares of the chamber, to diminish counting errors, the respective cell number was obtained through the following calculation:

$$\frac{\text{cell number} \quad x \quad \text{dilution factor}}{\text{counted area [mm}^2\text{]} \quad x \quad \text{chamber depth [mm]}} \times 1000 = \frac{\text{cells}}{\text{ml}}$$

Because the counted area consists of 16 squares of 0.04 mm^2 each, and taking into account a chamber depth of 0.1mm, a product of 0.064 was calculated for the 2 values below the fraction bar. The simplified version of the upper formula is thus:

$$\frac{\text{cell number} \quad x \quad \text{dilution factor}}{0.064\ \text{mm}^3} \times 1000 = \frac{\text{cells}}{\text{ml}}$$

The whole counting chamber and the cover glass were washed with 75% ethanol and dried after every count.

5.1.3 Assembly of Onkovidon®

Assembly of the Onkovidon® dye was achieved through dissolving 10mg/ml of β-cyclodextrin in ddH_2O followed by sonication, at 50°C for 25min, which resulted in a 10mM β-cyclodextrin solution. A 60µM ethanolic stock solution of Coumarin6 was then diluted 1:20 in the 10mM β-cyclodextrin solution, resulting in a 3µM Onkovidon® stock. This stock solution could be stored at 4°C for several days.

The 3µM Onkovidon® stock was then treated in 3 different ways. Either it was diluted 1:100, in 1 x PBS and used to incubate cells directly with the thereby achieved 30nM Onkovidon® staining solution, or it was lyophilized o/n by one of two possible ways.

The first possibility was to pipette 20µl of 3µM Onkovidon® stock into 2ml Eppendorf tubes with angled bottom. After o/n lyophilization, a dilution of scrapped cells was then pipetted into the Eppendorf tube, with the Onkovidon® powder, in an amount of 2ml, resulting in a 30nM Onkovidon® staining solution.

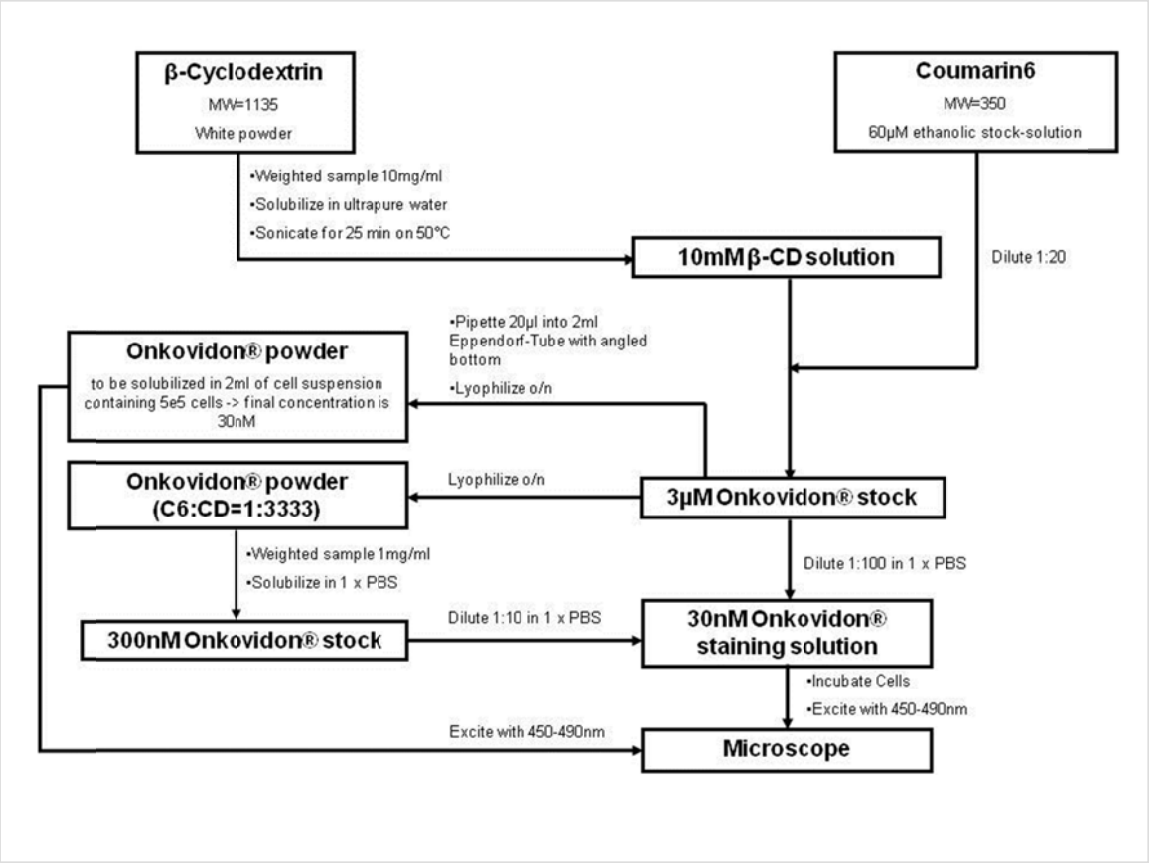

Figure 5-1: Exact assembly instructions of the Onkovidon® dye.
Because the basic components of the dye exist as powders, it was of crucial importance to bring them into solution to make staining of cultured cell lines possible. As cyclodextrins are very well water soluble and then still keep a hydrophobic cavity, they are very good delivering vectors to the plasma membrane, for hydrophobic compounds, like Coumarin6.

The second possibility was to lyophilize a large quantity of the 3µM Onkovidon® stock in a plastic capped 25ml glass, resulting in an Onkovidon® powder, with a ratio of Coumarin6:β-cyclodextrin of 1:3333. Dissolving 1mg/ml of this powder in 1 x PBS gave a 300nM Onkovidon® stock, which could then be diluted again 1:10, in 1 x PBS, to achieve a 30nM Onkovidon® staining solution.

5.1.4 Cholesterol Measurement

5.1.4.1 Preparation of membrane fractions of cultured cells

For the preparation of membrane fractions L929, HTB2, HTB9 and HTB5 cells were grown in 100mm cell culture dishes to a confluency of 80 to 100%. Cells were scrapped and centrifuged for 5 minutes at 735 x g, using a bench centrifuge. After discarding the supernatants, 100µl of Phosphate Extraction Buffer were added to each pellet and cells were observed every five minutes, using a light microscope, to verify cell death by osmolysis. When at least 80% of cells were osmolysed they were transferred to 15ml Falcons resuspended thoroughly through a 23gg syringe needle first and through a 27gg syringe needle afterwards, with 50 strokes each time. Suspensions were then transferred to Eppendorf tubes and centrifuged at 4°C for 10 minutes, at 82 x g, in a bench centrifuge for sedimentation of cell debris. Supernatants, which can be seen as a crude homogenate, were carefully removed and the pellets were discarded. 60µl of each crude homogenate were mixed with 60µl of 5x SDS- sample buffer and incubated for 5min, at 95°C. After cooling down they were stored at -80°C for subsequent analysis. The rest of each crude homogenate was then balanced in ultracentrifuge tubes and re-centrifuged at 4°C for 1h, at 53000rpm (TLA-120.2), in a Beckman TLX ultracentrifuge to pellet crude membrane vesicles. Supernatants, which can be seen as the cytosolic fractions, were again removed carefully with a needle and treated as described for the crude homogenates. Each pellet was rinsed with 300µl of phosphate extraction buffer and then re-homogenized in 1/8 volume, compared to the volume of phosphate extrac-

tion buffer used in the first homogenization step, of phosphate detergent extraction buffer by 50 times up and down pipetting, with a yellow pipette tip. Then they were incubated on a rocking platform, at 4°C for 1h to extract the membranes and again centrifuged at 4°C for 10min, at 20000rpm (TLA-45), in a Beckman TLX ultracentrifuge. Supernatants, which can be seen as crude membrane extracts, were again carefully removed to fresh Eppendorf tubes with a needle, and again 60µl aliquots were treated as described for the crude homogenates. The crude membrane extracts were used later on for extraction and quantification of membrane cholesterol.

Phosphate Extraction Buffer	Phosphate Detergent Extraction Buffer	5 x SDS-Sample Buffer
20mM sodium-pyrophosphate	20mM sodium-pyrophosphate	400mM Tris/HCl
20mM sodium phosphate	20mM sodium phosphate	10% (v/v) SDS
0,5mM EDTA	0,5mM EDTA	50% (v/v) Glycerol
1mM $MgCl_2$	1mM $MgCl_2$	500mM DTT
0,303M Sucrose	0,303M Sucrose	0,1% Bromphenolblue
pH 7,4	pH 7,4	pH 6,8
2mM PMSF	2mM PMSF	
Protease Inhibitor Cocktail	Protease Inhibitor Cocktail	
	Phosphatase Inhibitor Cocktail 1	
	Phosphatase Inhibitor Cocktail 2	
	1% (v/v) Triton X-100	
	0,1 % (v/v) SDS	

Table 5-2: Recipes, concentrations and amount of chemicals for phosphate extraction buffer, phosphate detergent extraction buffer and 5 x SDS-sample buffer.

For gathering cytoskeletal fractions the pellets of the last centrifugation step were rinsed in 300µl of phosphate extraction buffer again, followed by re-homogenization in 1/8 volume, compared to the volume of phosphate extraction buffer used in the first homogenization step, of 8M Urea and incubation on a rocking platform at RT for 30min. Again 60µl aliquots of these cytoskeletal fractions were treated as described for the crude homogenates. For subsequent analysis every aliquot should be incubated at 65°C for 10min before loading on gels.

5.1.4.2 Polyacrylamid gels

PAA-gels were used to prove successful membrane isolation and to quantify and compare the concentration of membrane isolates gathered from L929, HTB2, HTB9 and HTB5 cell lines. PAA-gels actually consisted of two gels that were casted in the same gel-casting equipment, starting with a 10 % resolving gel followed by 5% stacking gel. For producing the gels ddH_2O, 30% acrylamid mix, 10% SDS, 10% ammonium persulfate and 1.5M Tris, differing in pH for resolving and stacking gels were mixed together in 50ml Falcons, and TEMED was added in the end to start the polymerization process.

For 5ml of a 10% resolving gel	Ml	For 2ml of a 5% stacking gel	Ml
H20	1.9	H20	1.4
30% acrylamide mix	1.7	30% acrylamide mix	0.33
1.5M Tris pH 8.8	1.3	1.5M Tris pH 6.8	0.25
10% SDS	0.05	10% SDS	0.02
10% ammonium persulfate	0.05	10% ammonium persulfate	0.02
TEMED	0.003	TEMED	0.002

Table 5-3: Recipes and amount of chemicals for a 10% resolving gel and for a 5% stacking gel. Recipes differ only in the pH of Tris.

After casting the resolving gel it was covered with isopropanol and given approximately 20min to polymerize. Isopropanol was then removed and the stacking gel was casted on top, using a plastic comb to produce loading slots. After 20min for polymerization of the stacking gel, the comb was removed, after the equipment was put in an electrophoresis apparatus and was covered with an electrophoresis buffer, and membrane isolates were loaded. Electrophoresis was performed at 20mA and 500V for about 1.5h, till the gel ran out. Photodensiometric analysis was performed after Coomassie-staining and -destaining of the gels.

Electrophoresis buffer
25mM Tris
250mM Glycine
0,1% SDS

Table 5-4: Recipe and concentration of chemicals for electrophoresis buffer.

5.1.4.3 Coomassie-staining and -destaining

After electrophoresis the PAA-gels were incubated in Coomassie staining solution at RT for 30min, followed by incubation in destaining solution for approximately 1h, for reducing the background and to strengthen the contrast.

Coomassie staining solution	Coomassie destaining solution
0,5g Coomassie Blue R250	10% acetic acid
400ml methanol	30% methanol
70ml acetic acid	60% ddH_2O
ddH_2O to 1l	

Table 5-5: Recipes, concentrations and amounts of chemicals for Coomassie staining solution and Coomassie destaining solution.

5.1.4.4 Photodensiometric analysis of PAA-gels with Quantiscan

After application of the Coomassie-staining the gels were scanned and the pixel intensities of the most prominent bands were analyzed, with Quantiscan from Biosoft®. Thus, the crude membrane extracts could be normalized to each other.

5.1.4.5 Spectroscopic measurement of membrane cholesterol

Spectroscopic measurement of membrane cholesterol was performed using crude membrane extracts obtained through preparation of membrane fractions from L929, HTB2, HTB9, HTB5 cells, using a photospectrometer. Crude membrane extracts were either used pure or diluted, according to the values gathered from photodensiometric analysis. Cholesterol standard solutions, of 100mM, 50mM 25mM,

12.5mM, 6.25mM, 3.13mM, 1.56mM, 0.78mM, 0.39mM, 0.2mM and 0.1mM, were produced through dilution of pure Cholesterol in 95% EtOH. A ferric chloride solution was produced as stock by dissolving 100mg Iron (III) chloride hexahydrate in 100ml ethyl acetate. Reagent blanks were produced through the procedure described below, omitting crude membrane extracts or standard solutions and using the same amount of EtOH 95% instead.

100µl of pure or diluted crude membrane extracts or cholesterol standard solutions were added to 1.9ml of EtOH 95% and shaken on a vortex-mixer for 15sec, followed by centrifugation for 10min at 1000g. 0.5ml of each supernatant was then transferred to 15ml Falcons and 2ml of ferric chloride solution were added into each case. The resulting solutions were mixed and allowed to stand for 10min. Then, the Falcons were cooled by immersion on ice and 2ml of concentrated sulfuric acid were added very slowly while continually swirling the tubes. Again the resulting solutions were allowed to stand for 10min. 1ml out of each Falcon was then transferred to plastic cuvettes and the absorbance was read at 560nm; first for the reagent blank; second for the standard solutions against the reagent blank and then, for the crude membrane fractions against the reagent blank. A standard curve was drawn from the data gathered from the standard solutions and the values of the crude membrane extracts were plotted on this.

5.1.5 Viable staining of adherent cells for epifluorescence and laser scanning microscopy

Viable cell staining was performed on adherent L929, HTB2, HTB9 and HTB5 cells either grown in LabTek™ Chambered Coverglasses, to a density of $5x10^5$ cells per observed chamber, or in 60mm cell culture dishes to a population of $5x10^5$ cells per dish. Staining was performed in the device cells were grown in, and dyes were chosen and applied depending on the fluorescence microscopy method. Cells were then subjected to laser scanning or epifluorescence microscopy.

Due to the filterset on the inverted Zeiss AXIOVERT S100TV epifluorescence microscope, used in our lab, staining performed for epifluorescence microscopy was always a single staining, with only the Onkovidon® dye alone. Routinely, cells were washed with 1 x PBS twice, then incubated with the Onkovidon® staining solution, as described for staining with Onkovidon®, and observed under the epifluorescence microscope.

Staining for laser scanning microscopy was always a double staining, done with the Onkovidon® dye and either with Mito-Tracker® Orange CMTMRos (554/576), Lyso-Tracker® Red DND-99 (577/590) or BODIPY® 558/568 C_{12}, whereupon one of the three tracker substances, mentioned above, was applied first (see staining with Mito-Tracker® Orange CMTMRos (554/576), Lyso-Tracker® Red DND-99 (577/590) or BODIPY® 558/568 C_{12}), after removing the particular medium and rinsing the cells in 1 x PBS. After incubation with one of these tracker substances, cells were rinsed in 1 x PBS and incubated with appropriate media for 30min to recover from the staining procedure. Then the Onkovidon® staining solution was applied (see staining with Onkovidon®), followed by replacement of the dye with appropriate medium. Then cells were observed alive using a Zeiss LSM 510 confocal microscope. Due to the possible overlay of excitation and detection maxima of the chosen dyes, it was not possible to perform triple or quadruple staining.

5.1.5.1 Staining with Mito-Tracker® Orange CMTMRos (554/576)

1mM stock solutions were obtained by dissolving 50µg of lyophilized solid (which is the content of one vial) in 117µl of DMSO and can be stored at -20°C, when protected from light. After warming up one vial to room temperature it was briefly centrifuged, using a bench centrifuge, to deposit the DMSO solution at the bottom of the vial. Stock solutions were diluted in appropriate media to a final working concentration of 10nM, to prepare staining solutions. Cells were then incubated with the prewarmed staining solutions (37°C) for 10min and then treated, as described above, for laser scanning microscopy.

5.1.5.2 Staining with Lyso-Tracker® Red DND-99 (577/590)

This tracker substance was already delivered as 1mM stock solutions, one vial containing 50µl of DMSO stock solution. After warming up one vial to room temperature it was briefly centrifuged, using a bench centrifuge, to deposit the DMSO solution at the bottom of the vial. The stock solution was then diluted in appropriate media to a final working concentration of 50nM, to prepare staining solutions. Cells were then incubated with the prewarmed staining solutions (37°C) for 30min and then treated, as described above, for laser scanning microscopy.

5.1.5.3 Staining with BODIPY® 558/568 C_{12}

1mM stock solutions were obtained by dissolving 1mg of lyophilized solid (which is the content of one vial) in 2117µl of acetonitrile. After warming up one vial to room temperature it was briefly centrifuged, using a bench centrifuge, to deposit the acetonitrile solution at the bottom of the vial. The stock solution was then diluted in appropriate media, to a final working concentration of 20nM, to prepare staining solutions. Cells were then incubated with the prewarmed staining solutions (37°C) for 20min and then treated, as described above, for laser scanning microscopy.

5.1.5.4 Staining with Onkovidon®

For the purpose of cell staining a 300nM stock solution was obtained by dissolving 1mg of lyophilized Onkovidon®-Powder in 1ml of 1 x PBS, in a plastic capped 5ml glass, through shaking on a vortex-mixer. The stock solution was then diluted in 1 x PBS to a final working concentration of 30nM, to prepare staining solutions. Cells were then incubated with prewarmed staining solutions (37°C) for 10min and then treated, as described above, for laser scanning or epifluorescence microscopy.

5.1.6 Staining and fixing of adherent cells for epifluorescence and laser scanning microscopy

Staining and fixing procedures were performed on adherent L929, HTB2, HTB5 and HTB9 cells grown on coverslips, in 60mm cell culture dishes, to a density of $5x10^5$ cells per dish, as it was pointed out to be necessary because cells started to get apoptotic fast, when observed alive in a Zeiss LSM 510 confocal microscope. For the staining procedures the coverslips were transferred to 10mm cell culture dishes and they were always kept under 1 x PBS, to not run dry, when they were not in treatment.

The applied staining procedure was identical to the procedure described above for the viable staining of adherent cells, for laser scanning microscopy, with the difference that coverslips had to be treated, instead of using LabTek™ Chambered Coverglasses or cell culture dishes. At the step where Onkovidon® is replaced with appropriate media, cells were rinsed with 1 x PBS twice, instead. Then they were incubated with a 3.7% paraformaldehyde solution, at RT for 45min, in an extractor hood and immediately afterwards they were incubated with 0.1M glycine, at RT for 5min, for quenching issues. Again cells were rinsed with 1 x PBS, then in ddH_2O. After drying, the coverslips were mounted with Roti®Mount Fluo Care mounting medium, on object carriers. The gathered slides were then subjected to laser scanning microscopy, but can also be used for epifluorescence microscopy.

5.1.7 Giant unilamellar vesicle formation and staining

Giant unilamellar vesicles were prepared by electroformation in an investigation chamber, which consisted of two platinum wires fixed parallel in a polyvinylidene fluoride casing. The bottom of the chamber contained a 0.5mm piece of borosilicate glass glued to the casing and the top of the chamber was open to enable micromanipulation.

The chosen lipids were dissolved in methanol:diethylether (1:9, v/v), at a concentration of 0.2mg ml^{-1}. A drop of approximately 10µl was carefully deposited all along the two wires with a Hamilton Syringe. The lipid film was then dried under an argon stream for about one minute and afterwards dried under vacuum in a dessicator for at least 15h, preferentially o/n. The investigation Chamber was then put on the stage of a light/epifluorescence microscope (Zeiss Axiovert S100 TV) and connected to a frequency generator (HP 34401A Multimeter), generating an AC field of 2V and 10Hz. 900µl of ddH_2O were added to the chamber and the growing vesicles were directly observed by light microscopy. After 30min vesicle formation was stopped by switching off the frequency generator. If an adequate number of vesicles had formed, vesicles were then stained with Onkovidon®, at RT for 10min, directly on the stage of the microscope, by adding 100µl of 300nM stock solution, resulting in a final working concentration of 30nM Onkovidon®. Vesicles were then observed and detected using transmitted light and epifluorescence microscopy.

5.1.8 Inactivation of active transport processes

Inactivation of active transport mechanisms was performed on adherent L929, HTB2, HTB9 and HTB5 cells. Cells were grown in 60mm cell culture dishes to a density of $5x10^5$ cells per dish.

The dishes were simply transferred from the incubator to an especially designed cooling plate, located in a covered polystyrene box. The cooling plate was connected to a cooling trap, filled with an anti-freezing agent. The cooling trap had to be engaged 30min before the start of the experiments to allow the whole system to cool down. Temperature measurement of the anti-freezing agent as well as of the cooling plate itself, showed that the liquid was cooled down to -10°C, resulting in a temperature of the cooling plate of 0°C. Thus, it was possible to cool down the cell culture dishes to temperatures between 0°C and 4°C, within 30 minutes, thereby causing an inactivation of all active transport mechanisms.

Old medium was removed from the chilled cell culture dishes, which were then rinsed once with ice cold 1 x PBS and incubated with ice cold 30nM Onkovidon® staining solution for 10min, while dishes were held on the cooling plate in the box. They were then quickly subjected to epifluorescence microscopy.

5.1.9 Long term incubation with Onkovidon®

Long term incubation, with the Onkovidon® dye, was performed on L929, HTB2, HTB9 and HTB5 cells. Cells were grown in LabTek™ Chambered Coverglasses to a density of $5x10^5$ cells per observed chamber. Old medium was then removed from each chamber and cells were rinsed with 1 x PBS, followed by incubation at 37°C, with 30nM Onkovidon® staining solutions diluted in appropriate media for each cell type. These staining solutions were left on the cells for the next 48 hours. Cells were observed 10min after start of the incubation, as well as after 24 hours and after 48 hours. Cells were observed using epifluorescence microscopy and pictures were taken at the mentioned time points.

5.1.10 Neomycin-induced cell death

Adherent L929, HTB2, HTB9, HTB5 cells were killed through application of neomycin. Neomycin trisulfate salt hydrate-powder was dissolved at a concentration of 50mg/ml, in ddH_2O, resulting in a 55mM stock solution. This stock solution could be stored at 4°C for 2 weeks. The stock solution was diluted to working solutions of 1600mg/l, 800mg/l, 400mg/l, 200mg/l, 100mg/l and 50mg/l, to perform a screen on L929, HTB2, HTB9 and HTB5 cells, and to verify the optimal working concentration of 50mg/l proposed by the purchaser. The optimal working concentration was found to be between 100mg/l and the proposed 50mg/l for all 4 cell lines. As a consequence and to reduce incubation time, cells were killed by application of 100mg/l of neomycin trisulfate salt hydrate-powder, dissolved in ddH_2O for 1h.

After incubation, with neomycin, cells were stained with Onkovidon® staining solution, as described for the staining with Onkovidon®, and subjected to epifluorescence microscopy. Then cells were rinsed in 1 x PBS and incubated at RT for 4min, with a 0.4% Trypan Blue solution. Trypan Blue was then removed and cells were covered in 1 x PBS, and subjected again to the epifluorescence, as well as to transmitted light microscopy.

5.1.11 Epifluorescence microscopy

Epifluorescence images were taken using a Zeiss AXIOVERT S100TV epifluorescence microscope, with appropriate filter settings and at 10x, 20x or 63x magnifications. For quantification of images see Image analysis.

5.1.12 Laser scanning microscopy

Z-stack images were taken using a Zeiss LSM 510 confocal microscope, with appropriate filter settings and at 100x magnifications. 3-dimensional reconstruction of Z-stack images and post-processing of single layers of Z-stack images were done using the Zeiss Zen 2009 software, as well as the Zeiss LSM Image Browser.

5.1.13 Image analysis

For quantification, images were analyzed using the cell counting- and area determination-tool of Adobe® Photoshop CS4 (image processing software). Chosen images were counted for distinguishable cells and the covered area was also determined for each cell. Photoshop then calculated a grey scale value, as well as an area and perimeter value for each counted cell. Gathered values were cleaned from outliers and further processed using Microsoft Exel 2007, resulting in mean values for fluorescence intensity, cell size and perimeter and appropriate graphs.

5.1.14 Ab initio calculations

The quantum chemical calculations were performed using the GAUSSIAN09 program package [77]. The structures of coumarin 6 and β-cyclodextrin were fully optimized by HF, with 3-21G basis set. Complexes between coumarin 6 and β-cyclodextrins were built and optimized by HF/3-21G.

6 Abbreviations

%	Percent
°C	Degrees Celcius
µg	Microgram
µg/ml	Microgram per milliliter
µl	Microliter
µM	Micromole
μm^2	Square micrometer
AC	Alternating current
ADRP	Adipose differentiation-related protein = Adipophilin
ATCC	American Type Culture Collection
ATP	Adenosine tri-phosphate
C6	Coumarin 6
C6:CD	Coumarin 6 : Cyclodextrin
C6:β-CD complex	Coumarin 6 : β-Cyclodextrin complex
C-C axis	Carbon-carbon axis
C-C bond	Carbon-carbon bond
CD 51/54/68/138	Cluster of differentiation
CDs	Cyclodextrin(s)
CGTase	Cyclomaltodextrin glucanotransferase
Cis double bond	Carbon-carbon double bond, with both remaining H-atoms on the same side
CK 5/6/7/20	Cytokeratin 5/6/7/20
CO_2	Carbon dioxide
CTCs	Circulating tumor cells
Da	Dalton
ddH_2O	Double distilled water = ultrapure water
DMPC	Dimyristoylphosphatidylcholine
DMSO	Dimethylsulfoxide
DTT	Dithiothreitol
EDTA	Ethylenediaminetetraacetic acid
EggPC	Egg phosphatidylcholine
ER	Endoplasmic reticulum

EtOH	Ethanol
FCS	Fluorescence correlation spectroscopy
g	G-Force
GAG	Glycosaminoglycan
GUVs	Giant unilamellar vesicle(s)
H	Hour
H-bond	Hydrogen bond
HDL	High density lipoprotein
Hz	Hertz
IDL	Intermediate density lipoprotein
Ki67	Antigen KI-67
LDL	Low density lipoprotein
LMP	Lysosomal membrane permeabilization
LSM	Laser Scanning Microscope
M	Mol
mA	Milliampere
MAMs	Mitochondria associated membrane(s)
Mg	Milligram
mg ml^{-1}	Milligram per milliliter
mg/l	Milligram per liter
mg/ml	Milligram per milliliter
$MgCl_2$	Magnesium chloride
Min	Minute
Ml	Milliliter
mM	Milimol
Mm	Millimeter
mm^2	Square millimeter
mm^3	Cubic millimeter
N-linked	N-linked glycans are attached to a nitrogen of asparagine or arginine side-chains
Nm	Nanometer
nM	Nanomol
o/n	Over night
OH-group	Hydroxyl group
O-linked	O-linked glycans are attached to the hydroxyl oxygen of serine, threonine, tyrosine, hydroxylysine, or hydroxyproline side-chains, or to oxygens on lipids such as ceramide

p53	Tumor protein 53 = tumor suppressor
PAA	Poly acryl amide
PAA-gels	Poly acryl amide-gels
PBS	Phosphate buffered saline
PE	Phosphatidylethanolamine
PFA	Paraformaldehyde
PI	Phosphatidylinositol
PMSF	Phenylmethanesulfonylfluoride
POPC	Phosphatidylcholine
PS	Phospahtidylserine
Rpm	Rounds per minute
RT	Room temperature
SDS-gels	Sodium dodecyl sulfate-gels
Sec	Second
SM	Sphingomyelin
SNARE	**S**oluble NSF **A**ttachment **P**rotein **Re**ceptor
TEMED	Tetramethylethylenediamine
THF	Tetrahydrofuran
TTF-1	Transcription termination factor 1
U/ml	Units per milliliter
UV	Ultra violet
V	Volt
v/v	Volume per volume
VLDL	Very low density lipoprotein
β-CD	B-cyclodextrin
EpCAM	Epithelial cell adhesion molecule

7 Index of Figures

8 Index of Tables

9 Synopsis

Cyclodextrins are capable of forming host-guest complexes and thus, provide a hydrophilic envelope for otherwise poorly water-soluble substances. Thereby, they can function as a delivery system for hydrophobic molecules towards cells, no matter if tissue cultured or part of multicellular organisms. It was the aim of this study to gather basic information by microscopic imaging, for quantitative and qualitative analysis, about the staining properties of a newly developed dye. The dye, consisting of β-cyclodextrin complexed with the hydrophobic laser dye molecule coumarin 6, was applied on tissue cultured bladder cancer cells, as well as on artificially produced, transport protein free, giant unilamellar vesicles. Coumarin 6 was shown, by epifluorescence microscopy, to incorporate fast and nonspecifically into the plasma membranes of 4 chosen cell lines, in a temperature- and cell viability- independent manner. Applied on living cells, it did not affect cell viability and the staining process seemed to correlate with cholesterol concentration, exhibiting that higher cholesterol concentrations led to weaker staining. It also incorporated into the artificially produced membranes and thus, led to an overall strengthening of the theory, that the staining process functions by diffusion once the dye is delivered to the proximity of membranes by the complex-forming β-cyclodextrin. Laser scanning microscopy uncovered morphological flattening of cells, due to cytoskeletal breakdown, with rising malignancy. It showed intracellular staining of lysosomes, mitochondria and lipid droplets in each of the 4 cell lines. As the existence of droplets was only confirmed for the cells of highest malignancy (HTB5), we discovered that HTB2 and HTB9 human bladder cancels, as well as L929 murine fibroblasts harbor these organelles also, and that these localize basally in the cytoplasm. We conclude that the dye complex delivers the encased coumarin 6 to the plasma membrane, where it incorporates and diffuses further to stain intracellular membrane

systems and thus, making it possible to effectively stain tissue cultured cells, within short incubation times and without harming cells.

10 Synopsis (German)

Cyclodextrine sind geeignet Einschlussverbindungen zu bilden und bieten dadurch eine hydrophile Hülle für ansonsten in Wasser unlösliche Substanzen. Dadurch bieten sie die Möglichkeit hydrophobe Moleküle an Zellen zu liefern, unabhängig ob es sich dabei um Kulturzellen oder multizelluläre Organismen handelt. Ziel dieser Studie war es Grundlagen-Information über die Färbeeigenschaften eines neu entwickelten Farbstoffes, durch quantitative und qualitative Analyse mikroskopischer Bilder, zu sammeln. Der Farbstoff, bestehend aus β-Cyclodextrin, komplexiert mit dem hauptsächlich hydrophoben Laserfarbstoff Coumarin 6, wurde dazu sowohl auf Kulturzellen als auch auf künstlich erzeugte unilamellare Vesikel, welche keine Transportproteine beinhalteten, aufgebracht. Es konnte durch Epifluoreszenz-Mikroskopie gezeigt werden, dass Coumarin 6 schnell und unspezifisch, und das weder temperaturabhängig noch abhängig von der Zellviabiltät, an die Zellmembran von 4 ausgewählten Zelllinien bindet. Außerdem hatte der Färbeprozess keinen Einfluss auf die Lebensfähigkeit der Zellen und es stellte sich heraus, dass dieser mit der Cholesterin-Konzentration in Zusammenhang stand, als dass die Färbung bei höherer Cholesterin-Konzentration schwächer wurde. Dass der Farbstoff auch in die künstlich erzeugten Membranen inkorporierte, führte zu einer Stärkung der Theorie dass schlicht Diffusion für die Färbung verantwortlich ist, sobald dieser komplexiert mit β-Cyclodextrin in die Nähe der Zellmembran gelangt. Durch Laser Scanning Mikroskopie konnte außerdem festgestellt werden dass die morphologische Erscheinung der Zellen, bei zunehmender Malignität, flacher wurde, ausgelöst durch einen Zusammenbruch des Zytoskeletts. Außerdem konnte so gezeigt werden dass auch Lysosomen, Mitochondrien und Lipid Droplets in allen 4 Zelllinien gefärbt wurden. Da das Vorhandensein von Lipid Droplets nur für die Zellen höchster Malignität (HTB5) bekannt war, können wir darauf verweisen, dass diese außerdem in den humanen Blasenkrebslinien HTB2 und HTB9 und auch in

den murinen Fibroblasten, der Linie L929, vorkommen und basal im Zytosol lokalisiert sind. Zusammenfassend kann gesagt werden, dass mithilfe der Einschlußverbindung Coumarin 6 an die Zellmembran geliefert wird, von wo es nach erfolgter Inkorporation weiter diffundiert und intrazelluläre Membransysteme anfärbt. Dadurch ist eine effiziente, durch niedrige Inkubatuonszeiten gekennzeichnete, Färbung von Kulturzellen möglich, ohne diese zu schädigen.

11 Curriculum vitae

Personal Data

Name:	Christoph Miksch
Present address:	Ocwirkgasse 11/5/9, 1210 Vienna, Austria
Date of birth:	17.05.1983
Place of birth:	Vienna
Martial status:	Relationship
Parents:	Christine MIKSCH
	Dr. Georg MIKSCH

Education

1989-1993	Primary school, Maria Regina Döblinger Hauptstraße 83, Vienna
1993-2001	Secondary school, GRG19 Billrothstraße 73, Vienna
June 2001	High School Diploma
2001-2002	Military Service
2002-2004	Student of Dental Medicine

2004-2011 Student of Molecular Biology, and diploma thesis under the supervision of ao. Univ.-Prof. Dr. Gottfried KÖHLER, at the Department of Structural and Computational Biology, Max F. Perutz Laboratories GmbH, Campus Vienna Biocenter, University of Vienna, Dr. Bohrgasse 9, 1030 Vienna, Austria

Publications

2010 M. Edetsberger, M. Knapp, E. Gaubitzer, C. Miksch, K.E. Gvichiya, G. Köhler, Effective Staining of Tumor Cells by Coumarin-6 Depends on the Stoichiometry of Cyclodextrin Complex Formation, (2010).

2010 M. Edetsberger, E. Gaubitzer, C. Miksch, M. Knapp, B. Baluch, K.E. Gvichiya, I. Attassi, W. Smetana, G. Köhler, Detection of Malign Cells in Bio-Fluids for Diagnostic Purposes, (2010).

Language skills

German (native), English (fluent), French (basic), Italian (basic), Latin (basic)

12 References

[1] J.C. Skou, M. Esmann, The Na,K-ATPase, J Bioenerg Biomembr 24 (1992) 249-261.

[2] Y. Hatefi, ATP synthesis in mitochondria, Eur J Biochem 218 (1993) 759-767.

[3] J. Biarc, R.J. Chalkley, A.L. Burlingame, R.A. Bradshaw, Receptor tyrosine kinase signaling - a proteomic perspective, Advances in Enzyme Regulation (2010).

[4] G. van Meer, D.R. Voelker, G.W. Feigenson, Membrane lipids: where they are and how they behave, Nat Rev Mol Cell Biol 9 (2008) 112-124.

[5] M.A. Schwarz, K. Owaribe, J. Kartenbeck, W.W. Franke, Desmosomes and hemidesmosomes: constitutive molecular components, Annu Rev Cell Biol 6 (1990) 461-491.

[6] S.A. Carr, M.J. Huddleston, M.F. Bean, Selective identification and differentiation of N- and O-linked oligosaccharides in glycoproteins by liquid chromatography-mass spectrometry, Protein Sci 2 (1993) 183-196.

[7] M. Buckley, P. Xin, S. Washington, N. Herb, D. Erickson, V.P. Bhavanandan, Lectin histochemical examination of rabbit bladder glycoproteins and characterization of a mucin isolated from the bladder mucosa, Arch Biochem Biophys 375 (2000) 270-277.

[8] S. Teneberg, T.R. Hirst, J. Angstrom, K.A. Karlsson, Comparison of the glycolipid-binding specificities of cholera toxin and porcine Escherichia coli heat-labile enterotoxin: identification of a receptor-active non-ganglioside glycolipid for the heat-labile toxin in infant rabbit small intestine, Glycoconj J 11 (1994) 533-540.

[9] E.M. Bevers, P.L. Williamson, Phospholipid scramblase: an update, Febs Letters 584 (2010) 2724-2730.

[10] P. Bostrom, L. Andersson, M. Rutberg, J. Perman, U. Lidberg, B.R. Johansson, J. Fernandez-Rodriguez, J. Ericson, T. Nilsson, J. Boren, S.O. Olofsson, SNARE proteins mediate fusion between cytosolic lipid droplets and are implicated in insulin sensitivity, Nat Cell Biol 9 (2007) 1286-1293.

[11] G. Koster, M. VanDuijn, B. Hofs, M. Dogterom, Membrane tube formation from giant vesicles by dynamic association of motor proteins, Proc Natl Acad Sci U S A 100 (2003) 15583-15588.

[12] T. Rog, K. Murzyn, R. Gurbiel, Y. Takaoka, A. Kusumi, M. Pasenkiewicz-Gierula, Effects of phospholipid unsaturation on the bilayer nonpolar region: a molecular simulation study, J Lipid Res 45 (2004) 326-336.

[13] C.R. Gault, L.M. Obeid, Y.A. Hannun, An overview of sphingolipid metabolism: from synthesis to breakdown, Adv Exp Med Biol 688 (2010) 1-23.

[14] T. Rog, M. Pasenkiewicz-Gierula, Cholesterol-sphingomyelin interactions: a molecular dynamics simulation study, Biophys J 91 (2006) 3756-3767.

[15] D. Sarnataro, C. Grimaldi, S. Pisanti, P. Gazzerro, C. Laezza, C. Zurzolo, M. Bifulco, Plasma membrane and lysosomal localization of CB1 cannabinoid receptor are dependent on lipid rafts and regulated by anandamide in human breast cancer cells, Febs Letters 579 (2005) 6343-6349.

[16] R.H. Gensure, M.L. Zeidel, W.G. Hill, Lipid raft components cholesterol and sphingomyelin increase H+/OH- permeability of phosphatidylcholine membranes, Biochem J 398 (2006) 485-495.

[17] T. Irie, M. Otagiri, M. Sunada, K. Uekama, Y. Ohtani, Y. Yamada, Y. Sugiyama, Cyclodextrin-induced hemolysis and shape changes of human erythrocytes in vitro, J Pharmacobiodyn 5 (1982) 741-744.

[18] T. Kiss, F. Fenyvesi, I. Bacskay, J. Varadi, E. Fenyvesi, R. Ivanyi, L. Szente, A. Tosaki, M. Vecsernyes, Evaluation of the cytotoxicity of beta-cyclodextrin derivatives: evidence for the role of cholesterol extraction, Eur J Pharm Sci 40 (2010) 376-380.

[19] B. Alberts, A. Johnson, J. Lewis, M. Raff, K. Roberts, P. Walter, Molecular Biology of the Cell, 5th Edition, 2008.

[20] Z. Marijanovic, D. Laubner, G. Moller, C. Gege, B. Husen, J. Adamski, R. Breitling, Closing the gap: identification of human 3-ketosteroid reductase, the last unknown enzyme of mammalian cholesterol biosynthesis, Molecular Endocrinology 17 (2003) 1715-1725.

[21] A. Fredenrich, P. Bayer, Reverse cholesterol transport, high density lipoproteins and HDL cholesterol: recent data, Diabetes Metab 29 (2003) 201-205.

[22] S.G. Dahl, I. Sylte, A.W. Ravna, Structures and models of transporter proteins, Journal of Pharmacology and Experimental Therapeutics 309 (2004) 853-860.

[23] J.K. Zehmer, Y. Huang, G. Peng, J. Pu, R.G. Anderson, P. Liu, A role for lipid droplets in inter-membrane lipid traffic, Proteomics 9 (2009) 914-921.

[24] M. Jaattela, C. Cande, G. Kroemer, Lysosomes and mitochondria in the commitment to apoptosis: a potential role for cathepsin D and AIF, Cell Death Differ 11 (2004) 135-136.

[25] G. Daum, J.E. Vance, Import of lipids into mitochondria, Prog Lipid Res 36 (1997) 103-130.

[26] E.J. Lesnefsky, C.L. Hoppel, Oxidative phosphorylation and aging, Ageing Res Rev 5 (2006) 402-433.

[27] T. Kirkegaard, M. Jaattela, Lysosomal involvement in cell death and cancer, Biochim Biophys Acta 1793 (2009) 746-754.

[28] T. Kolter, K. Sandhoff, Lysosomal degradation of membrane lipids, Febs Letters 584 (2010) 1700-1712.

[29] T.C. Walther, R.V. Farese, Jr., The life of lipid droplets, Biochim Biophys Acta 1791 (2009) 459-466.

[30] C. Thiele, J. Spandl, Cell biology of lipid droplets, Current Opinion in Cell Biology 20 (2008) 378-385.

[31] M.T. Accioly, P. Pacheco, C.M. Maya-Monteiro, N. Carrossini, B.K. Robbs, S.S. Oliveira, C. Kaufmann, J.A. Morgado-Diaz, P.T. Bozza, J.P. Viola, Lipid bodies are reservoirs of cyclooxygenase-2 and sites of prostaglandin-E2 synthesis in colon cancer cells, Cancer Res 68 (2008) 1732-1740.

[32] P.T. Bozza, J.P. Viola, Lipid droplets in inflammation and cancer, Prostaglandins Leukot Essent Fatty Acids 82 (2010) 243-250.

[33] P. Targett-Adams, D. Chambers, S. Gledhill, R.G. Hope, J.F. Coy, A. Girod, J. McLauchlan, Live cell analysis and targeting of the lipid droplet-binding adipocyte differentiation-related protein, J Biol Chem 278 (2003) 15998-16007.

[34] S. Jagerstrom, S. Polesie, Y. Wickstrom, B.R. Johansson, H.D. Schroder, K. Hojlund, P. Bostrom, Lipid droplets interact with mitochondria using SNAP23, Cell Biol Int 33 (2009) 934-940.

[35] R.E. Hurst, R.M. Moldwin, S.G. Mulholland, Bladder defense molecules, urothelial differentiation, urinary biomarkers, and interstitial cystitis, Urology 69 (2007) 17-23.

[36] P. Rathert, S. Roth, (Eds.), Urinzytologie - Praxis und Atlas, 4th Edition, Springer Meizin Verlag, Heidelberg, 2007.

[37] S.P. Jost, J.A. Gosling, J.S. Dixon, The morphology of normal human bladder urothelium, J Anat 167 (1989) 103-115.

[38] P. Khandelwal, S.N. Abraham, G. Apodaca, Cell biology and physiology of the uroepithelium, Am J Physiol Renal Physiol 297 (2009) F1477-1501.

[39] J.H. Shanks, K.A. Iczkowski, Divergent differentiation in urothelial carcinoma and other bladder cancer subtypes with selected mimics, Histopathology 54 (2009) 885-900.

[40] R.M. Hicks, J.J. Wakefield, Membrane changes during urothelial hyperplasia and neoplasia, Cancer Res 36 (1976) 2502-2507.

[41] A.P. van der Meijden, Bladder cancer, BMJ 317 (1998) 1366-1369.

[42] S. Mustjoki, N. Sidenius, C.F. Sier, F. Blasi, E. Elonen, R. Alitalo, A. Vaheri, Soluble urokinase receptor levels correlate with number of circulating tumor cells in acute myeloid leukemia and decrease rapidly during chemotherapy, Cancer Res 60 (2000) 7126-7132.

[43] Y. Terada, H. Sanbe, T. Takaha, S. Kitahata, K. Koizumi, S. Okada, Comparative study of the cyclization reactions of three bacterial cyclomaltodextrin glucanotransferases, Appl Environ Microbiol 67 (2001) 1453-1460.

[44] T. Loftsson, D. Duchene, Cyclodextrins and their pharmaceutical applications, Int J Pharm 329 (2007) 1-11.

[45] V.J. Stella, Q. He, Cyclodextrins, Toxicol Pathol 36 (2008) 30-42.

[46] K.A. Connors, The Stability of Cyclodextrin Complexes in Solution, Chem Rev 97 (1997) 1325-1358.

[47] T. Loftsson, M.E. Brewster, Pharmaceutical applications of cyclodextrins. 1. Drug solubilization and stabilization, J Pharm Sci 85 (1996) 1017-1025.

[48] R. Challa, A. Ahuja, J. Ali, R.K. Khar, Cyclodextrins in drug delivery: an updated review, AAPS PharmSciTech 6 (2005) E329-357.

[49] D. Duchene, D. Wouessidjewe, G. Ponchel, Cyclodextrins and carrier systems, Journal of Controlled Release 62 (1999) 263-268.

[50] Z. Li, M. Wang, F. Wang, Z. Gu, G. Du, J. Wu, J. Chen, gamma-Cyclodextrin: a review on enzymatic production and applications, Appl Microbiol Biotechnol 77 (2007) 245-255.

[51] H.J. Buschmann, E. Schollmeyer, Applications of cyclodextrins in cosmetic products: A review, J Cosmet Sci 53 (2002) 185-191.

[52] P.J. Salustio, G. Feio, J.L. Figueirinhas, J.F. Pinto, H.M. Cabral Marques, The influence of the preparation methods on the inclusion of model drugs in a beta-cyclodextrin cavity, Eur J Pharm Biopharm 71 (2009) 377-386.

[53] K. Nakanishi, T. Nadai, M. Masada, K. Miyajima, Effect of cyclodextrins on biological membrane. II. Mechanism of enhancement on the intestinal absorption of non-absorbable drug by cyclodextrins, Chem Pharm Bull (Tokyo) 40 (1992) 1252-1256.

[54] B. Bang, R. Gniadecki, B. Gajkowska, Disruption of lipid rafts causes apoptotic cell death in HaCaT keratinocytes, Exp Dermatol 14 (2005) 266-272.

[55] F.A. Haskins, H.J. Gorz, Glucosides of coumarinic and o-coumaric acids in the tonka bean, Science 139 (1963) 496-497.

[56] J.R. Stoker, D.M. Bellis, The biosynthesis of coumarin in Melilotus alba, J Biol Chem 237 (1962) 2303-2305.

[57] NTP Toxicology and Carcinogenesis Studies of Coumarin (CAS No. 91-64-5) in F344/N Rats and B6C3F1 Mice (Gavage Studies), Natl Toxicol Program Tech Rep Ser 422 (1993) 1-340.

[58] G.A. Reynolds, K.H. Drexhage, New Coumarin Dyes with Rigidized Structure for Fashlamp-pumped Dye Lasers, Optical Communications 13 (1975) 222-225.

[59] M. Knapp, P. Wolschann, G. Köhler, Threading of β-Cyclodextrins on Coumarin-6 monitored by fluorescence spectroscopy, (2011).

[60] K. Rechthaler, G. Köhler, Excited State Properties and Deactivation Pathways of 7-Aminocoumarins, Chemical Physics 189 (1994) 99-116.

[61] K.P. Link, The discovery of dicumarol and its sequels, Circulation 19 (1959) 97-107.

[62] M.J. Fasco, P.P. Dymerski, J.D. Wos, L.S. Kaminsky, A new warfarin metabolite: structure and function, J Med Chem 21 (1978) 1054-1059.

[63] A. Lopes, J. Seixas de Melo, A.J. Martins, A.L. Macanita, F.S. Pina, H. Wamhoff, E. Melo, Partition of Pesticides of the Coumarin Family between Water and Amphiphilic Aggregates, Environmental Science & Technology 29 (1995) 564-570.

[64] M. Edetsberger, M. Knapp, E. Gaubitzer, C. Miksch, K.E. Gvichiya, G. Köhler, Effective Staining of Tumor Cells by Coumarin-6 Depends on the Stoichiometry of Cyclodextrin Complex Formation, (2010).

[65] M. Edetsberger, E. Gaubitzer, C. Miksch, M. Knapp, B. Baluch, K.E. Gvichiya, I. Attassi, W. Smetana, G. Köhler, Detection of Malign Cells in Bio-Fluids for Diagnostic Purposes, (2010).

[66] A.M. Denadai, K.I. Teixeira, M.M. Santoro, A.M. Pimenta, M.E. Cortes, R.D. Sinisterra, Supramolecular self-assembly of beta-cyclodextrin: an effective carrier of the antimicrobial agent chlorhexidine, Carbohydr Res 342 (2007) 2286-2296.

[67] J. Rodriguez, R. Semino, D. Laria, Building up nanotubes: docking of "Janus" cyclodextrins in solution, J Phys Chem B 113 (2009) 1241-1244.

[68] E.E. Daniel, K. Robinson, The relation of sodium secretion to metabolism in isolated sodium-rich uterine segments, J Physiol 154 (1960) 445-460.

[69] J.A. Harris, A.G. Cheng, L.L. Cunningham, G. MacDonald, D.W. Raible, E.W. Rubel, Neomycin-induced hair cell death and rapid regeneration in the lateral line of zebrafish (Danio rerio), J Assoc Res Otolaryngol 4 (2003) 219-234.

[70] J. Park, B.C. Sutradhar, G. Hong, S.H. Choi, G. Kim, Comparison of the cytotoxic effects of bupivacaine, lidocaine, and mepivacaine in equine articular chondrocytes, Vet Anaesth Analg 38 (2011) 127-133.

[71] S. Adler, C. Pellizzer, M. Paparella, T. Hartung, S. Bremer, The effects of solvents on embryonic stem cell differentiation, Toxicol In Vitro 20 (2006) 265-271.

[72] A.E. Ahmed, J.P. Loh, B. Ghanayem, G.I. Hussein, Studies on the mechanism of acetonitrile toxicity. I: Whole body autoradiographic distribution and macromolecular interaction of 2-14C-acetonitrile in mice, Pharmacol Toxicol 70 (1992) 322-330.

[73] M.S. Jablin, M. Flasinski, M. Dubey, D.R. Ratnaweera, M. Broniatowski, P. Dynarowicz-Latka, J. Majewski, Effects of beta-cyclodextrin on the structure of sphingomyelin/cholesterol model membranes, Biophys J 99 (2010) 1475-1481.

[74] A. Abulrob, J.S. Tauskela, G. Mealing, E. Brunette, K. Faid, D. Stanimirovic, Protection by cholesterol-extracting cyclodextrins: a role for N-methyl-D-aspartate receptor redistribution, Journal of Neurochemistry 92 (2005) 1477-1486.

[75] Coumarin, IARC Monogr Eval Carcinog Risk Chem Man 10 (1976) 113-119.

[76] H.T. Cheng, Megha, E. London, Preparation and properties of asymmetric vesicles that mimic cell membranes: effect upon lipid raft formation and transmembrane helix orientation, J Biol Chem 284 (2009) 6079-6092.

[77] M.J.T. Frisch, G. W.; Schlegel, H. B.; Scuseria, G. E.; Robb, M. A.; Cheeseman, J. R.; Scalmani, G.; Barone, V.; Mennucci, B.; Petersson, G. A.; Nakatsuji, H.; Caricato, M.; Li, X.; Hratchian, H. P.; Izmaylov, A. F.; Bloino, J.; Zheng, G.; Sonnenberg, J. L.; Hada, M.; Ehara, M.; Toyota, K.; Fukuda, R.; Hasegawa, J.; Ishida, M.; Nakajima, T.; Honda, Y.; Kitao, O.; Nakai, H.; Vreven, T.; Montgomery, Jr., J. A.; Peralta, J. E.; Ogliaro, F.; Bearpark, M.; Heyd, J. J.; Brothers, E.; Kudin, K. N.; Staroverov, V. N.; Kobayashi, R.; Normand, J.; Raghavachari, K.; Rendell, A.; Burant, J. C.; Iyengar, S. S.; Tomasi, J.; Cossi, M.; Rega, N.; Millam, N. J.; Klene, M.; Knox, J. E.; Cross, J. B.; Bakken, V.; Adamo, C.; Jaramillo, J.; Gomperts, R.; Stratmann, R. E.; Yazyev, O.; Austin, A. J.; Cammi, R.; Pomelli, C.; Ochterski, J. W.; Martin, R. L.; Morokuma, K.; Zakrzewski, V. G.; Voth, G. A.; Salvador, P.; Dannenberg, J. J.; Dapprich, S.; Daniels, A. D.; Farkas, Ö.; Foresman, J. B.; Ortiz, J. V.; Cioslowski, J.; Fox, D. J. Gaussian, Inc., Wallingford CT,, GAUSSIAN 09, Revision A.1, (2009).

13 Appendix

A Detection of Malign Cells in Bio-Fluids for Diagnostic Purposes

B Effective Staining of Tumor Cells by Coumarin-6 Depends on the Stoichiometry of Cyclodextrin Complex Formation

Appendix A

Detection of Malign Cells in Bio-Fluids for Diagnostic Purposes

Detection of Malign Cells in Bio-Fluids for Diagnostic Purposes

Michael Edetsberger[1*], Erwin Gaubitzer[2*], Christoph Miksch[2*], Martin Knapp[1], Bruno Baluch[1], Khatuna Elizbarowna Gvichiya[1], Ibrahim Attassi[3], Walter Smetana[3] and Gottfried Köhler[2]

[1] OnkoTec GmbH, Vestenötting 1, 3830 Waidhofen/Thaya, Austria

[2] Max F. Perutz Laboratories - Dept. f. Computational and Structural Biology, Campus Vienna Biocenter, 1030 Vienna, Austria

[3] Technical University Vienna - Institute for Sensor and Actuator Systems, Gusshausstrasse, 1040 Vienna, Austria

*these authors contributed equally

Abstract: *ONKOVIDON®, a new and patent registered, green fluorescent marker substance helps to detect potential malign cells in different body fluids. Specific dye enrichment in intracellular compartments provides a defined staining pattern for different cell types. The stained cells are first separated in a microfluidic sedimentation device. Prototypes of this chip are built in LTCC technology. The images of these isolated cells are than characterized, classified, and counted for quantitative diagnostics. The whole process, i.e. isolation and imaging of cells and their quantitative characterization is fully automated using a newly developed software package.*

1. Introduction:

Despite significant advances in treatment, bladder cancer is a common disease with a high mortality rate but intensive screenings have shown to decrease mortality rates[1].

Therefore, for an optimized treatment and more important early diagnosis it is essential to have a fast, reliable and high quality diagnostic tool. Auto fluorescence of cells is an appealing technique as no markers or dyes have to be used to detect morphological changes of cells. This method can differentiate between normal, healthy tissue and papillary tumors but the diagnosis of carcinoma in situ remains problematic [2] and detection of low grade tumors is also highly critical. Intravesical instillation of fluorophores, with limited systemic absorption and thus systemic side effects, is the method of choice when considering fluorescence diagnosis of bladder cancer [1]. Three fluorophores can be proposed to this purpose: ALA, h-ALA and hypericin. All three have been shown to have an excellent sensitivity (>90%), with various specificities ranging from 70 over 80 to 90%, respectively [2]. Cellular markers, particularly abnormal cells, like red blood cells or shed cells from tumors, which appear in the urine have been utilized to help diagnose bladder cancer [3]. Performed at repeated intervals, cytoscopy using either bladder wash or voided urine is the golden standard. It should be recalled, that this technique is not perfect as has been demonstrated by using hematoporphyrin derivate cytoscopy [4] or other marker tests, which have detected tumors that cytoscopy has overlooked [5]. Several modeling studies have indicated that replacing some or all surveillance cytoscopy examinations with a marker test, might significantly reduce costs [6]. Although different marker tests show a better performance than cytoscopy also these rapid diagnostic techniques have strong draw backs. For some of the markers, particularly Uro Vysion FISH, 10 to 15% of specimens from patients with bladder cancer have been reported to be uninterpretable [2].

There is no doubt that fluorescent molecules play an important role in the development of Biosensors, photo catalytic instruments, opto-electronic devices and for cellular staining reactions. The aim of OnkoTec is the development of a cost effective non-invasive Automated Rapid Diagnostic Tools (ARDT) for the detection of malign cells out of body-fluids, starting with bladder cancer, detecting fluorescent labeled cancer cells out of urine samples. Commercial available test systems detect cancer-markers

using specific monoclonal antibodies, which is very expensive on one hand and which show a wide range of sensitivity on the other hand [7]. OnkoTec developed a new markers substance providing a fast labeling of potential candidates.

ONKOVIDON® is a novel, patent registered, green fluorescent marker substance that provides strongly different staining patterns for cells of different origin due to the highly specific interaction of the dye with certain cellular compartments. These different patterns allow to differentiate between cells of different malignancy and to distinguish them from healthy cells. After separating the labeled cells from urine in a microfluidic sedimentation chamber the cells are imaged. Prototypes for this device were built and optimized using LTCC technology. The images of these isolated cells are characterized, classified, and counted for quantitative diagnostics in a fully automated process using a newly developed instrument and software package.

2. Results:

The first step for a specific detection of malign cells in bio fluids is the effective and specific staining of potential malign candidates. This specific staining has to be verified with different microscopic techniques.

2.1 Fluorescence Microscopy and Laser Scanning microscopy:

Different cell lines were imaged after 10 minute incubation with 10nM Onkovidon in phosphate buffered saline[1] (PBS). Epifluorescence images were performed with a Zeiss AXIOVERT S100TV[2] and Laser Scanning images were performed with a Zeiss 510 Meta[3]. In figure 1 the results of co-staining experiments are presented. Adherent bladder cancer cells, surrounded by a 1000 fold majority of erythrocytes, harvested by finger-pad punction, show a strong fluorescent signal, if they are incubated with

[1] Phosphate buffered saline (137mM NaCl, 2.7mM KCl), 10mM Na2HPO4, 1.76mM KH2PO4, pH 7.4)
[2] Zeiss Axiovert S100TV with appropriate filter setting at 10x magnification
[3] Zeiss 510 Meta with appropriate filter and laser settings at 100x magnification

Onkovidon and imaged at appropriate excitation and emission wavelength[4]. In contrast the erythrocytes do not show any fluorescent signal, although both cell types were incubated with the fluorescent dye simultaneously. Additionally the malign bladder cancer cells (red arrow) show a typical, cytoplasmatic dye enrichment, which cannot be observed in fibroblasts or benign bladder cancer cells in such an extent.

This cell dependent intracellular dye enrichment and the intracellular distribution of the dye was also shown using Laser Scanning Microscopy. Also in this case different adherent cell lines were washed with PBS and stained with 30nM Onkovidon in PBS for 10 minutes. The results of the LSM experiment is presented in figure 2.

Using Fibroblast (fig.2 left), the dye is distributed homogeneously over the cytoplasm, whereas the nucleus is not stained with this dye which was also shown by a counter stain with 10mM HOECHST 33342 (figure 3). Using benign bladder cancer cells the dye is still distributed homogeneously but a pattern specific enrichment of the dye could be observed (fig. 2 middle). In contrast to Fibroblasts or benign bladder cancer cells, an enrichment of the dye in the peri-nuclear region can be observed in malign bladder cancer cells (fig.2 right)

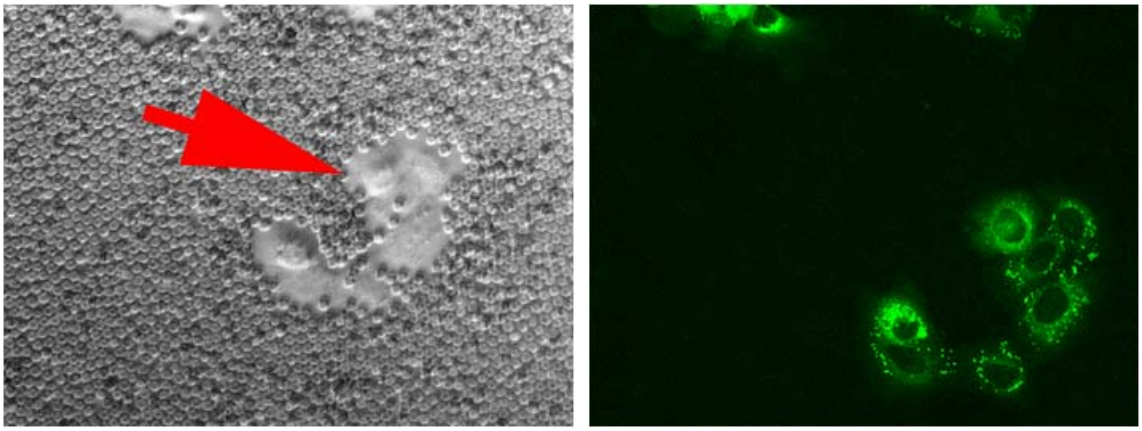

Fig1: Cultivated bladder tumor cells (HTB5 – malign bladder cancer-grade IV) incubated with Onkovidon® in the presence of human erythrocytes (direct blood from finger pad). Left: Transmission micrograph (10 x magnifications). The red arrow indicates adherent tumor cells surrounded by erythrocytes (small round structures). Right: Fluorescence micrograph (10 x magnifications). Only the adherent cancer cells show a strong fluorescent signal.

[4] λex= 488nm/ λem=514nm

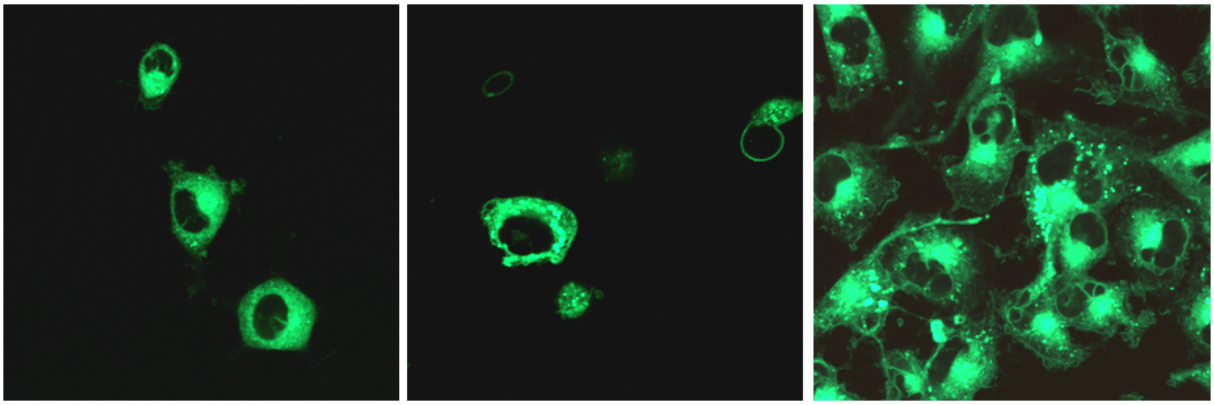

Fig2: Laser Scanning Micrographs of different cell types incubated with Onkovidon®. Every image represents a slice of about 1µm. Left: LSM Images of Fibroblasts. The fluorescent dye is distributed homogeneously over the cytoplasm, but does not enter the nucleus. Middle: LSM images of benign bladder cancer cells. Still the dye is distributed homogeneously, but a beginning accumulation of the dye can be observed. Right: LSM images of malign bladder cancer cells. The intracellular dye accumulation is in high gear. Additionally these cells show an inhomogeneous distribution of the dye.

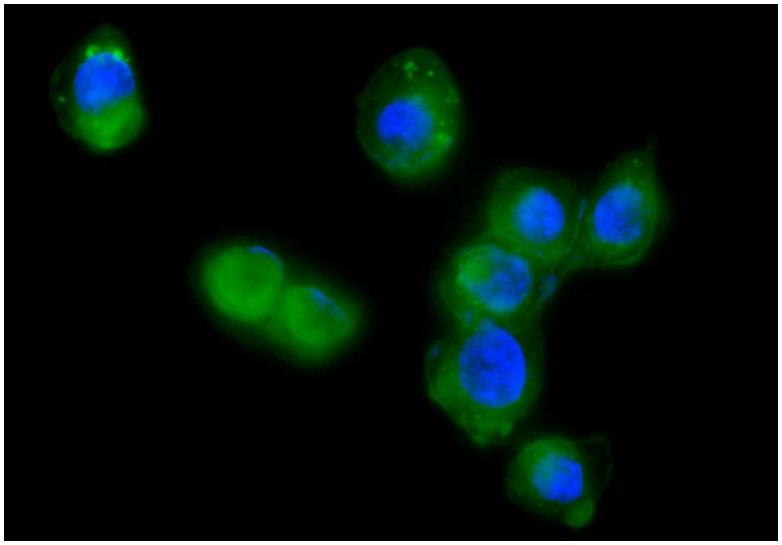

Fig3: Fluorescent micrographs of Fibroblasts stained with Onkovidon and counterstained with Hoechst 33342. As there is no cross talk in the different detection channels, the different dyes stain different cellular compartments as the nucleus appears blue and the cytoplasm appears green.

If tumor cells stained with Onkovidon and counterstained with the red fluorescent, lipophilic dye BODIPY 558/568, are imaged with a laser scanning microscope a very interesting result can be observed. Onkovidon stains membranes clearly and intensively with high contrast between the stained membrane, cytoplasm, nucleus and

other stained structures (fig. 4 arrow). In contrast to the cellular membrane appearing in green other yellow structures are observed. The yellow color results as overlay of green fluorescence (Onkovidon) and red fluorescence, originating from the lipid-body specific dye BODIPY. In contrast to lipid bodies, which can be identified by co-localization of green and red fluorescence, in other compartments of the cell green and red fluorescence can be observed separately

2.2 Sedimentation of cells

After specific staining of the cells in the body fluid, these cells are separated from the fluid and collected for imaging and analysis. For this purpose a microfluidic device was built using LTCC technology (GC tapes) (see figure 5, left), as it provides rapid prototyping during design and optimization of the construction. The principle set up of the sedimentation chamber is shown in figure 5 (right).

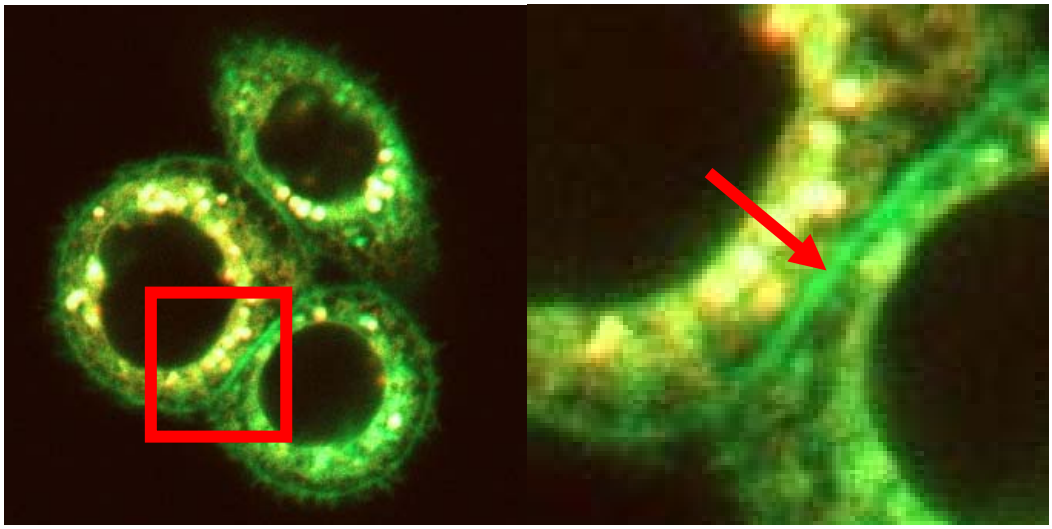

Fig4: Laser scanning micrographs of bladder cancer cells incubated with Onkovidon and counterstained with BODIPY, a lipid-body specific dye (Overlay of green and red channel). Onkovidon shows a strong affinity to stain all lipid structures (green) in contrast to BODIPY-Red, which stains preferentially lipid bodies (red). Lipid bodies appear thus orange to yellow in the overlay. The plasma membrane is only stained by Onkovidon as is seen in the right figure (red arrow)

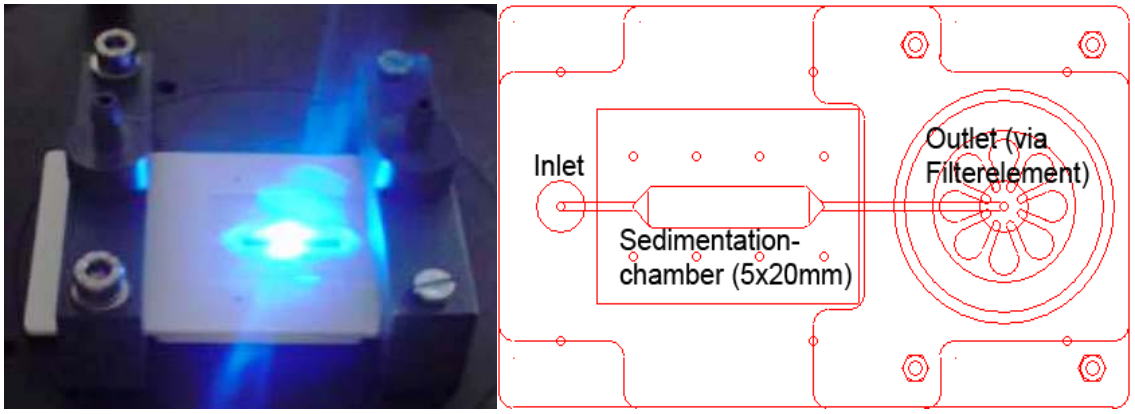

Fig5 Left: Microfluidic device build up in LTCC for cell sedimentation. The cells enter the device from the right side. They are passing the imaging chamber (blue eliminated area) and the supernatant is leaving the device on the right side. Right: Schematic set up of the sedimentation device.

Green fluorescent Fibroblasts enter the device at a flow rate of 20ml/min at the inlet port. Then the cells pass the imaging area (0.5x20mm) and already at this very high flow rate the cells start to sediment effectively, with could be shown by epifluorescence micrographs at different positions within the observation area figure 6). After the cells sedimented within the observation chamber the supernatant leaves the device at the outlet port. Cells which did not sediment are collected at the outlet port which is closed with a filter element. These collected cells can additionally be harvested by a reverse flow technique. The sedimented cells are imaged at 10x magnification and the images analyzed with a newly developed software package.

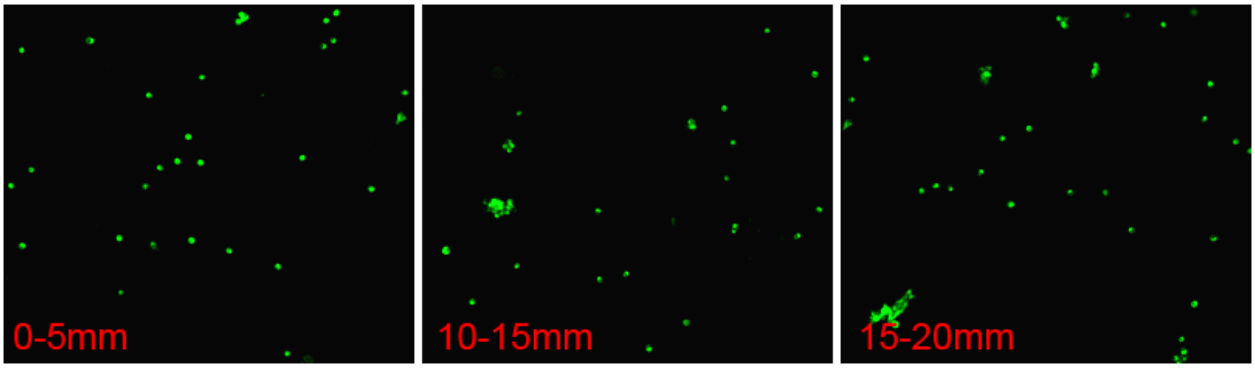

Fig6: Epifluorescent micrographs at 4x magnification, representing a 0.8x0.8mm section of the observation area. Left: represents the sedimentation behavior of Fibroblasts within 5mm after the cells enter the imaging chamber. Middle: represents an area within 10 to 15mm after the entrance channel. Right: represents the last 5mm within the imaging area.

2.3 Characterization of cells:

Different cell types have different fluorescence patterns after staining. Images of cells with 10x magnifications can be used to characterize the different fluorescence distribution in the cells. In our case a standard monochrome CCD camera was used and the fluorescence intensity distribution was extracted from the gray channel with a resolution of 12 bit. For an automatic evaluation of the images only single, segregated cells were used, as conglomerates of cells, which appear sometimes in the images, may hide significant features due to the overlap of the single images. Conglomerates of cells, which might be significant for certain diagnostic purposes, will be evaluated in future studies.

Evaluation and characterization of the cell images are performed in three main steps:

1. Discrimination of the background and partition of the foreground into individual objects (recognition of single objects)
2. Pre-selection of objects with shapes similar to cells of interest.
3. Description of cellular objects on the basis of fluorescence intensity, size and internal structure.

The three descriptors used are selected because they allow a clear characterization of the objects and there independence from each other. The internal structure parameter represents a newly developed descriptor, which takes into account the internal structure of a given cell independent of the total fluorescence intensity.

The applicability and meaningfulness of these descriptors was tested on samples obtained from cultural cell lines (immortal tumor cells of different type and grading). Although, each property shows a broad statistical distribution for the individual cells, in the (currently) three-dimensional property space the different cell lines can be clearly separated from each other. In our examination we used 4 cell lines of which Fibroblasts (L929), high grade bladder tumor cells (HTB5) and benign bladder tumor cells (HTB2) occupy specific subsectors of the property space (figure 7). Only

squamous bladder tumor cells are not clearly discriminable. Therefore, this analysis is currently limited to a smaller range of cell lines because of overlapping areas in their distributions, but additional descriptors are developed and will be implemented shortly.

In the case of urine samples there are several different cell types present as mixtures. In this case it is necessary to find that distribution, which is typical for respective cancer patients. This is currently performed in an empirical study where a large number of samples comprising all states of carcinoma of the urogenital tract are examined and checked against different properties. Already in the current status it is possible to discriminate bladder positive samples from samples of inflammations or other urogenital diseases. We could also show that, using additional or revised descriptors, it is possible to differentiate between different grading of the tumor cells (data not presented).

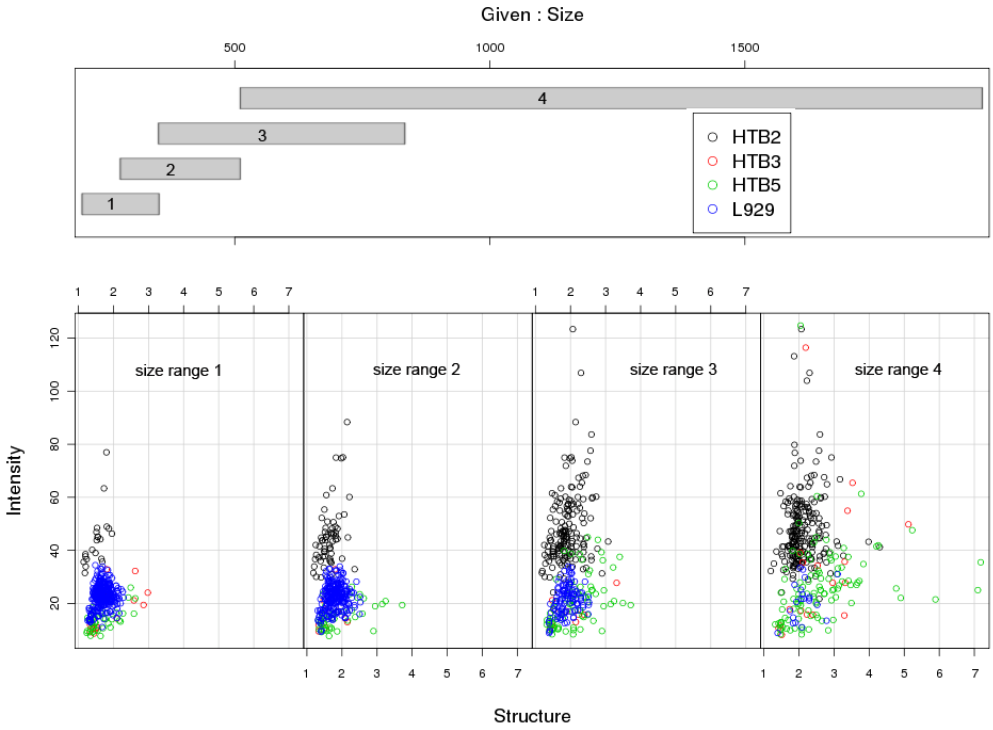

Fig7: The 3-dimensional space of cell properties is subdivided into 4 sizes and for each size the intensity is plotted versus its structural property. The different colored circles represent individual cell objects of the different cell lines.

3. Conclusion:

It could be shown that using ONKOVIDON® a specific detection of malign cells in bio fluids and the effective and specific staining of malign, cultivated cells could be obtained. Using a newly developed software package we were able to discriminate between benign and malign cell lines of the same origin and even more we were able to differentiate between cell lines of different origins. Using a sedimentation unit fabricated in LTCC technology it was possible to separate the stained cells from the supernatant very effective and additionally it should be elucidated that LTCC technology is a very powerful tool for rapid prototyping for the different microfluidic architecture, which is essential for the development of an effective sedimentation unit.

4. References

[1] S.P. Shirodkar, V.B. Lokeshwar, Potential new urinary markers in the early detection of bladder cancer, Curr Opin Urol 19 (2009) 488-493.

[2] M.A. D'Hallewin, L. Bezdetnaya, F. Guillemin, Fluorescence detection of bladder cancer: a review, European Urology 42 (2002) 417-425.

[3] E. Messing, Markers of detection, Urol Oncol 25 (2007) 344-347.

[4] D. Jocham, F. Witjes, S. Wagner, B. Zeylemaker, J. van Moorselaar, M.O. Grimm, R. Muschter, G. Popken, F. Konig, R. Knuchel, K.H. Kurth, Improved detection and treatment of bladder cancer using hexaminolevulinate imaging: a prospective, phase III multicenter study, J Urol 174 (2005) 862-866; discussion 866.

[5] H.B. Grossman, M. Soloway, E. Messing, G. Katz, B. Stein, V. Kassabian, Y. Shen, Surveillance for recurrent bladder cancer using a point-of-care proteomic assay, JAMA 295 (2006) 299-305.

[6] Y. Lotan, C.G. Roehrborn, Cost-effectiveness of a modified care protocol substituting bladder tumor markers for cystoscopy for the followup of patients with transitional cell carcinoma of the bladder: a decision analytical approach, J Urol 167 (2002) 75-79.

[7] P.R.a.S. Roth, Urinzytologie, 4. Edition ed., Springer, 2007.

Appendix B

Effective Staining of Tumor Cells by Coumarin-6 Depends on the Stoichiometry of Cyclodextrin Complex Formation

Effective Staining of Tumor Cells by Coumarin-6 Depends on the Stoichiometry of Cyclodextrin Complex Formation

Michael Edetsberger[*1], Martin Knapp[*1], Erwin Gaubitzer[1], Christoph Miksch[2], Kathuna Elizbarowna Gvichiya[1] and Gottfried Köhler[2]

[1] *Onkotec Gmbh, Vestenötting 1, Waidhofen/Thaya, Austria*

[2] *Max F. Perutz Laboratories, Department for Computational and Structural Biology, Campus Vienna Biocenter 5/1, 1030 Vienna, Austria*

*these authors contributed equally

Phone: 0043 1 4277 52244

Email: michael.edetsberger@onkotec.eu

Abstract

In a comprehensive picture of inclusion complex formation of the highly fluorescent dye coumarin-6 (C6) and betacyclodextrin (beta-CD), which was obtained using various fluorescence spectroscopic methods, it was demonstrated that up to three beta-CD rings can thread on the rod like dye molecule. Interaction of coumarins and modified coumarins with cellular organelles or proteins has been reported in several publications. Especially 7-amino-coumarins are characterized by unique properties like high fluorescence quantum yield and are thus already used successfully in different areas, like staining of fluorescent nanoparticles. We could show that Coumarin-6 made soluble by complexation with beta-cyclodextrin is able to stain eukaryotic cells specifically dependent on their origin and cellular behaviour. The staining reaction is independent from pH, is photo stable, and shows no cross talk with proteins in the cytoplasm and other staining procedures or erythrocytes. Staining with Coumarin6/cyclodextrin complexes can thus be used for fast discrimination of different cell types. Importantly, it could be shown that the ideal staining reaction is dependent on the stoichiometry of the complex-formation.

Keywords: *Cyclodextrines, Coumarin-6, Fluorescence Correlation Spectroscopy (FCS), Cell staining, Fluorescence Microscopy*

Introduction

Self-assembling phenomena attract considerable interest as basic issues for supramolecular chemistry, molecular biology and fields like nanotechnology and nanofabrication [1]. A specific example for molecular self-assembly is the formation of host-guest complexes where an active small guest molecule binds into a cavity of a macromolecular host. Complexation due to the hydrophobic effect is a widely found phenomenon in chemistry and can be applied to increase the solubility of hydrophobic molecules in water [2,3]. Cyclodextrines are well known hydrophilic host molecules, consisting of six (alpha-cyclodextrin), seven (beta-cyclodextrin) or eight (gamma-cyclodextrin) α-1,4-glycosidically linked glucopyranose subunits providing a hydrophobic cavity. They are known to complex a variety of guest molecules unspecifically [4,5] providing a hydrophilic envelope for a hydrophobic guest in water.

Fluorescent molecules play an important role in the development of biosensors, photo catalytic systems, opto-electronic devices and for staining reactions of specific compartments in living cells to make them discernable in microscopic imaging. Especially the staining of hydrophobic compartments in cells like membranes needs hydrophobic molecules which are generally not soluble in an aqueous environment. Using organic co-solvents to increase their solubility interferes, however, with cellular function. This limitation could be overcome using cyclodextrines to solubilize the dyes, as they can be used at rather low concentration.

One example we used recently is coumarin-6 complexed with β-cyclodextrines, which has been shown to stain cancer cells specifically [6]. Commercially available systems to detect cancer-markers on the cell surface make use of specific monoclonal and fluorescent labeled antibodies, which have a wide range of sensitivity, high selectivity but are very expensive and can often be used only for to detect specific cancer cells [7]. Despite significant advances in treatment, bladder cancer is a common disease with a high mortality rate but intensive screenings have shown to decrease mortality rates [8]. Therefore, for an optimized treatment and more important early diagnosis it is essential to have a fast, reliable and high quality diagnostic tool, which allows detecting cancer cells or other cells characteristic for a disease directly from urine.

In this paper we show that specific staining of cancer cells in urine is highly dependent of the stoichiometry of the coumarin-6 complexes with β-cyclodextrin, which depends strongly on the β-cyclodextrin concentration in relation to the dye concentration.

Materials and Methods

Preparation of β-cyclodextrin solution:

A nearly saturated 10^{-2}M stock solution of β-cyclodextrin was obtained by adding 10mg/mL β-cyclodextrin to purified water followed by 15 minutes sonication at 65°C. This procedure gave a clear and stable solution.

Preparation of coumarin-6 solution:

A 60μM coumarin-6 stock solution was obtained by dissolving coumarin-6 in absolute ethanol resulting in a clear, green fluorescent solution.

Complex formation between coumarin-6 and β-cyclodextrin

Ethanolic coumarin-6 and aqueous β-cyclodextrin was mixed in varying amounts to obtain the desired dye/β-cyclodextrin concentration ratios. This mixture was stirred for 10 minutes at room temperature and this procedure gave a clear, highly green fluorescent solution in the case the β-cyclodextrin concentration exceeded 20 μM. To stain cells this solution was added to the growing buffer for a final concentration of 30 nM for the dye.

Fluorescence Correlation Spectroscopy (FCS) measurements:

A confocal microscope (Confocor1-Carl Zeiss, Jena, Germany) was used to measure dynamics of complex formation by fluorescence correlation spectroscopy (FCS). An argon ion laser supplied 488 nm light for excitation of coumarin-6, filtered using a 488 ± 10 nm interference filter. The excitation light was focused by a water immersion objective (C-Apochromat 63×, 1.2 NA) in the solution and the fluorescence light was collected through the same objective and passed through a broad band filter (520-560 nm) before passing the confocal pinhole with a diameter of 45 μm. The instrument was calibrated using a 10 nM aqueous solution of rhodamine 6G. FCS measurements were performed in aqua bidest or PBS respectively. The experiments were analyzed with the FCS ACCESS software package obtained from Zeiss/EVOTEC, using a multicomponent fit model. Analysis was performed for a fixed structural parameter defining the ratio between the height and the width of the detection volume. This parameter was also obtained from the calibration procedure.

Epifluorescent Images

Bladder cancer cells were grown in chambered cover slides in MEM medium. For imaging the medium was replaced by phosphate buffered saline (137mM NaCl, 2.7mM KCl, 10mM Na2HPO4, 1.76mM KH2PO4, pH 7.4) containing the coumarin-6/β-cyclodextrin complex at a final concentration of 30nM for coumarin-6. Epifluorescence images were taken after 10 minutes incubation using a Zeiss AXIOVERT S100TV, appropriate filter settings and 10 x magnifications. For quantification of the images they were analyzed using the cell counting module of ImageJ (free image processing software).

Theoretical Methods

The quantum chemical calculations were performed using the GAUSSIAN09 program package [9]. The structures of coumarin-6 and β-cyclodextrin were fully optimized by HF with 3-21G basis set. Complexes between C coumarin-6 and one β-cyclodextrins were built and were optimized by HF/3-21G.

Results

FCS measurements of complex formation

The mean diffusion times for coumarin-6/β-cyclodextrin complexes were measured for 30nM coumarin-6 and varying the β-cyclodextrin concentrations, in between relative concentrations of the two partners of 1: 300 up to 1:150.000 (coumarin-6/β-cyclodextrin), by FCS. The autocorrelation function ($G_{(t)}$) was measured and fitted to the following model [10]:

$$G_{(t)} = 1 + \frac{1}{N}\left[\frac{1}{1+\frac{4Dt}{\omega_1^2}}\sqrt{\frac{1}{1+\frac{4Dt}{\omega_2^2}}}\right]$$

where N is the number of fluorescent molecules in the confocal volume, D the diffusion coefficient, ω_1 the radius of the confocal ellipsoid horizontally and ω_2 its length. The mean diffusion time was obtained from the fit procedure and its mean values are shown in figure 1 as a function of the relative concentrations of coumarin-6 and β-cyclodextrin.

Adding less than 20 μM β-cyclodextrin to 30 nM aqueous coumarin-6 gives mean diffusion times near to that typical for the free dye, however, with a large statistical error. This is most likely due to the low solubility of coumarin-6 in water and hence aggregation of the dye. Small dye aggregates were also denoted by the observation of particles moving through the observation volume of higher brightness and longer diffusion time than a single dye molecule. In comparison the complex with cyclodextrines has the same brightness but a long diffusion time as it consists only of one dye molecule. Increasing the β-cyclodextrin concentration above ca. 50 μM the particle distribution becomes more homogeneous as no dye aggregates are observed and the statistical error of the mean diffusion time decreased significantly. Self-aggregation of cyclodextrines should not contribute at these low concentrations. These results indicate, however, coumarin-6/β-cyclodextrin complex formation even in concentration range below 20 μM. Increasing the β-cyclodextrin concentration the mean diffusion time increased and becomes nearly 37 μs near to 150 μM host, which is near to an estimated diffusion time for the 1:1 coumarin-6/β-cyclodextrin complexes. At even higher β-cyclodextrin concentrations larger complexes are formed. Around 900 μM

β-cyclodextrin complexes of a 1:2 stoichiometry dominate. Formation of even 1:3 coumarin-6/β-cyclodextrin complexes is indicated by the value of the mean diffusion time when the host concentration becomes larger than 1 mM. These data indicate that coumarin-6 forms strong inclusion complexes with β-cyclodextrin with complexation constants near to 10000 M^{-1} for the formation of the 1:1 complex, about 2000 to 3000 M^{-1} for the formation of the 1:2 complex from the 1:1 complex and about 1000 M^{-1} for further addition of an cyclodextrin-molecule.

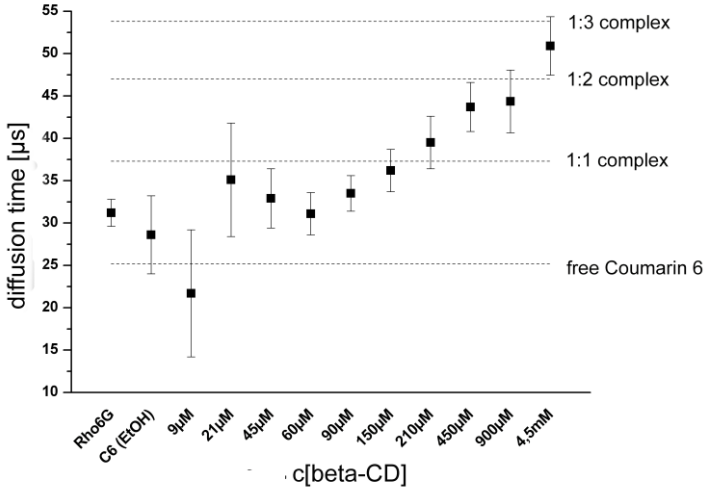

Fig1: Results of the FCS measurements of different stoichiometric mixtures of coumarin-6 (concentration 30nM) and β-cyclodextrin (final concentrations between 9µM and 4.5mM). Dashed lines represent estimated diffusion times of free coumarin-6, and 1:1-, 1:2- and 1:3 complexes with β-cyclodextrin. Measurements for coumarin-6 in ethanol are also shown (C6-EtOH). The error bars were obtained from the subsequent repetition of the measurements.

Influence of complex formation on staining reaction

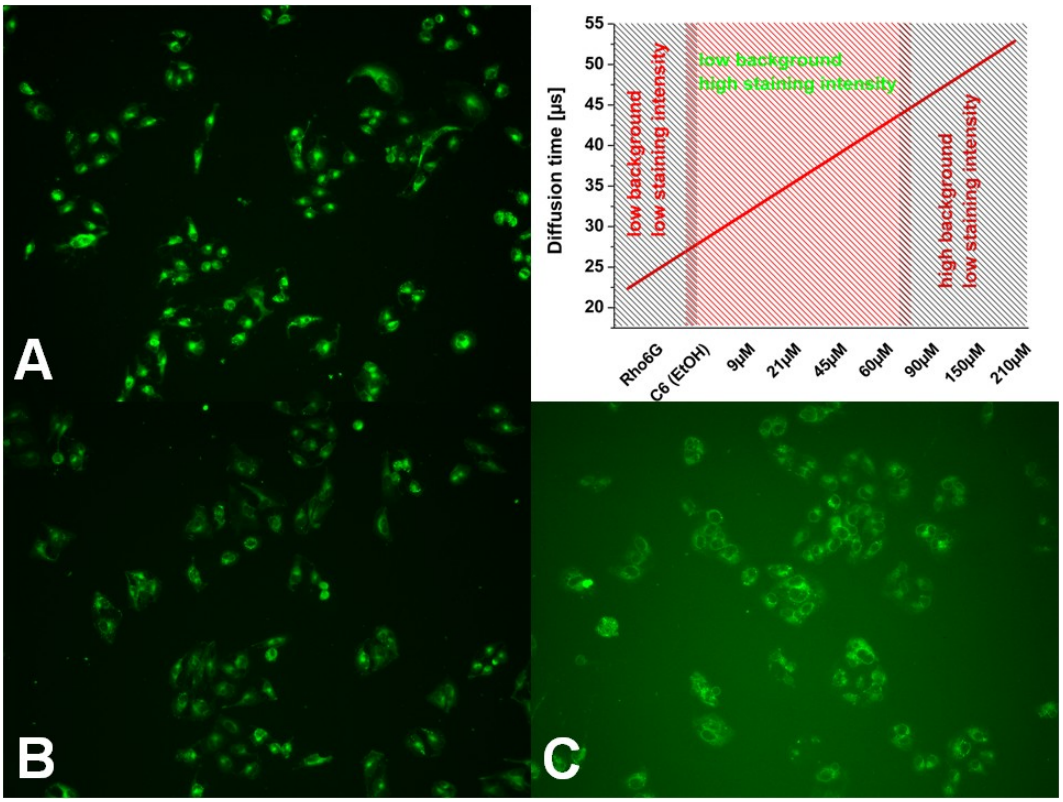

Fig2: Human bladder tumor cells stained with coumarin-6 (30 nM)/β-cyclodextrin complexes of different stoichiometrical composition. Cells are stained using a 1:3.000 (A), 1:750 (B) and 1:30.000 (C) coumarin-6 to β- cyclodextrin mixture. Upper-right panel: Comparison between complex stoichiometry and staining intensity. The red line indicates a linear regression of the mean diffusion time caused in dependence of an increased concentration of β-cyclodextrin. The black boxes indicate the mean intensity of the stained cells using different concentration of β-cyclodextrin. Generally a final concentration of 30 nM coumarin-6 was applied in all cases.

In a further series of experiments the staining efficiency of living cells when complexes of different stoichiometry are used. The results of these experiments are summarized in Figure 2. It has already been shown that different cell types show significantly different fluorescence patterns after staining with coumarin-6/β-cyclodextrin. Images of cells obtained with 10x magnification can be used to characterize the different fluorescence distribution in the cells [6]. From these images a mean brightness of the stained cells could be calculated for given cell type by integrating the intensity pattern over the area of the cell. This defines the staining capability of the dye. Representative results obtained for bladder tumor cells are presented in figure 2. The results show clearly that it is very important to use mainly 1:1 coumarin-6/β-cyclodextrin complexes, i.e. to apply a ca. 100 µM β-cyclodextrin solution, to assure an intensive staining reaction without a significant background (see fig2-A). Cells stained at these conditions show a mean intensity of about 27 a.u. Using primarily uncomplexed dye for staining, i.e. at a cyclodextrin concentration below 45 µM (see fig2-B for staining of the same cells with 21 µM β-cyclodextrin) or stable 1:2 complexes (see fig2-B for staining of the same cells

with 900 μM β-cyclodextrin) yield much less fluorescence intensity under identical condition and background fluorescence becomes much more intensive. The overall fluorescence intensity drops below 10 a.u. in both cases, which compares to nearly 1/3 of the intensity that is obtained using preferentially 1:1 complexes. It should be mentioned that these intensity values are corrected for background fluorescence, which becomes increasingly important when even higher β-cyclodextrin concentrations are applied corresponding to the predominant formation of 1:3 complexes. In that case the dye is not significantly incorporated into the cells and most of the Coumarin fluorescence is found in the medium outside the cells (see fig.3a). Cells stained with 1:3 complexes show almost the same total intensity as cells stained with pure coumarin-6 solution (see fig 3b) with the main difference that the background is much less intense most likely due to quenching by aggregation.

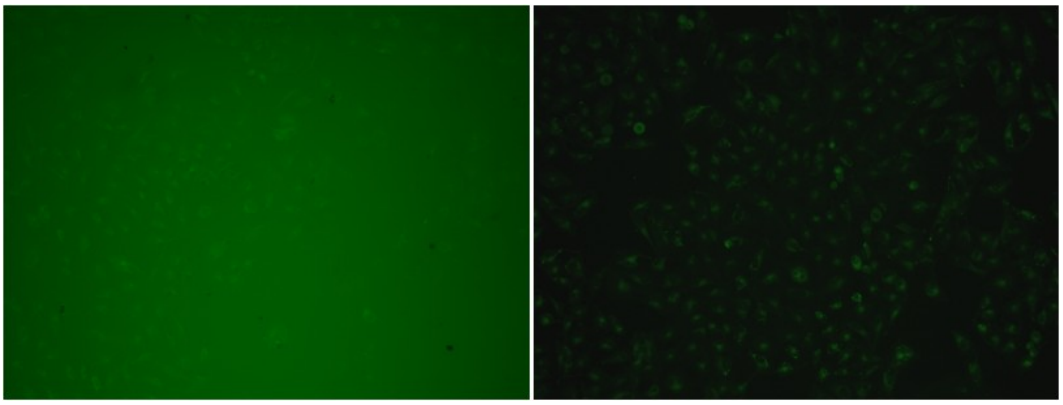

Fig3: Left: Human Bladder tumor cells stained with coumarin-6 (30nM)/β-cyclodextrin (4.5mM). The cells do not show a significant fluorescent signal and the fluorescence originating from the cells is hidden by the background fluorescence. Right: Human Bladder tumor cells incubated with coumarin-6 without cyclodextrines added. Although a fluorescent pattern can be observed, the fluorescence of stained cells is much weaker, compared to the fluorescence of cells incubated using a cyclodextrin concentration around 100 μM.

The results indicate clearly the importance of the complex stoichiometry for the interaction with life cells and the uptake of the dye.

Model calculations

An *ab initio* model of the 1:1 complex of dye and β-cyclodextrin was calculated and is shown in fig. 4 as these complexes are the most efficient structures to stain the cells. The figure shows clearly that at least two further cyclodextrin rings fit to the size of the dye molecule and this supports the interpretation of the FCS measurements. The position of the cyclodextrin ring threaded on the dye molecule suggests a slow dissociation of the complex, which could explain the high association constant found for the 1:1 complex. On the other hand side, the two additional rings in 1:2 and 1:3 guest to host complexes associate only with free end of the dye molecule and this accounts for the lower binding constants for association of an additional sugar molecule.

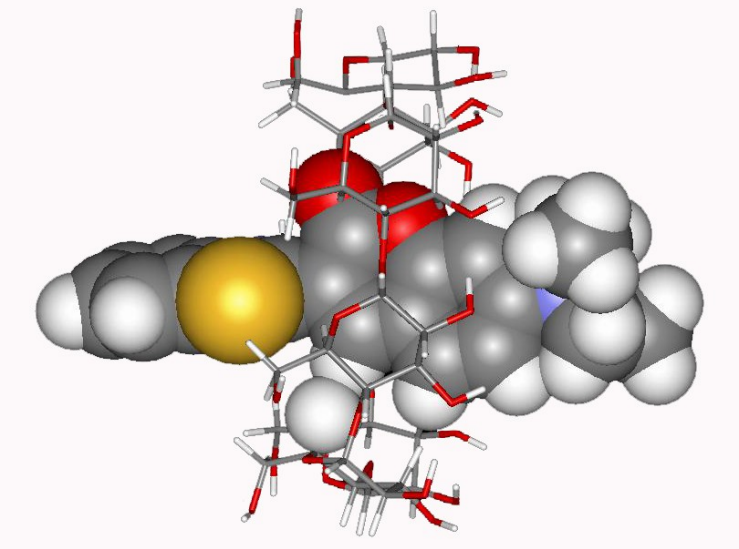

Fig4: A typical geometry of a complex between coumarin-6 and β-cyclodextrin, fully optimized at HF/3-21G level.

Summary

Coumarin-6 is an amphipatic dye with high fluorescence in the green spectral region and high photochemical stability. The amphipatic character of the dye and its lipid like structure allows specific staining of lipid structures in eukaryotic cells. As it has, however, only low solubility in aqueous solution delivery of the dye to the cell membrane is an important issue. It was demonstrated that threading of β-cyclodextrines on the rod like molecule accounts for increases the staining capability of dye efficiently when complexes of a low 1:1 stoichiometry are used. Higher complex structures like 1:2 or 1:3 coumarin-6 per β-cyclodextrin molecules reduces the uptake of the dye by the cells efficiently. The mechanisms and the thermodynamics governing this behavior is currently studied in detail, as this is an important issue for understanding of drug delivery to cells using cyclodextrines. The results could be used for the development of effective drug delivery systems pharmacological applications of cyclodextrines.

References

[1] M. Knapp, P. Wolschann, G. Köhler, Threading of β-Cyclodextrins on Coumarin-6 monitored by fluorescence spectroscopy, (to be published).

[2] K.A. Connors, The stability of cyclodextrin complexes in solution, Chemical Reviews 97 (1997) 1325-1357.

[3] G. Grabner, K. Rechthaler, B. Mayer, G. Kohler, K. Rotkiewicz, Solvent influences on the photophysics of naphthalene: Fluorescence and triplet state properties in aqueous solutions and in cyclodextrin complexes, Journal of Physical Chemistry A 104 (2000) 1365-1376.

[4] G. Grabner, S. Monti, G. Marconi, B. Mayer, C. Klein, G. Kohler, Spectroscopic and photochemical study of inclusion complexes of dimethoxybenzenes with cyclodextrins, Journal of Physical Chemistry 100 (1996) 20068-20075.

[5] G. Marconi, S. Monti, B. Mayer, G. Kohler, Circular-Dichroism of Methylated Phenols Included in Beta-Cyclodextrin - an Experimental and Theoretical-Study, Journal of Physical Chemistry 99 (1995) 3943-3950.

[6] M. Edetsberger, E. Gaubitzer, C. Miksch, M. Knapp, B. Baluch, K.E. Gvichiya, I. Attassi, W. Smetana and G. Köhler, Detection of Malign Cells in Bio-Fluids for Diagnostic Purposes, Proceedings of the EUREKA Conference (2010).

[7] P.R.a.S. Roth, Urinzytologie, 4. Edition ed., Springer, 2007.

[8] S.P. Shirodkar, V.B. Lokeshwar, Potential new urinary markers in the early detection of bladder cancer, Curr Opin Urol 19 (2009) 488-493.

[9] Gaussian 09, Revision **A.1**, Frisch, M. J.; Trucks, G. W.; Schlegel, H. B.; Scuseria, G. E.; Robb, M. A.; Cheeseman, J. R.; Scalmani, G.; Barone, V.; Mennucci, B.; Petersson, G. A.; Nakatsuji, H.; Caricato, M.; Li, X.; Hratchian, H. P.; Izmaylov, A. F.; Bloino, J.; Zheng, G.; Sonnenberg, J. L.; Hada, M.; Ehara, M.; Toyota, K.; Fukuda, R.; Hasegawa, J.; Ishida, M.; Nakajima, T.; Honda, Y.; Kitao, O.; Nakai, H.; Vreven, T.; Montgomery, Jr., J. A.; Peralta, J. E.; Ogliaro, F.; Bearpark, M.; Heyd, J. J.; Brothers, E.; Kudin, K. N.; Staroverov, V. N.; Kobayashi, R.; Normand, J.; Raghavachari, K.; Rendell, A.; Burant, J. C.; Iyengar, S. S.; Tomasi, J.; Cossi, M.; Rega, N.; Millam, N. J.; Klene, M.; Knox, J. E.; Cross, J. B.; Bakken, V.; Adamo, C.; Jaramillo, J.; Gomperts, R.; Stratmann, R. E.; Yazyev, O.; Austin, A. J.; Cammi, R.; Pomelli, C.; Ochterski, J. W.; Martin, R. L.; Morokuma, K.; Zakrzewski, V. G.; Voth, G. A.; Salvador, P.; Dannenberg, J. J.; Dapprich, S.; Daniels, A. D.; Farkas, Ö.; Foresman, J. B.; Ortiz, J. V.; Cioslowski, J.; Fox, D. J. Gaussian, Inc., Wallingford CT, 2009.

[10] P. Schwille, U. Haupts, S. Maiti, W.W. Webb, Molecular dynamics in living cells observed by fluorescence correlation spectroscopy with one- and two-photon excitation, Biophysical Journal 77 (1999) 2251-2265.